~~The~~ Studies of ~~Some~~ Molecular Conformations by Vibrational Spectroscopy

by Richard Maxwell Barrett, B.Sc.

A thesis presented to the Faculty of Science
of the University of London in candidature
for the degree of Dector of Philosophy.

Chemistry Department,
Royal Holloway College,
(University of London),
Englefield Green,
Surrey.

December 1972.

To Linda Mary

Acknowledgements

The author wishes to express his most sincere gratitude to Dr. Derek Steele for his advice, guidance and encouragement during the tenure of this work.

Thanks are also due to my colleague Mr. Robert A.R. Pearce for many hours of helpful discussion and to Dr. Duncan G. Gillies for his advice and help on the N.M.R. aspects of this work.

The use of the London University inter-collegeate spectroscopic services and computing facilities is gratefully acknowledged.

The author wishes to thank the Science Research Council for financial support in the form of a Postgraduate Studentship.

Abstract

The impact of conformational analysis in chemistry was clearly demonstrated in 1969, during the tenure of this work, when the Nobel Prize for Chemistry was awarded to Professor D. H. R. Barton.

The first part of this thesis deals with the vibrational analysis of biphenyl and its 4,4'-dihalogeno derivatives with respect to the dihedral angle between the two rings. It is clearly demonstrated that change in conformation for biphenyl and 4,4'-difluorobiphenyl from D_{2h} (solid state) to D_2 symmetry (solution, molten and gaseous states) is accompanied by changes in position and spectral activity of certain normal modes. These shifts, together with supplementary data derived from some deuterated derivatives of biphenyl, give an estimate of the dihedral angle in the solution state. The structure of 4,4'-dichloro and 4,4'-dibromobiphenyl is D_2 irrespective of phase.

The second part of the thesis presents the vibrational analysis of tetrahydropyran and its 4-chloro and 4-bromo derivatives. Variable temperature NMR measurements give a quantitative estimate of the conformational equilibrium.

The final part of this work presents the liquid band shape analysis of the 215 cm^{-1} band of hexafluorobenzene in mixed benzene-cyclohexane solvents. It is shown from the computed correlation functions that vibrational relaxation occurs during the split of the hexafluorobenzene-benzene complex.

Contents

CHAPTER 1

The Vibrational Problem

1.1 General Introduction

Normal coordinate analysis refers to the mathematical treatment involved in the computation of the 3N-6 normal modes of vibration for a molecule (3N-5 for a linear molecule). The solution involves the construction of a three-dimensional potential energy surface or its force-field which may or may not be unique. For small molecules the vibrational assignment is well established, often for several isotopic species. In addition, the molecular geometric data is usually very accurate and Coriolis coupling and centrifugal distortion constants can be readily determined. The dimension of the secular equation is small such that the effort involved in manual calculation is not prohibitive. The consequence of this situation, i.e. amount of data available plus limited dimension of the problem, is that the most general harmonic field for these molecules involves a number of parameters normally lower or at least equivalent to the number of observables available. Research in this case is essentially orientated towards the determination of a complete potential function and the emphasis is on the unicity of the

solution, on the nature of the force-field and on the validity of the harmonic approximation. Recent work (1,2) on non-harmonic force fields has produced cubic and quartic terms for a number of molecules.

For larger molecules, however, the problem is far more complicated and the vibrational assignment is not always completely established. The molecular geometry is often known only approximately and supplementary data usually arises from deuterated species. The secular equation involves symmetry blocks of considerable dimensions which can only be solved by the availability of a fast, large-storage computer. As a consequence the most general harmonic field involves a number of parameters which largely exceeds the number of experimental data. Research on large molecules therefore involves the transferability of various types of force field of simpler molecules to more complex molecules of similar chemical constitution, to predict vibrational assignments. If this is done satisfactorily it is then feasible to use iterative techniques to improve the force field of the complex molecule.

To a first approximation molecular vibrations may be treated independently of rotation and electronic motions. Various coordinate systems can be used to solve the problem but the

following general treatment will show how the Hamiltonian is set up and solved.

A Cartesian framework for a molecule of N atoms will lead to 3N coordinates,

$$x_1, x_2, x_3 \ldots\ldots x_{3N}$$

The total kinetic energy is given by

$$2T = \sum_i m_i \frac{dx_i}{dt}^2 = \sum_i m_i \dot{x}_i^2 \qquad (1.1.1)$$

The potential energy of the molecule in terms of the same coordinates is given by a Taylor series expansion.

$$V = V_o + \sum_i \left(\frac{\partial V}{\partial x_i}\right)_o x_i + \frac{1}{2}\sum_{ij}\left(\frac{\partial^2 V}{\partial x_i \partial x_j}\right)_o x_i x_j$$

$$+ \frac{1}{6}\sum_{i,j,k}\left(\frac{\partial^3 V}{\partial x_i \partial x_j \partial x_k}\right)_o x_i x_j x_k + \ldots\ldots \text{higher terms}$$

(1.1.2)

As V_o is independent of the coordinate system it is arbitrarily set equal to zero.

If the coordinates are independent $\frac{\partial V}{\partial x_i}$ must be zero at the equilibrium position. A further simplification arises

if the molecular vibration comprises small displacements in which case it can be assumed that $x_i x_j x_k \ll x_i x_j$. Hence only quadratic terms need be considered in a first-order theory.

The second derivatives are constants being the force constants of the potential function.

$$\text{Hence} \quad 2V = \sum_{i,j} f_{ij} x_i x_j \tag{1.1.3}$$

The mass-adjusted displacements can be simply formulated by the help of the mass-weighted coordinates. The definition of such coordinates is

$$q_i = m_i^{\frac{1}{2}} x_i \tag{1.1.4}$$

Hence the kinetic and potential energy expressions are

$$2T = \sum_i \dot{q}_i^2 \tag{1.1.5}$$

$$2V = \sum_{i,j} c_{ij} q_i q_j \tag{1.1.6}$$

or in a matrix notation

$$2T = \dot{q}^t \dot{q} \tag{1.1.7}$$

$$2V = q^t C q \tag{1.1.8}$$

Newton's equation of motion can be written in Lagrangian form as

$$\frac{d}{dt}\left(\frac{T}{\dot{q}_i}\right) + \left(\frac{V}{q_i}\right) = 0 \qquad (i = 1, 3N) \tag{1.1.9}$$

A system of 3N second order differential equations is obtained of the form

$$\ddot{q}_i + \sum_j c_{ij} q_j = 0 \qquad (1.1.10)$$

or in matrix form

$$\ddot{q} + cq = 0 \qquad (1.1.11)$$

The solution of such a simple harmonic problem is

$$q_i = A_i \sin(\lambda^{\frac{1}{2}} t + \delta) \qquad (1.1.12)$$

where A_i, δ and λ are constants.

By substituting these 3N solutions back into the original differential equations the constants can be calculated and the following system is arrived at

$$\sum_j c_{ij} A_j = \lambda A_j = 0 \qquad (i = 1,2 \ldots 3N) \qquad (1.1.13)$$

which can be transformed into

$$\sum_{j\,i} c_{ij} A_j + A_j (c_{ii} - \lambda) = 0 \qquad (1.1.14)$$

or in matrix form

$$(c - \lambda E)A = 0 \qquad (1.1.15)$$

where E is the unit matrix.

Such a set of simultaneous equations can have a non-trivial solution only if the determinant of the coefficients vanishes

$$\begin{vmatrix} c_{11} - \lambda & c_{1,2} & \cdots & c_{1,3N} \\ c_{21} & c_{22} - \lambda & \cdots & \\ \vdots & \vdots & & \\ c_{3N,1} & & & c_{3N,3N} - \lambda \end{vmatrix} = 0$$

or $$\left| c_{ij} - \lambda \delta_{ij} \right| = 0 \qquad (1.1.16)$$

where δ_{ij} is the Kronecker delta ($\delta_{ij} = 1$ if $i = j$ but $= 0$ otherwise).

In matrix notation the secular equation is

$$c - E = 0 \qquad (1.1.17)$$

The normal frequencies ν_i are related to the roots λ_i by

$$\lambda_i = 4\pi^2 \nu_i^2 \qquad (1.1.18)$$

On back substituting λ_i a relationship between the amplitudes $A_{1i}, A_{2i} \ldots A_{3N,i}$ and the i th normal frequency is obtained. This defines 3N simultaneous equations.

$$\begin{aligned} (c_{11} - \lambda_i)A_{1i} + c_{12} A_{2i} + \cdots \quad & c_{1,3N} A_{3N,i} = 0 \\ c_{21} A_{1i} + (c_{22} - \lambda_i)A_{2i} + \cdots \quad & c_{2,3N} A_{3N,i} = 0 \\ \vdots \qquad\qquad\qquad & \vdots \\ c_{3N,1} A_{1,i} + \cdots \quad & (c_{3N,3N} - \lambda_i)A_{3N,i} = 0 \end{aligned}$$

This system can only be solved for the ratios of $A_{1i}, A_{2i} \ldots$ etc., but an arbitrary set A^1_{ki} may be obtained by putting $A_{1i} = 1$.

1.2 Internal Coordinates

Since the above treatment includes the three transalatory and three rotational degrees of freedom, the secular equation will have six roots which are zero. It is therefore far more convenient to construct the vibrational Hamiltonian in a set of coordinates which translate and rotate with the molecule, namely internal coordinates. They involve changes in bond distances, angles between chemical bonds and dihedral angles in torsional movements. These are particularly important because they provide the most physically significant set for use in describing the potential energy of the molecule. Since the kinetic energy, on the other hand, is more easily set up in cartesian displacement coordinates, a relation between the two types is therefore needed. The following treatment is covered in many standard texts (3,4,5).

$$T = \frac{1}{2} \sum_{k=1}^{3N} \frac{1}{m_k} p_k^2 \qquad (1.2.1)$$

where p_k is the momentum associated with the cartesian displacement x_k.

$$p_k = \frac{\partial T}{\partial \dot{x}_k} = m_k \dot{x}_k \qquad (1.2.2)$$

Now let p_i and $p_{t,r}$ be the momenta associated with internal and with translational and rotational motions respectively.

Hence

$$p_i = \frac{\partial T}{\partial \dot{R}_i} \quad \text{and} \quad p_{t,r} = \frac{\partial T}{\partial (\dot{tr}\,;\dot{rot})}$$

Substitution gives

$$p_k = \frac{\partial T}{\partial \dot{x}_k} = \sum_{i=1}^{3N-6} \frac{\partial T}{\partial \dot{R}_i}\frac{\partial R_i}{\partial x_k} + \sum_{t,r} \frac{\partial T}{\partial (\dot{tr};\dot{rot})}\frac{\partial (tr;rot)}{\partial x_k} \tag{1.2.3}$$

The first term relates to the internal coordinates whereas the second will be zero because the cartesian axes rotate and translate with the molecule, thus having no kinetic energy.

Hence

$$2T = \sum_k^{3N} \frac{1}{m_k}\left(\sum_i^{3N-6} p_i \frac{\partial R_i}{\partial x_k}\right)^2 \tag{1.2.4}$$

$\frac{\partial R_i}{\partial x_k}$ is abbreviated to B_{ik} and represents the transformation between internal and cartesian coordinates. In matrix form

$$R = BX \tag{1.2.5}$$

Hence

$$2T = \sum_k^{3N} \frac{1}{m_k}\left(\sum_i^{3N-6} p_i B_{ik}\right)^2$$

$$= \sum_{i,j}\left(\sum_k \frac{1}{m_k} B_{ik} B_{jk}\right) p_i p_j$$

$$= \sum_{i,j} G_{ij} p_i p_j \tag{1.2.6}$$

where

$$G_{ij} = \sum_k \frac{1}{m_k} B_{ik} B_{jk} \quad \text{or in matrix form}$$

$$G = B M^{-1} B^t \tag{1.2.7}$$

Hence $2T = P^t G P$ (1.2.8)

Using Hamilton's equation

$$\dot{R}_i = \frac{\partial T}{\partial P_i}$$

Hence substitution will give the kinetic energy in terms of the velocities.

$$2T = \dot{R}^t G^{-1} \dot{R} \tag{1.2.9}$$

As before the potential energy will be given in internal coordinates as

$$2V = \sum_{i,j} f_{ij} R_i R_j$$

or $2V = R^t F R$ (1.2.10)

Hence the Hamiltonian in internal coordinate space becomes

$$\tfrac{1}{2}\left[R^t F R + \dot{R}^t G^{-1} \dot{R}\right]\psi = E\psi \tag{1.2.11}$$

The form of the secular equation must be

$$\left| F - (G^{-1})\lambda \right| = 0$$

or multiplying from the left by G

$$\left| GF - E\lambda \right| = 0 \tag{1.2.12}$$

1.3 Symmetry and Normal Coordinates

For a large molecule the dimension of the matrix involved can be factored into a number of symmetry blocks because the normal modes form a basis for a representation of the group involved. The problem is essentially unaltered because any symmetry operation must leave the potential and kinetic energies invariant. The symmetry and internal coordinates are related by the U matrix.

$$S = UR \tag{1.3.1}$$

Since the U matrix is orthogonal, $U^{-1} = U^t$.

Substituting for R in the expressions for T and V

$$R = U^{-1}S = U^tS$$

Hence $$2T = (U^t\dot{S})^tG^{-1}(U^t\dot{S})$$

$$= \dot{S}^t U G^{-1} U^t \dot{S}$$

$$= \dot{S}^t G_s^{-1} \dot{S} \tag{1.3.2}$$

where G_s represents the symmeterised G matrix.

Similarly

$$2V = (U^tS)^tF(U^tS)$$

$$= S^tU F U^t S$$

$$= S^t F_s S \tag{1.3.3}$$

and F_s $(=U F U^t)$ is the symmeterised F matrix.

The U matrix is constructed manually from standard group tables (6) by means of the Wigner operator. The rule for non-degenerate coordinates is

$$S^{(\gamma)} = N \sum_T \chi^{(\gamma)}_T \, {}_T R_1 \qquad (1.3.4)$$

where γ refers to a species (irreducible representation), N is the normalising constant and χ_T is the character for operation T of that species. The rule has to be modified for degenerate species but can usually be formulated using a linear combination of internal coordinates.

The solution of the Lagrange equation in mass-weighted or internal coordinates is complicated by the presence of the cross-terms in the secular equation. It is therefore necessary to construct a particular coordinate system composed of 3N-6 parameters that gives both the kinetic and potential energy expressions in a diagonal form. This is done by the introduction of normal coordinates (Q).

Then

$$2T = \sum_i^{3N-6} \dot{Q}_i^{\,2} = \dot{Q}^t \dot{Q} \qquad (1.3.5)$$

and

$$2V = \sum_i Q_i^{\,2} = Q^T \lambda Q \qquad (1.3.6)$$

λ being a diagonal matrix.

The secular equation is now

$$|\lambda - \lambda E| = 0 \qquad (1.3.7)$$

The transformation involved between other sets of coordinates is given by the L matrix.

$$R = L_R Q \text{ or } S = L_S Q \qquad (1.3.8)$$

The solution of equation is

$$Q_k = Q_k^{\,o} \sin(\lambda_k^{\frac{1}{2}} t + \delta_k) \qquad (k=1, \ldots 3N-6) \qquad (1.3.9)$$

Because there is a linear relationship between normal coordinates and mass-weighted cartesians each q_i will be given by a similar expression

$$q_{ik} = q_{ik}^{\,o} \sin(\lambda_k^{\frac{1}{2}} t + \delta_k) \quad (i=1, \ldots 3N) \qquad (1.3.10)$$

Hence in each normal coordinate every cartesian oscillates with the same frequency ν_k and the same phase δ_k but in general the amplitudes will be different.

Substituting for S

$$2T = \dot{S}^t G_s^{-1} \dot{S} = \dot{Q}^t \dot{Q}$$

$$= (L_s \dot{Q})^t G_s^{-1} (L_s \dot{Q})$$

$$= \dot{Q}^t (L_s^{\,t} G_s^{-1} L_s) \dot{Q}$$

$$2V = S^t F_s S = Q^t \lambda Q$$

$$= (L_s Q)^t F_s (L_s Q)$$

$$= Q^t (L_s^{\,t} F_s L_s) Q$$

Comparing these equations it follows that

$$\lambda = L_s^{\,t} F_s L_s \qquad (1.3.11)$$

and $\quad L_s^{\,t} G_s^{-1} L_s = E$

or $\quad G_s = L_s L_s^{\,t} \qquad (1.3.12)$

These two equations combined give

$$G_s F_s L_s = L_s \lambda$$

or $\quad (G_s F_s - \lambda E) L_s = 0 \qquad (1.3.13)$

1.4 Methods of Constructing the G matrix

By far the most convenient method of constructing G matrix elements is the Wilson s vector technique. The s vector for each atom comprising a certain type of internal coordinate, is defined such that it lies in the direction which will produce the largest distortion in the internal coordinate and it is of a magnitude equal to the distortion produced in the internal coordinate by a unit displacement in this most effective direction. The unit displacement is assumed to be infinitesimally small.

$$s_{ij} = \frac{\partial R_i}{\partial x_j} \qquad \begin{array}{l} i = 1, \ldots 3N-6 \\ j = 1, \ldots 3N \end{array}$$

But $$G_{ij} = \sum_{k=1}^{3N} \frac{\partial R_i}{\partial x_k} \cdot \frac{\partial R_j}{\partial x_k} \cdot \frac{1}{m_k}$$

$$= \sum_{k=1}^{3N} s_{ik} \cdot s_{jk} \mu_k$$

There are six types of internal deformation used to describe the molecular distortions.

(a) <u>Bond stretching</u> (R)

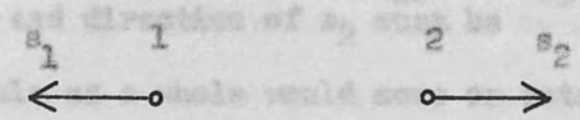

The most effective way of accomplishing a bond stretch between atoms 1 and 2 is by constructing s_1 and s_2 as shown in the above figure.

Hence $$G(r_{12}^2) = \frac{e_{21} \cdot e_{21}}{m_1} + \frac{e_{12} \cdot e_{12}}{m_2}$$

$$= \frac{1}{m_1} + \frac{1}{m_2} = (\mu_1 + \mu_2)$$

Considering an interaction term between two stretches r_{12} and r_{23} the only contribution comes from atom 2.

$$G(r_{12}, r_{23}) = \frac{e_{12} \cdot e_{23}}{m_2} = \mu_2 \cos\theta$$

where θ is the interbond angle.

(b) <u>Angle bending</u> (α)

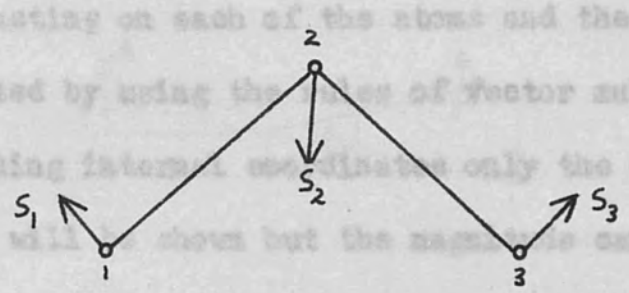

To produce a unit displacement in angle the vectors s_1 and s_3 will have a magnitude $\frac{1}{r_{12}}$ and $\frac{1}{r_{23}}$ respectively. The magnitude and direction of s_2 must be $-s_1 - s_3$ otherwise the molecule as a whole would move or rotate.

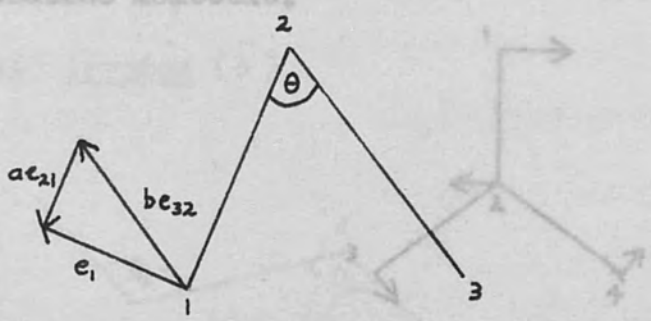

Let e_{32} and e_{21} be the unit vectors along the two bonds, and e_1, a unit vector perpendicular to r_{12}.

Then $\quad e_1 = a\, e_{21} + b\, e_{32} \quad$ where a and b are some constants.

Since $\cos\theta = \frac{a}{b}$ and $\sin\theta = \frac{1}{b}$

$$e_1 = \frac{e_{21}\cos\theta}{\sin\theta} + e_{32}$$

Hence $$s_1 = \frac{\cos\theta\, e_{21} - e_{23}}{r_{12}\sin\theta}$$

Similarly s_3 can be calculated, and then s_2 from the above relationship.

Hence in general any internal coordinate can be represented by s vectors acting on each of the atoms and the B matrix element computed by using the rules of vector multiplication. For the remaining internal coordinates only the direction of the s vectors will be shown but the magnitude can be found from the appropriate text.

(c) <u>In-plane wag</u> (β)

We usually consider the special case where the four atoms of the internal coordinate lie in the same plane, as in the benzene molecule.

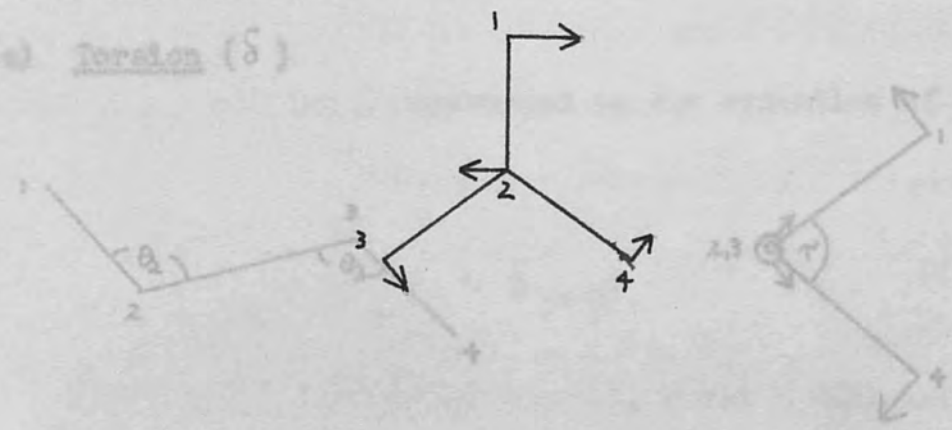

It is essentially represented as the summation of two angle bending coordinates. In the above figure $\beta \equiv (\alpha_{123} - \alpha_{124})$. It is defined to be positive when atom 1 is moving in an anti-clockwise direction (opposite to that shown in the figure).

The three following internal coordinates are out-of-plane internal coordinates because the s vectors are directed perpendicular to the plane containing the associated atoms.

(d) Out-of-plane wag (γ)

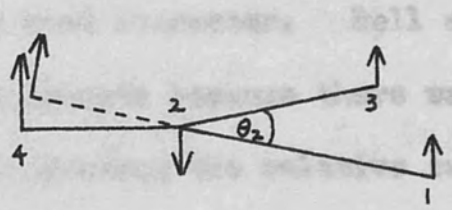

The out-of-plane s vectors are formed from the unit vectors by means of the vector product rule, i.e. $\frac{(e_{12} \wedge e_{23})}{\sin \theta_2}$ is a unit vector perpendicular to the plane (1,2,3).

(e) Torsion (δ)

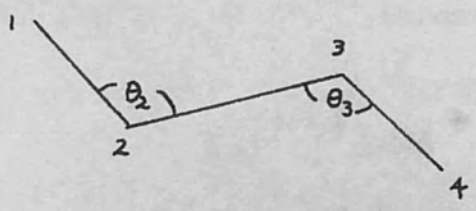

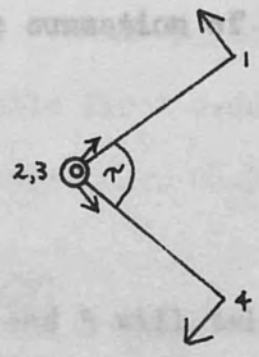

(f) Special torsion (ϕ)

Bell introduced a new internal coordinate to improve on Wilson's Valence Force field (V.F.F.) for the out-of-plane vibrations of benzene. The major objection to the torsional force constant involved was its magnitude being three times as

great as that of ethylene, when the benzenoid C-C bond has only partial double bond character. Bell suggested that the δ-coordinate was inadequate because there was no physical justification for neglecting the relative twist of associated C-H bonds, especially when lighter hydrogen atoms will usually have greater displacements.

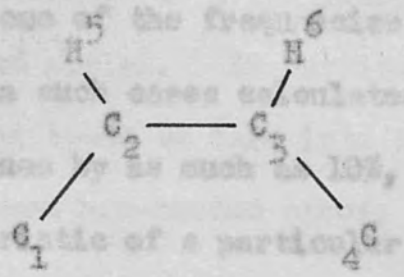

Hence the ϕ torsion is expressed as the summation of two δ-torsions

$$\phi_{2,3} = (\delta_{1234} + \delta_{5236})$$

The plane described by atoms 1, 2 and 5 will twist with respect to the plane 4, 3 and 6 about the joining C-C bond.

1.5 Types of Force Field

(i) Valence Force Field (V.F.F.)

This form of the potential function is the simplest known because it consists of diagonal F matrix elements only.

Interaction constants are neglected. Hence for a simple molecule the potential energy will take the form

$$2V = \sum_i f_{ii} (\Delta r_i)^2 + \quad f_{jj} (r\Delta\alpha_j)^2$$

The number of force constants is usually less then the number of frequencies so that the force constants can be calculated from some of the frequencies and the others used for checking. In such cases calculated frequencies may deviate from observed values by as much as 10%, and force constants are very characteristic of a particular kind of bond, e.g. a C=C double bond would have a force constant of about 9.7 mdynes/Å regardless of environment. When applied to linear XY_2 molecules the VFF becomes a reasonable first order approximation except for conjugated bond systems (e.g. CO_2)

(ii) <u>General Quadratic Force Field (GQFF)</u>

In its absolute form all the elements $\frac{\partial^2 V}{\partial R_i \partial R_j}$ are included and the number of terms involved increases approximately as the square of the dimension ($= \frac{1}{2} n(n+1)$ since F is symmetric). This obviously introduces far more parameters than observables, and only in a few simple cases has the complete GQFF been derived. In practice, however, all the remote interaction terms are reduced to zero and some interaction constants can be identified to be

zero from their transformational properties under symmetry operations. For example, any interaction term involving the β-internal coordinate (which is converted to $-\beta$ under σ_v) and any second coordinate which is transformed into itself, must be identically zero.

(iii) Urey-Bradley Force Field (UBFF)

This field consists of a VFF plus terms involving forces between non-bonded nuclei. In physical terms, this sort of potential function seeks to take into account the van der Waals forces between non-bonded atoms. The potential energy has the form

$$V = (\text{VFF terms}) + \sum_i \left(\tfrac{1}{2}F_i(\Delta q_i)^2 + F_i^{\,1} q_i(\Delta q_i)\right)$$

$$+ \sum_i k_i^{\,1} r_i (\Delta r_i) + \sum_i H^{\,1} r^{\,2} (\Delta \alpha_i)$$

where q is the distance between a non-bonded pair of atoms. In this case the linear terms are not necessarily zero because r, α and q are not independent.

The conditions for a potential minimum near the equilibrium positions are now of the form

$$\frac{\partial V}{\partial(\Delta r_i)} = r_i k_i^{\,1} + q_i F_i^{\,1} \frac{\partial q}{\partial r} = 0$$

When the expansion is worked out, the relationship between the force constant of the GQFF and the UBFF of a simple molecule

can be compared. If it is assumed that the repulsive energy between non-bonded atoms is proportional to r^{-9}, F^1 is taken to be $-\frac{1}{10}F$.

The UBFF has achieved popularity simply because of the difficulty in assigning physical meaning to many off-diagonal VFF constants in terms of molecule structure. Shimanouchi (8) and his coworkers derived values of the non-bonded interaction constants between the halogen atoms of CCl_4 and CBr_4 and found them very close to the isoelectronic systems argon-argon and krypton-krypton, at the same internuclear distances.

Since the UBFF is a specific case of the GQFF one should have no doubts in deciding which one is better. Whenever the UBFF fails to work for a molecule, one can automatically assume that other interaction constants, between non-adjacent coordinates, play an important role in the F matrix. A well known example of the failure of the UBFF to reproduce all the observed frequencies is that of ethylene. Later, however, Overend and Scherer (9) showed that the introduction of a trans-bending-bending interaction constant was sufficient to put the modified Urey-Bradley force field (MUBFF) to work. For all aromatic systems the basic UBFF fails to reproduce the observed spectrum correctly, the error being concentrated in those ring modes which correspond to the famous B_{2} ring vibration of

benzene. For this molecule Overend and Scherer (10) suggested an elegant way of introducing into the force field the ortho, meta and para stretch-stretch interactions condensed into a single term, the so-called Kekule constant. This MUBFF works correctly and was later transferred with success to naphthalene and anthracene.

(iv) Mill's Hybrid Orbital Force Field

Several people have tried to correlate the signs of interaction constants, with the change in electronic charge movements accompanying nuclear distortion. Heath and Linnett (11) argued that changes in sp hybridisation with vibration could account for the interaction constants of water and heavy water. Thus for pure p bond character the oxygen atom would be expected to form two bonds at right angles, whereas complete sp^3 hybridisation would lead to shorter O-H bonds forming a tetrahedral angle. Considering the α internal coordinate, the molecule will tend to contract stiffening the OH bonds and hence giving a positive sign for $F_{r\alpha}$. Likewise an extension of either OH bond would increase the p character of both bonds, i.e. increase the extension of the other bond producing a decrease in the potential energy. F_{rr} will therefore be negative as observed. Similarly a C-H stretch in a benzene nucleus will be accompanied by an increase in the associated C-C-C angle.

In this way many stretch-bend interaction constants have been shown to be negative, e.g. C=O and HCH of formaldehyde, C=C and HCH of ethylene.

Mills succeeded in formulating these qualitative arguments on quantitative grounds by introducing the hybridisation parameter λ. When applied to the simple system of methyl halides the interaction constants were derived as products of the diagonal constants and the derivative of the internal coordinate concurred with respect to λ. Detailed force constant calculations confirmed the predicted signs of these terms $\left(\frac{\partial r}{\partial \lambda}\right)$ CH or CX as positive, consistent with the assumption that p character increases with bond length. Duinker (12) used the HOFF treatment in deriving his in-plane force field for benzene.

(v) Compliance Constants

"Inverse" force constants (i.e. elements of F^{-1}) have certain properties which make the solution of the vibrational problem in the form $|F^{-1} G^{-1} - \lambda^{-1} E| = 0$ more convenient. Decius(13) points out that additional sources of information, in particular mean amplitudes of vibration from electron diffraction (r^2) and centrifugal distortion constants from microwave spectroscopy both involve compliance constants in a more direct and natural way. The most important property, however, lies in their invariance in different sets

of coordinates. This was most aptly illustrated by and Slater (14) using the force constants derived from $^{14}NO_2$ and $^{15}NO_2$ for two sets of internal coordinates.

1.6 Solution of the Secular Matrix

When the G matrix has been calculated from the B matrix and the form of F matrix decided, it is required to solve

$$(G_s F_s - \lambda_s E) L_s = 0 \qquad (1.6.1)$$

This is done by calculating the eigen vectors (D) and eigen values (Γ) of the symmeterised G matrix

$$G_s D_s = D_s \Gamma_s \qquad (1.6.2)$$

The eigen vectors are normalised such that $D_s D_s^{\,t} = E$. Γ_s is a diagonal matrix containing the eigen values whose corresponding eigen vectors are given by the columns of D.

A matrix $\bar{D}_s$ is then formed by

$$\bar{D}_s = D_s \Gamma_s^{\frac{1}{2}} \qquad (1.6.3)$$

It is easily shown that

$$\bar{D}_s \bar{D}_s^{\,t} = G_s \qquad (1.6.4)$$

Multiplying (1.6.2) from the right by $D_s^{\,t}$

$$G_s D_s D_s^{\,t} = D_s \Gamma_s D_s^{\,t}$$

$$\therefore \quad G_s = D_s \Gamma_s D_s^{\,t}$$

$$= (D_s \Gamma_s^{\frac{1}{2}})(D_s \Gamma_s^{\frac{1}{2}})^t$$

$$= \underline{\bar{D}_s \bar{D}_s^{\,t}} \qquad \text{(Q.E.D.)}$$

A matrix $\bar{D}_s^{\,t} F_s \bar{D}_s$ is then formed whose eigen vectors are Y_s and eigen values Λ_s.

i.e. $$(\bar{D}_s^{\,t} F_s \bar{D}_s) Y_s = Y_s \Lambda_s \qquad (1.6.5)$$

Multiplying from the left by $\bar{D}_s$

$$\bar{D}_s \bar{D}_s^{\,t} F_s \bar{D}_s Y_s = \bar{D}_s Y_s \Lambda_s$$

It then follows from (1.6.4) that

$$G_s F_s (\bar{D}_s Y_s) = (\bar{D}_s Y_s) \Lambda_s \qquad (1.6.6)$$

Hence comparison of the two equations (1.6.1) and (1.6.6) gives

$$L_s \equiv \bar{D}_s Y_s \quad \text{and} \quad \lambda_s \equiv \Lambda_s$$

The units of G and F will influence the units of λ_s and hence the appropriate factors are introduced.

From (1.1.18) the eigen values λ_k are related to the frequencies in Hz by

$$\lambda_k = 4\pi^2 \nu_k^{\,2}$$

Using c.g.s. units λ_k will have the dimensions of CF, i.e.

amu^{-1} dyne cm^{-1} $10^5 \equiv amu^{-1}$ gm sec^{-2}

But $\quad 1 \text{ amu} = \frac{1}{N_o} \text{ gms}$

Hence $\quad N_o \lambda_k = 4\pi^2 (c\bar{\nu}_k)^2 \quad$ where c is the velocity of light and $\bar{\nu}$ the wave number (cm^{-1}).

Hence $\quad \lambda_k = \frac{4^2 c^2}{N_o} \bar{\nu}_k^{\,2}$

or $\quad \bar{\nu}_k = 1307.1 \lambda_k^{\frac{1}{2}} \qquad (1.6.7)$

L will have units of $(amu)^{-\frac{1}{2}}$ and Q $(amu)^{+\frac{1}{2}}$ Å.

If the secular equation is solved in symmetry coordinates some of the eigen values for certain symmetry species will take on a value of zero. These are known as the redundant roots and occur when there are more symmetry coordinates than normal coordinates. Their presence implies that at least of the deformation coordinates are dependent on one another. In simple cases the redundancy condition can easily be spotted, e.g. in benzene A_{1g} species.

$$\sum_{i=1}^{1g} \alpha_i = 0$$

Redundant coordinates must be eliminated if the secular equation is set up in the form $|F - G^{-1}\lambda| = 0$, because now G is singular and has no inverse.

1.7 Cartesian Displacement Representation (CD)

Once the secular equation has been solved it is often convenient to transform the normal coordinates back into their cartesian representation so as to vectorially represent the motions of the individual atoms during the normal vibration.

Let A be the transformation between cartesian and internal coordinates such that

$$X = A\,R \qquad (1.7.1)$$

Because $R = B\,X$ $\qquad A\,B = E = B\,A$

From (1.2.7)

$$G_R = BM^{-1}\,B^t$$

Postmultiplying by A

$$A\,G_R = ABM^{-1}\,B^t$$

$$\therefore \qquad A\,G_R = M^{-1}\,B^t$$

Premultiplying by G_R^{-1}

$$A = M^{-1}\,B^t\,G_R^{-1} \qquad (1.7.2)$$

Therefore

$$X = (M^{-1}\,B^t\,G_R^{-1})R \qquad (1.7.3)$$

From (1.3.1) $S = UR$

Hence $\quad X = (M^{-1} B^t G_R^{-1} U^t) S \qquad (1.7.4)$

From (1.3.8) $S = L_s Q$

Hence $\quad X = (M^{-1} B^t G_R^{-1} U^t L_s) Q \qquad (1.7.5)$

From above

$$G_s = U G_R U^t$$

Hence premultiplying by U^t and postmultiplying by U

$$U^t G_s U = G_R$$

Hence $\quad (G_R)^{-1} = (U^t G_s U)^{-1}$

$$= U^t G_s^{-1} U$$

Substituting in (1.7.5) gives

$$X = (M^{-1} B^t U^t G_s^{-1} L_s) Q \qquad (1.7.6)$$

From $\quad L_s L_s^t = G_s \quad$ and therefore

$$X = (M^{-1} B^t U^t (L_s^t)^{-1}) Q \qquad (1.7.7)$$

Both equations (1.7.6) and (1.7.7) involve the inverse of a matrix which may or may not contain one or more redundancies for a certain symmetry block. If this is the case no inverse will exist because the matrix is singular.

Gussoni and Zerbi (15) introduced a set of symmetry coordinates derived from the eigen vectors of the G matrix

$$\xi = D_R^t R \qquad (1.7.8)$$

The new sigma coordinates form a completely reduced representation of the symmetry point group to which the molecule belongs and are therefore symmetry coordinates themselves. It may be pointed out that the Σ coordinates are closer to the normal coordinates than the Wigner type and could be called quasi-normal coordinates since they reduce the kinetic energy to diagonal form.

The Σ coordinates can be placed in symmetry block form as

$$\Sigma = D_s^{\,t}\, S \qquad (1.7.9)$$

Any redundancy now present can be removed by omitting the column of zeros in D_s corresponding to the zero root in Γ_s.

It is now required to find an expression for $(L_s^{\,t})^{-1}$ in equation (1.7.7).

From $\quad L_s = \bar{D}_s\, Y_s$

Hence $\quad L_s^{\,t} = Y_s^{\,t}\, \bar{D}_s^{\,t}$

Therefore

$$(L_s^{\,t})^{-1} = \left[Y^{\,t}(D\,\Gamma^{\frac{1}{2}})^{t}\right]^{-1} \qquad (1.7.10)$$

(where D is the reduced D_s matrix and Γ the reduced Γ_s matrix.)

$$= \left[Y^{-1}(\Gamma^{\frac{1}{2}}\, D^{t})\right]^{-1}$$

$$= (D^{t})^{-1}\Gamma^{-\frac{1}{2}}\, Y$$

Hence $\quad (L_s^{\,t})^{-1} = D\,\Gamma^{-\frac{1}{2}}\, Y$

and

$$X = (M^{-1}\, B^{t}\, U^{t}\, D\,\Gamma^{-\frac{1}{2}}\, Y)Q \qquad (1.7.11)$$

Q can be regarded as defining the scale of the distortions and is in effect a normalising constant. An absolute value is assigned by utilising the expression for the root mean square displacement for a harmonic oscillator in one dimension

$$\left(\frac{h(v+\frac{1}{2})}{4\pi^2\nu_i}\right)^{\frac{1}{2}} \qquad (1.7.12)$$

Fundamental vibrations involve the transition in the vibrational energy levels from $v = 0 \rightarrow v = 1$ where v is the vibrational quantum number. Defining the increase in mean square amplitude in the $0 \rightarrow 1$ transition by $(\bar{Q}_i^{\,2})^{\frac{1}{2}}$ we have

$$(\bar{Q}_i^{\,2})^{\frac{1}{2}} = \frac{h}{4\pi^2\nu_i} \qquad (1.7.13)$$

In reality, however, not all molecules are in the ground state at room temperature and a correction factor of $\frac{1}{2}\coth\frac{h\nu}{2kT}$ allows for the population of excited states.

1.8 Potential Energy Distribution (PED)

The solution of the vibrational problem for a particular normal mode k is

$$GF\ell_k = \lambda_k \ell_k$$

From $\quad R = L_R Q$

and the relation between the internal coordinates and the normal coordinates will therefore be

$$R_1 = l_{11} Q_1 + l_{12} Q_2 \quad \cdots\cdots \quad l_{1k} Q_k$$

$$\vdots$$

$$R_i = l_{i1} Q_1 + l_{i2} Q_2 \quad \cdots\cdots \quad l_{ik} Q_k$$

Hence for mode k the relative ratio of the amplitudes of the internal coordinates will be

$$l_{1k} : l_{2k} \cdots : l_{ik}$$

If one of these elements is relatively large compared with others, the normal mode is said to be predominantly due to the vibration caused by the change of this internal coordinate.

Morino and Kuchitsu (17) have shown that the PED in each internal coordinate gives a better measure of the band assignments than the simple ratio of elements.

Since $2V = Q^t \lambda Q$ and $\lambda = L^t F L$

the potential energy of the whole molecule for mode Q_k is expressed as

$$2V = Q_k^{\,2} \sum_{ij} F_{ij} L_{ik} L_{jk} \qquad (1.8.1)$$

Since, in general, the summation terms are large when $i = j$, only the $F_{ii} L_{ik}^2$ terms are significant. Thus the ratios of such terms provide a reasonable measure of the relative contribution of each internal coordinate to the normal mode, and if any one term is relatively large compared to the rest the normal mode can be assigned to that particular internal coordinate.

1.9 Computational Solution

The most prominent work for computerising the vibrational problem with or without iterative techniques was due to Snyder and Schachtschneider (16). The essential logic is outlined in Fig. I(i). Diagonalisation of the appropriate matrices is carried using a subroutine EA03A from the University of London Computer Centre. This subroutine involves Jacobi's method where the off-diagonal elements are progressively reduced to zero and the transformations involved are then applied to a unit matrix to give the eigen vectors.

Begin

Cycle No. of molecules

Read No. of atoms - Natoms
Read cartesian co-ords of nuclei - X
Read No. of int. co-ords - NR
Read masses in amu - AMASS

Cycle NR

Read counter for coordinate deformation

R	α	γ	δ	β	ϕ
1	2	3	4	5	6

Read numbers of nuclei involved in deformation

Form $\bar{e}$ vectors between bonded nuclei

Form $\bar{s}$ vectors for each atoms

Compile B matrix row with consistent dimensions

Form $G = BM^{-1} B^t$

Read F (mdyne/Å)

Read No. of symmetry blocks - NSYMB

Cycle NSYMB

Read U matrix

Form G_s and F_s

Form D and Γ from EAO3A

Eliminate redundancies

Form $\bar{D}^t F \bar{D}$

Form Y and Λ from EAO3A

$L = \bar{D} Y$

Output $\bar{\nu} = 1303 \lambda^{\frac{1}{2}}$ and L

Cartesian displacements

End

Fig. I(i) Flow diagram of Program 'LINDA' in Appendix 1.

CHAPTER 2

The Vibrational Analysis of Biphenyl

2.1 Introduction

Many of the earlier studies on the vibrational spectra of biphenyl (18-21) left many of the assignments in considerable doubt. Recent work of Pascuier and Lebas (22) gives a fairly complete assignment based on purely qualitative reasoning and normal coordinate calculations for the in-plane vibrations of the planar molecule by Zerbi and Sandroni (23,24) give reasonably good predictions. It has therefore been an embarrassing fact that despite so many studies, convincing evidence of spectral changes accompanying change of state has been lacking. This has partly been due to the fact that both the low-frequency infrared and Raman spectra in different physical states had been either inadequately determined or obscured by solvent bands.

Many physical techniques have been used to determine the conformation of biphenyl in different physical states. Early work on the X-ray crystallographic study of crystalline biphenyl by Dhar (25) suggested that the molecule was planar within the limits of experimental error and the inter ring C-C bond length

was 1.48 Å. More recent work by Trotter (26) revises this distance to 1.506 Å. The interpretation of the 247 nm "conjugation band" in the ultraviolet spectrum in solution is still uncertain but present views are based on the assumption that change in conformation will alter the $\pi - \pi$ interaction thus affecting the position and intensity of the transition. The high-resolution N.M.R. spectra in the molten and solution states of some poly-phenyls (27) give results which are inconclusive for biphenyl but which indicate that m-terphenyl is non-planar. Electron spin resonance spectra (28) of the biphenyl radical are interpreted in terms of a molecule with a dihedral angle of 38°. Unquestionable evidence of the existence of a twisted structure in the vapour phase (29) comes from electron diffraction work, the angle obtained being 45 ± 10°. U.V. spectra (30) suggest that the deviation from planarity should be larger in the vapour state than the solution state value of 20-25°.

2.2 Experimental

The biphenyl used in all spectroscopic studies was purchased from B.D.H. Ltd. and used without further purification. All the near infrared spectra were recorded with a Perkin-Elmer 325 grating spectrophotometer. The solid state spectra were run either as a potassium bromide disc or as a solidified melt. This was obtained by allowing crystalline biphenyl to melt on

a warm KBr plate and then leaving to cool very slowly. The solution spectra were recorded using solvents with negligible absorption over particular ranges, i.e. 400 cm^{-1} to 1000 cm^{-1} with spectroscopic carbon disulphide and 1000 cm^{-1} to 1700 cm^{-1} with spectroscopic carbon tetrachloride. All the far-infrared spectra were recorded on a R.I.I.C. FS 720 Michelson interferometer using a 25gauge beam-splitter to accommodate the 40-400 cm^{-1} spectral range. The solid samples were recorded at liquid nitrogen temperature to prevent evaporation of biphenyl under vacuum. The solution spectra were run in either benzene or cyclohexane, both solvents having very small absorption in the far infra red. The polythene cells were made and sealed using apparatus designed in this Department (31).

The Raman spectra were recorded with either a Cary 81 (180° scattering and He/Ne 6328 Å exciting line) at Imperial College or a Spex Ramalog (90° scattering and Ar^+ 5147 Å exciting line) at University College. ~~Molten~~ Raman spectra of melts were taken in a specially-designed, glass heating finger and the gas-phase spectra using facilities at Southampton University. The principle bands of biphenyl are listed in Table II (1) and spectra below 1000 cm^{-1} are shown in Fig. II (i).

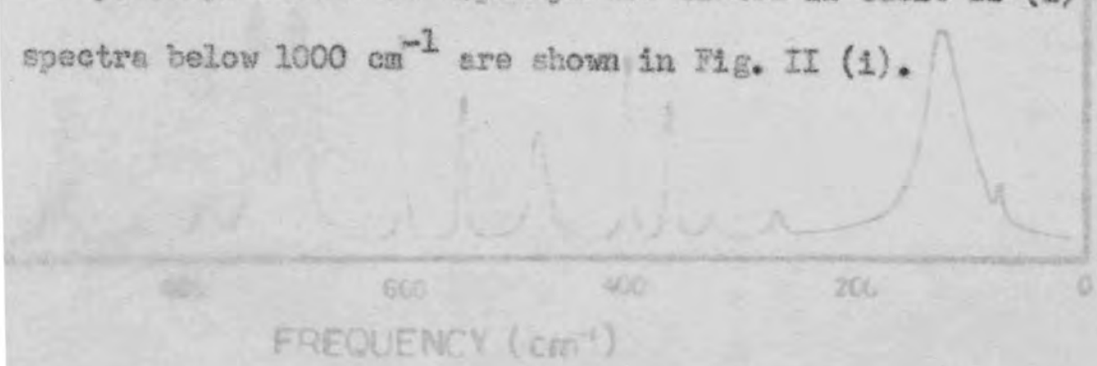

FIG (II) i

BIPHENYL

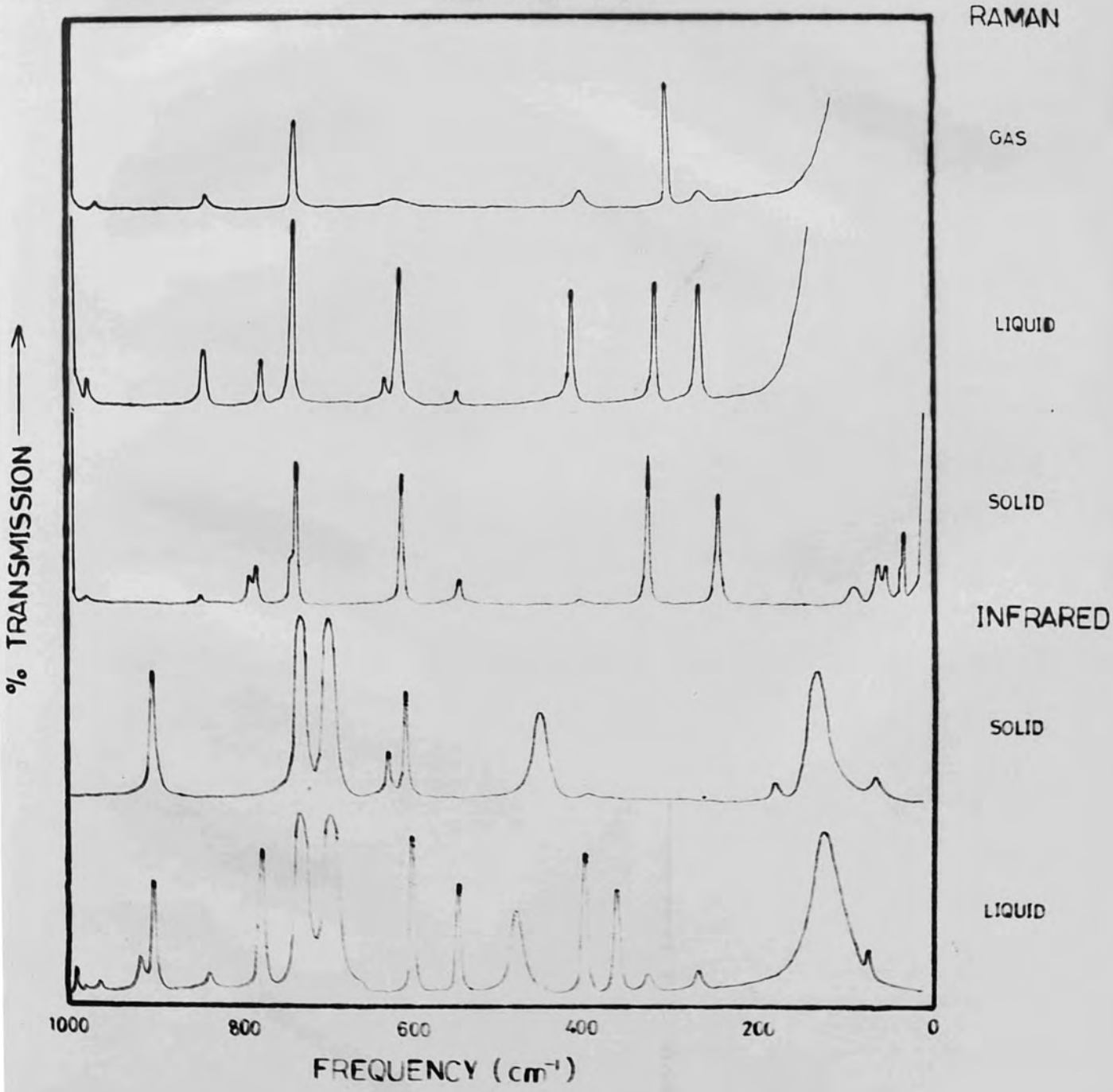

Calculations were carried out using magnetic tape facilities on the London University CDC 6600 with programmes written in Fortran IV. The aromatic rings were assumed to be regular hexagons and the bond lengths were taken as $R_{CC} = 1.40$ Å; $R_{1-7} = 1.48$ Å and $r_{CH} = 1.084$ Å. The in-plane force field was transferred from the field of Duinker and Mills (12) for benzene and the out-of-plane force field was transferred from a study on the out-of-plane vibrations of some halogenated benzenes (32). The inter-ring stretching force constant was assumed to be 4.9 mdynes/Å - a value chosen on the basis of a simple force constant-bond length relationship for C-C bonds. No inter-ring force constants were introduced because of the uncertainty concerning any resonance interactions. Since no data was available to describe the in-plane and out-of-plane wags for a carbon substituent on a ring, it was assumed that the energy required to produce unit angular deformation was independent of substituent. A list of force constants used is shown in Table II (2). The symmetry coordinates were compiled to represent the D_2 point group and are given in Appendix (1).

In the calculations below only 59 normal modes are computed, the missing fundamental being attributed to the lowest a_u mode, namely the "butterfly" mode. This deformation was omitted on account of the uncertainty concerning the nature of the torsion in solution, i.e. whether the torsion occurs about a fixed

Table II(1)

The Principle Infrared and Raman bands of Biphenyl at Frequencies below 1700 cm^{-1}

Infrared		Raman			Assignment
Solid	Liquid	Solid	Liquid	Gas	
1690w	1683w				
1650w	1655w				
		1620sh			
1617w	1612w				
		1610vs	1612vs	1613vs	a_g
1597s	1595s				b_{3u}
		1592vs	1595s	1596vs	b_{1g}
1568s	1567s				b_{2u}
		1513m	1509m (0.27)	1505w	a_g
1480vs	1481s				b_{3u}
	1455m	1462w	1462w		b_{1g}
1428vs	1430s				b_{2u}
1380w	1381m				
1344m	1337m				b_{2u}
	1317w	1333w			b_{1g}
1307w	1300w				
1280w	1280w				
		1276vs	1285vs (0.18)	1282vs	a_g
1268w	1266m				b_{2u}
	1242w	1265shw	1249m	1233w	b_{1g}
		1208w	1192m(br) (0.18)		a_g

Table II(1) (continued)

Infrared		Raman			Assignment
Solid	Liquid	Solid	Liquid	Gas	
1181m	1174w				b_{3u}
		1165m) 1149m)	1158m (0.81)		b_{1g}
1169s)) 1154w)	1155m				b_{2u}
1110m	1107w				
		1097w	1094w		b_{1g}
1090s)) 1075m)	1072s				b_{2u}
1041s	1042s				b_{3u}
		1036s	1031s (0.06)	1029m	a_g
1006s	1007s				b_{3u}
		1002vs	1004vs (0.09)	1003vs	a_g
985w	990w				b_{3u}
	979vw	978w			b_{2g}
968w					b_{1u}
	964vw		967m (0.29)	964w	a_u/b_{3g}
	917m				b_{2g}
902s	902s				b_{1u}

Table II(1) (continued)

Infrared		Raman			Assignment
Solid	Liquid	Solid	Liquid	Gas	
	838m	846w	841m (0.33)	838w	a_u/b_{3g}
	778s	790) 783) d-m	782m		b_{2g}
		743sh) 739)m	741vs (0.08)	740s	a_g
729vs	735vs				b_{1u}
695vs	697vs				b_{1u}
626w			626w		b_{2u}
610m	609s				b_{3u}
		610m	614m (0.75)	615w	b_{1g}
-	543s	546w	546w		b_{2g}
458s	486s				b_{1u}
-	403s	409vw	410m (0.56)	405m	a_u/b_{3g}
-	367m				b_{1g}
-	315w	329m	316m (0.18)	307s	a_g
-	269m	251m	269m (0.88)	265w	b_{2g}
174w					
118vs	112vs				b_{2u}
		89m			
73w	77w				b_{1u}
		52m			)
		41m			)Lattice
		22m			)modes

dihedral angle if the vibration becomes a rotational degree of freedom. This approximation can be justified because the lowness of the frequency results in little mixing with other normal coordinates. It is very common experience that these torsions factor out as a lone vibration.

2.3 Theoretical Predictions

The sixty normal modes of biphenyl form a basis for a representation of either the D_{2h} (dihedral angle $\theta = 0^{o}$), the D_2 ($0^{o} < \theta < 90^{o}$), or the D_{2d} ($\theta = 90^{o}$) point groups depending on its conformation. The representations, together with the corresponding activities and correlations are listed in Table II(3). It can be seen that as the centre of symmetry is lost the symmetry classes of the D_{2h} group coalesce in pairs. This means that, provided the in-plane and out-of-plane wave-functions mix, the modes in each pair will push one another apart and a relaxation of the spectral activities will result. Perturbations in the eigen values and eigen vectors on change of conformation can be expected from the following phenomena.

(i) Steric interactions

The normal modes which are most affected by possible steric interactions between the ortho hydrogens can be picked out from the cartesian displacement calculations. The Van

Table II(2)

The quadratic force constants used in calculating the frequencies of the systems $XC_6H_4.C_6H_4X$. Interaction constants are shown in parentheses. The units are mdynes $Å^{-1}$ for stretching constants, mdynes rad^{-1} for stretch-bend interactions and mdynes Å rad^{-2} for bending constants.

Force constant no.	Force constant for coordinate	X=H	=F	=Cl	=Br
1	r_i^2 (H)	5.125	5.125	5.125	5.125
2	r_i^2 (X)	-	5.80	3.70	3.12
3	β_i^2 (H)	1.035	1.012	1.028	1.036
4	β_i^2 (X)	-	1.741	1.656	1.117
5	R_i^2	7.015	6.97	6.87	6.95
6	β^2 (C)	1.035	1.012	1.028	1.036
7	R^2 (C)	4.9	4.9	4.9	4.9
8	α_i^2 (H)	1.103	1.070	1.213	1.149
9	α_i^2 (X)	-	1.394	1.405	1.207
10	(R_i, R_{i+1})	0.531	0.526	0.480	0.558
	$= -m = p$	-	-0.0056	0.0013	0.0160
11	(R_i, β_i)	0.364	0.347	0.379	0.414
12	$(R_i, \beta_i(X))$	-	0.448	0.425	0.476
13	$(r_i, \alpha_i(X))$	-	-0.637	-0.772	-0.557
14	(β_i, β_{i+1})	0.028	0.047	0.022	0.015
15	(β_i, β_{i+2})	-0.022	-0.022	-0.019	-0.008
16	(β_i, β_{i+3})	-0.032	-0.073	-0.065	-0.080
17	(α_i, α_{i+1})	-0.098	-0.096	0.000	-0.043

Table II(2) (continued)

Force constant no.	Force constant for coordinate	X=H	=F	=Cl	=Br
18	(R_i, α_i)	0.442	0.463	0.441	0.462
19	$(r_i(X), R_i)$	-	0.429	0.334	0.336
20	(β_i, α_{i+1})	0.064	0.064	0.064	0.064
21	γ_H^2	0.307	0.306	0.311	0.310
22	γ_X^2	-	0.359	0.354	0.321
23	ϕ_{HH}^2	0.0706	0.0700	0.0700	0.0700
24	ϕ_{HX}^2	-	0.0676	0.0561	0.0684
25	$(\gamma_H \gamma_H^o)$	0.0153	0.0155	0.0145	0.0155
26	$(\gamma_H \gamma_H^m)$	-0.0129	-0.0132	-0.0153	-0.0148
27	$(\gamma_H \gamma_H^p)$	-0.0141	-0.0142	-0.0135	-0.0159
28	$(\gamma_H \gamma_X^o)$	-	0.0234	0.0284	0.0281
29	$(\gamma_H \gamma_X^m)$	-	-0.0058	-0.0116	-0.0040
30	$(\gamma_H \gamma_X^p)$	-	-0.0056	0.0013	0.0160
31	$(\phi\phi_o)$	-0.0137	-0.0141	-0.0131	-0.0129
32	$(\gamma_H\phi_o)$	0.0182	0.0187	0.0190	0.0191
33	$(\gamma_X\phi_o)$		-0.0196	-0.0081	-0.0123
34	$(\gamma_X\phi_m)$		-0.0122	-0.0055	-0.0115

Table II(3)

Correlation tables and selection rules for biphenyl and its 4-4' dihalogeno substituted derivatives

D_{2h} ($\theta=0^\circ$)	D_2 ($0^\circ < \theta < 90^\circ$)	D_{2d} ($\theta=90^\circ$)
In-plane		
A_g (11, R)	A (15, R)	A_1 (11, R)
B_{1g} (10, R)		B_1 (4, R)
B_{2u} (10, 1.R)	B_1 (16, R+1.R)	E (16, 1.R+R)
B_{3u} (10, 1.R)		
Out-of-plane		
A_u (4, inactive)	B_2 (16, R+1.R)	A_2 (3, inactive)
B_{1u} (6, 1.R)	B_3 (13, R+1.R)	B_2 (10, R+1.R)
B_{2g} (6, R)		
B_{3g} (3, R)		

der Waals radius of the hydrogen atom (1.24 Å) is large compared with the equilibrium distance between the two ortho hydrogen nuclei (1.75 Å) for planar biphenyl and since the largest displacement is approximately 0.3 Å, strong repulsion should occur. In the a_g motions both pairs of ortho hydrogens are bouncing against one another and in the b_{2u} modes only one pair is colliding. Hence the a_g and b_{2u} fundamentals involving strong β deformations will be more affected than the corresponding b_{1g} and b_{3u} modes on steric relaxation. Steric repulsion could account for the increased bond length in the solid state.

(ii) Resonance interaction

It is generally assumed that the biphenyl molecule is a resonance hybrid of several canonical structures one of which involves an inter-ring double bond. Zerbi and Sandroni (23) showed that the b_{1g} and b_{2u} modes are greatly affected by the extent of π-delocalisation, and the extent of resonance could be obtained from the values of the Kekule resonance parameter (ρ) in their perturbed UBSF or by the values and signs of the C-C/C-C interactions in their GVFF for the planar conformation. The possible existence of a small contribution to the hybrid from the double-bonded structure was shown in the signs of certain inter-ring force constants, although their values were

small. To support this they repeated their calculations omitting these inter-ring force constants in the GVFF and in erting only one ρ parameter in the UBFF, only to find that a very satisfactory fit was still obtained.

A small delocalisation of π electrons across the inter-ring bond (1.51 Å) accounts for the almost normal length of a single C-C bond and the vapour phase value of 1.48 Å may imply a slightly higher bond order.

The double-bond structure will contribute even less on twisting and this would be reflected in a force constant change. When biphenyl is considered as two mono substituted benzene molecules (C_{2v} symmetry) each of the C_{2v} motions will combine into the in- and out-of-phase motions of biphenyl giving rise to a splitting of the original degenerate levels: a_1 (C_{2v}) split into a_g (in-phase) and b_{3u} (out-of-phase) parallel modes whilst b_1 modes (C_{2v}) split into b_{1g} (in-phase) and b_{2u} (out-of-phase) perpendicular modes. Zerbi showed that only the a_g vibrations were affected by the value of C-C inter-ring force constant. It will be shown from the calculations below that no interaction occurs between the a_g and a_u, nor between the b_{1g} and b_{3u} vibrations with change in geometry and hence any spectral shift must be attributed to a force constant variation.

(iii) G-matrix changes

The usual exercise in vibrational analysis is to fit the observables to the theoretical frequencies in order to improve the force field.

$$G(F + \Delta F)(L + \Delta L) = (L + \Delta L)(\lambda + \Delta \lambda)$$

The calculations in Table II below are based on the assumption that a change in the geometry of biphenyl will leave the force-field unaffected. This turns out to be a justified assumption because of the ability to reproduce the experimental spectral changes. The vibrational problem now takes the form:

$$F(G + \Delta G)(L + \Delta L) = (L + \Delta L)(\lambda + \Delta \lambda)$$

All the large frequency shifts encountered in the molecules considered below can be explained in terms of the appearance of G matrix interaction elements on twisting. Following first order perturbation theory the interaction between levels depends:

(i) on the interaction integral. If the wavefunctions are localised on the rings, then change in dihedral angle will not affect this integral.

(ii) Inversely on the difference between the energy levels. This implies that interaction will only be significant if there are similar vibrational frequencies in the species which coalesce.

The in-plane fundamentals lie between 3000 cm^{-1} to about 70 cm^{-1} whilst the out-of-plane modes occur only below 1000 cm^{-1}. Hence from (ii) it follows that perturbations will lie at low frequency within a certain species. Inter-ring coupling can only occur through deformations which span the rings near the joining C-C bond and since interaction cannot occur within the A species this excludes the C-C stretch. Other internal deformations which may lead to coupling are γ_c (out-of-plane) carbon wag external to the ring), β_c (in-plane carbon wag) and the torsions (ϕ) near the function. These predictions are fully substantiated by the calculations reported below.

The practical shifts are able to give an estimate of the dihedral angle when compared with the theoretical trends of the modes which move.

2.4 Results and Interpretation

The calculations for four dihedral angles with the corresponding assignments are tabulated for each symmetry species in Table II (4). Previous investigations have established the majority of the assignments for biphenyl beyond any reasonable doubt and reference will therefore be made to the main points of interest.

Table II (4)

Calculated and observed frequencies (cm^{-1}) for biphenyl for biphenyl for various dihedral angles. (Asterisk * denotes double assignment)

A Species (D_{2h} - A_g, A_u)

	Calculated frequencies for all θ	Observed Frequencies				
		Raman			Infrared	
		Solid	Liquid	Gas	Solid	Liquid
A_g	3073					
	3072					
	3069					
	1690	1610	1612	1613	-	-
	1527	1513	1509	1505	-	-
	1338	1276	1285	1282	-	-
	1192	1208	1192	-	-	-
	1024	1036	1031	1029	-	-
	998	1002	1004	1003	-	-
	745	739	741	740	-	-
	272	331	316	307	-	315
A_u	963	-	967	964*	-	-
	833	-	841	838*	-	-
	409	-	410	405*	-	-

Table II (4) (continued)

B_3 Species (D_{2h} - B_{3u}, B_{3g})

	Calculated frequencies for all θ	Observed Frequencies				
		Raman			Infrared	
		Solid	Liquid	Gas	Solid	Liquid
B_{3u}	3073					
	3072					
	3069					
	1610				1597	1595+
	1483				1480	1481
	1193				1181	1174
	1040				1041	1042
	1020				1006	1007
	992				985	990
	611				610	609
B_{3g}	963	-	969	964*	-	964*
	833	846	841	838*	-	838
	409	409	-	405*	-	403

Table II (4) (continued)

B_1 Species (D_{2h} - B_{1g}, B_{1u})

	Calculated frequencies for θ				Observed Frequencies				
					Raman			Infrared	
	0°	30°	60°	90°	Solid	Liquid	Gas	Solid	Liquid
B_{1g}	3070	3070	3070	3070	-	-	-	-	-
	3069	3069	3069	3069	-	-	-	-	-
	1609	1608	1606	1605	1592	1595	1596	-	1595*
	1449	1448	1443	1439	1462	1462	-	-	1455*
	1337	1336	1332	1328	1333	-	-	-	1317
	1292	1293	1294	1296	1263	1249	1233	-	1243
	1155	1155	1156	1158	1165/ 1149	1158	-	-	-
	1069	1068	1065	1062	1097	1094	-	-	-
	607	608	610	613	610	614	615	-	-
	342	326	300	275	-	-	-	-	367
B_{1u}	987	987	987	987	-	-	-	968	964*
	898	899	900	902	-	-	-	903	902
	726	728	735	746	-	-	-	729	735
	703	703	703	703	-	-	-	695	697
	431	449	479	502	-	-	-	458	486
	91	91	91	91	-	-	-	73	77

Table II (4) (continued)

B_2 Species (D_{2h} - B_{2u}, B_{2g})

	Calculated frequencies for θ =				Observed Frequencies				
					Raman			Infrared	
	0°	30°	60°	90°	Solid	Liquid	Gas	Solid	Liquid
B_{2u}	3070	3070	3070	3070					
	3069	3069	3069	3069					
	1608	1607	1605	1605				1568	1567
	1430	1431	1433	1439				1428	1430
	1326	1326	1326	1328				1344	1337
	1295	1296	1296	1296	-	-	-	1268	1266
	1161	1160	1159	1158	-	-	-	1153/ 1169	1155
	1055	1055	1058	1062	-	-	-	1075/ 1090	1075
	622	621	617	613	-	626	-	626	-
	96	95	93	91	-	-	-	118	112
B_{2g}	987	987	987	987	978	987	-	-	979
	909	908	906	902	-	-	-	-	917
	755	755	752	746	779/ 786	782	-	-	778
	694	696	699	703	-	-	-	-	670
	515	514	512	502	546	546	-	-	543
	239	244	257	275	251	269	265	-	269

A Species

The agreement between calculated and observed a_g and a_u frequencies is good except for ν_4 which is 80 cm^{-1} too high. It has been shown, however, in subsequent work (33) that the fit of the ring modes greatly improves when inter-ring interaction constants are introduced into the force field. The assignments are easily recognised by their strength in the Raman - all the bands being strongly polarised in the melt and very sharp in the gaseous phase. Shifts are observed for ν_7 and ν_{11} of 16 cm^{-1} and 15 cm^{-1} respectively going from D_{2h} to D_2. These downward shifts are consistent with a lowering of bond order. Although ν_7 is not observed in the gaseous phase, ν_{11} moves a further 9 cm^{-1} indicating that the molecule twists to a greater dihedral angle. This conclusion is consistent with the vapour-phase U.V. spectrum. From Appendix 3 giving the P.E.D. amongst the normal modes it can be seen that ν_{11} has a very large contribution from f.c.5 of 32% and f.c.8 of 29% adjacent to it. The distribution for ν_7 comes entirely from the ortho- and meta-β_{C-H} deformations. The calculated cartesian displacements illustrate the increase in steric hindrance due to these two modes. It is worth pointing out that ν_{11} can be seen in the solution far-infra-red spectrum - a direct violation of the selection rules.

The three a_u modes are absent from the solid Raman spectrum as would be predicted, and appear with moderate strength in the melt. Confusion now arises because the three b_{3g} modes are calculated at exactly the same frequencies and these are Raman active. The depolarisation ratios in the melt are greater than the a_g counterparts indicating that a double assignment is best assumed. In accord with what was said earlier the calculated a_g and a_u frequencies do not vary with dihedral angle and hence the shifts have to be explained in terms of either a force constant change or steric hindrance.

B3 Species

Zerbi (6) recorded the infra-red spectrum of a single crystal of biphenyl with linearly polarised radiation. From Table II (5) the direction cosines give the orientation of

Table II (5)

Direction cosines and dichroic ratios for crystalline biphenyl

Molecular axis	Crystal axis a	b	c	Dichroic ratio
x	0.2930	-0.0065	0.9552	
y	0.5203	-0.8375	-0.1670	0.38
z	-0.8002	0.5464	0.2472	2.15

the biphenyl molecules in the lattice with respect to the ab crystal plane. It can be seen that the component of the total dipole moment change for B_{3u} motions (which transforms as T_x) on the ab face is very small. Since the intensity of an infra-red transition is proportional to the square of this component in a given direction $I \propto \left(\frac{\partial \mu_x}{\partial Q_k}\right)^2$, the intensity of the B_{3u} fundamentals is expected to be very small when the ab cleavage is observed. The same effect was observed using biphenyl which was slowly allowed to anneal on a KBr plate. It can be clearly seen from Fig. II (ii) that the B_{3u} modes can be identified by their reduction in intensity going from the disc, where the orientation is random, to the solidified melt. This indicates that the melt must crystallise with its ab plane parallel to the plate.

The calculations again indicate that there is no change in frequency with dihedral angle. None of the b_{3u} modes can be identified as appearing in the Raman molten spectrum although the selection rules allow this. It can be generally observed that there are many more infra-red solution bands than Raman bands and that the Raman spectra are completely devoid of combination or overtone bands. In contrast the infra-red region between 2000 cm^{-1} and 1600 cm^{-1} contains numerous out-of-plane combination and overtone modes characteristic of an aromatic molecule.

Fig. II(ii)

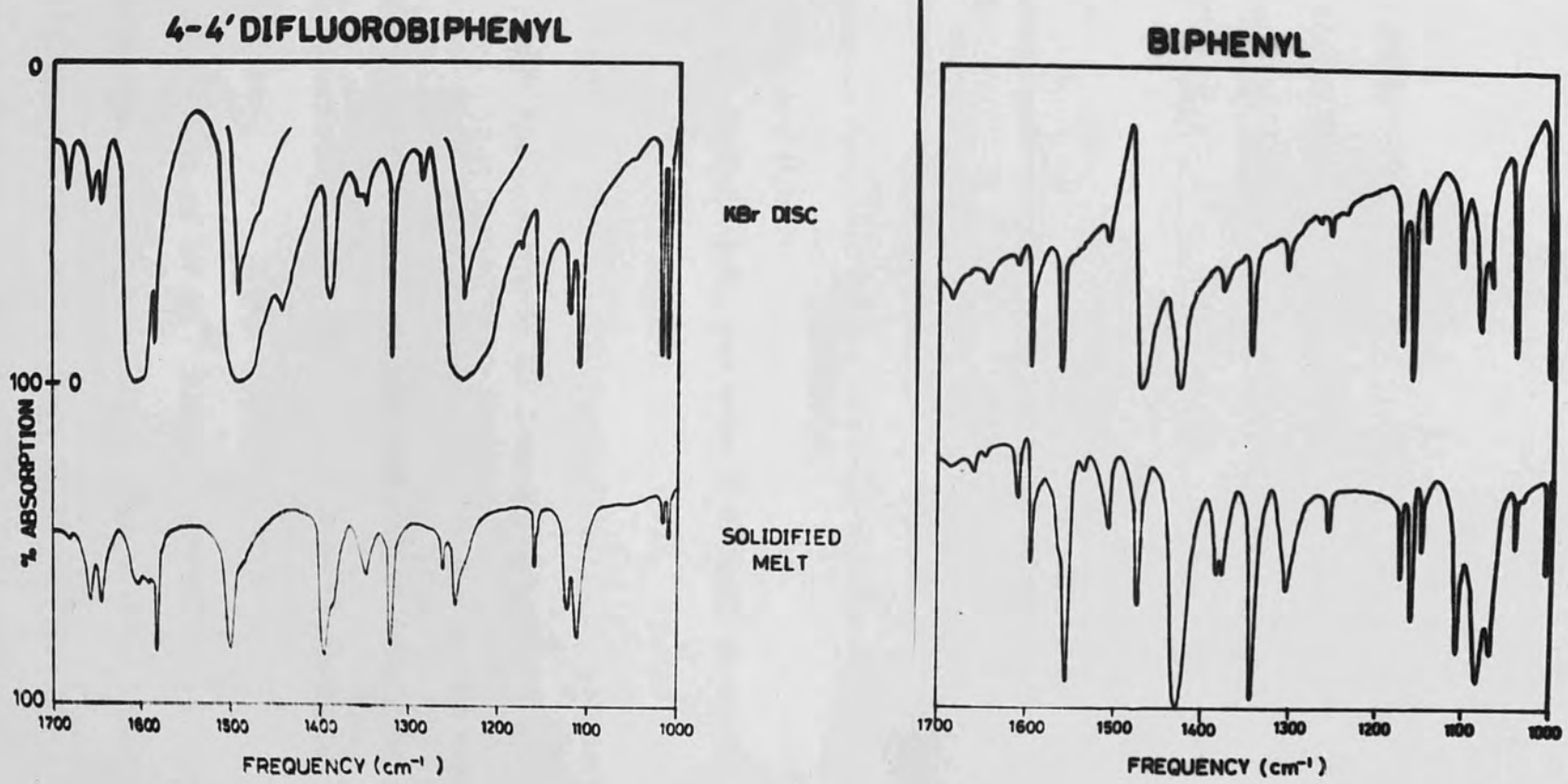

FIG( ). Relative intensities of the infrared bands for disc and solidified melt.

B_{3u} fundamentals should give rise to A type band shapes in the gaseous infra-red spectrum. From the data of Pasquier and Lebas (22) such bands are clearly recognised at 611 cm^{-1}, 1012 cm^{-1}, 1046 cm^{-1} and 1486 cm^{-1}.

The b_{3g} modes have been doubly assigned with the a_u fundamentalsaand they also appear at 964 cm^{-1}, 838 cm^{-1} and 403 cm^{-1} in the solution infra-red.

B1 Species

The big fundamentals are very difficult to spot because their strength in the Raman is very weak. Hence only a few depolarisation ratios can be measured with any degree of accuracy but the assignment is facilitated above 1000 cm^{-1} because the modes must be in-plane. A few of the modes have correlations with infra-red solution data. The only mode which is predicted to shift, ν_{10}, cannot be observed in the Raman spectrum, but a broad infra-red band at 367 cm^{-1} with a half-band width of 14 cm^{-1} becomes active in solution. A perturbational analysis now in progress gives this mode a zero weighting factor and a value of approximately 400 cm^{-1} is always calculated. This tends to suggest that if the fundamental was active it would appear near this value. The change in observed frequency then corresponds to a change in

dihedral angle of approximately 55°. ν_6 is observed to move from 1263 cm^{-1} in the solid to 1249 cm^{-1} in solution and to 1233 cm^{-1} in the gas phase. It is difficult to identify the accuracy of these positions because the fundamental lies as a weak shoulder of the very strong ν_6 a_{1g} mode. The reason for this shift is open to speculation. The P.E.D. for ν_{10} shows that the in-plane β_c force constant contributes 89% to the motion, again confirming the predictions above that shifts arise through G matrix interactions involving deformations near the joining C-C bond.

The out-of-plane b_{1u} modes appear as moderately strong bands in the infra-red except for ν_1 where γ_{C-H} modes are always weak. This time a frequency increase of 28 cm^{-1} is observed for ν_5 which also has a large half-band width. Because the vibrational energy within a given species must remain constant regardless of conformation, the decrease in frequency of the ν_{10} b_{1g} is now confirmed indicating that a strong perturbation exists between these two levels. The corresponding angle change for this shift is approximately 35° but it must be remembered that the calculated planar frequency is 27 cm^{-1} too low.

About 34% of the energy associated with ν_5 is derived from the out-of-plane γ_c deformation.

B_{1u} fundamentals should give rise to C-type envelopes in the infra-red spectrum of the gas corresponding to a dipole moment change parallel to the largest principal axis of inertia. Such band shapes can be definitely identified at 484 cm^{-1}, 699 cm^{-1} and 737 cm^{-1}. No dichroic effects are anticipated in the solidified melt and none of the bands became Raman active in the molten state.

B2 Species

The infra-red b_{2u} fundamentals are easily identified as fairly strong bands in the disc, melt and solution spectra. The calculations show that they are rather insensitive to dihedral angle, the maximum shift predicted over 90° being 9 cm^{-1}. ν_{10}, however, is a very strong band which is seen to shift by 6 cm^{-1} from solid to solution state. In the solid state, ν_7 and ν_8 seem to be affected by crystal splitting, and this phenomenon could explain the appearance of the 1149 cm^{-1} solid Raman band allocated to ν_7 in the b_{1g} series above. Only ν_9 at 626 cm^{-1} appears in the Raman melt spectrum. B_{2u} motions give rise to B-type band shapes and these can be identified at 1431 cm^{-1}, 1156 cm^{-1} and 1070 cm^{-1}.

The out-of-plane b_{2g} fundamentals are characterised by their appearance as strong bands in the solution infra-red spectrum. This is quite surprising because the bands are very weak in the Raman spectra (only one dipolarisation ratio is determined) and ν_2 and ν_4 cannot be located at all. The lowest frequency fundamental ν_6 is calculated to have a small shift and a change of 18 cm^{-1} is observed from solid to melt. This corresponds to a change in dihedral angle of approximately 60° if the shift is attributed entirely to G matrix effects.

2.5 Discussion

The agreement between the spectral frequencies reported here and those reported by Zerbi and Sandroni (24) and Pasquier and Lebas (22) is very good. The assignments differ from those of Pasquier and Lebas only in minor details, mainly in the weak b_{1g} modes. The assignments of Zerbi and Sandroni for the in-plane fundamentals are again in good agreement as might be expected since they too were based on calculations.

The one outstanding gap in our present knowledge is the frequency of the torsion "butterfly" mode. Zerbi (34) suggests that this might be at 70 cm^{-1} corresponding to an absorption in the neutron scattering spectrum. As a band appears at

this frequency in the far-infra-red spectrum and has alternative explanations as a fundamental this assignment may be discounted.

The only band below 1000 cm^{-1} not to be assigned occurs in the infra-red solid spectrum at 174 cm^{-1} and this disappears in solution. Although the "butterfly" torsion is infra-red inactive for D_{2h} symmetry, a slight deviation from planarity of the ortho- hydrogens could perhaps explain this weak band. A more obvious explanation, however, would be for this band to be an external (lattice) mode, disappearing on dissolution.

More recently Lim and Li (35) have re-examined the luminescence spectra of biphenyl and its substituted derivatives. In excited electronic states the molecule has been shown to have a planar conformation (36) and calculations based on the extended Hückel treatment (37) indicate that the increased conjugation energy outweights the non-bonded, ortho-ortho repulsion energy. Lim and Li predict that an electronic transition between states of radically different geometry is characterised by the appearance of a long progression in the vibrational mode that carries the geometry of one state into that of the other - namely the "butterfly" mode. They assign this mode to a strong band in the fluorescence spectrum at 635 cm^{-1}, and observe odd quanta in the fluorescence spectrum and even quanta in the phosphorescence spectrum at 77°K in n-heptane. A weak band at 626 cm^{-1}

does indeed appear in the Raman melt spectrum but this has been assigned as a b_{2u} fundamental. In fact, all the bands present in both fluorescence and phosphorescence can be accounted for by corresponding Raman fundamentals. The phosphorescence spectrum comprises nearly all the a_{1g} modes whilst the fluorescence spectrum contains a mixture of species.

From the work of Fateley and Miller on torsional modes of aromatic compounds in the far infra-red (38), such a high frequency would require an enormous torsional barrier. A semi-empirical computation of the internal energy of biphenyl as a function of dihedral angle θ, adjacent H-C-C angle and inter-ring bond length has been made by Simonetta et al (39). Their calculations on the isolated molecule gave a minimum in energy of 181.4 kJ/mole for r = 1.51 Å, $\theta = 35^\circ$ and $\chi = 121^\circ$. The barrier height predicted was 9.2 kJ/mole at $\theta = 0^\circ$ and 14.2 kJ/mole at $\theta = 90^\circ$.

The solution of the wave equation for the torsional energy of a molecule assumes that the potential energy may be adequately described by a Fourier series in terms of θ (40).

$$2V = \sum_{n=1}^{n=\infty} V_n (1 - \cos n\theta)$$

For biphenyl the barrier is two-fold (n=2), and following Fateley et al, V_4 is taken as zero.

Hence $2V = V_2 (1 - \cos 2\theta)$

On substitution into the wave equation, a function in the form of Mathieu's equation is obtained.

$$y'' + (b - S \cos^2 x)y = 0$$

For a fixed value of S there exists an infinite sequence of characteristic b values, corresponding to which the solutions y are periodic.

The torsional eigen value is given by:

$$E_v = \frac{n}{2}^2 F b_v$$

where n is the barrier symmetry, v is the principle torsion quantum number, b_v is an eigen value of the Mathieu equation and F is given by the expression:

$$F = \frac{h}{8\pi^2 c\, I_{red}} \qquad (\text{in } cm^{-1})$$

$$= \frac{16.852}{I_{red}}$$

Now $I_{red} = I_\alpha \left[1 - I_\alpha \sum_i \frac{\lambda_i^2}{I_i} \right]$

where I_α = moment of inertia of the internal top, (i.e. C_6H_5)

about its own symmetry axis, λ_i = cosine of the angle between the axis of the internal top and the ith principle axis of inertia of the entire molecule (I_i).

For biphenyl $I_{red} = \frac{I}{2} = 44.54$ amu $\mathring{A}^2$ giving F a value of 0.378 cm^{-1}.

Now $\frac{V_n}{n^2} = \frac{FS}{4}$

Hence $V_2 = FS$ and using $V_2 = 9.2$ kJ/mole the corresponding value of S is 2106.

Also $E = F\Delta b_{o\rightarrow 1}$

A refinement of Herschbach's tables of $\Delta b/S$ can be found in Ref. (4) and the "butterfly" torsion is predicted to be 43 cm^{-1}. It is perhaps fortuitous that a Raman band is found at 41 cm^{-1} in the solid state.

2.6 Conclusion

It has been clearly demonstrated that change in conformation for biphenyl from D_{2h} to D_2 symmetry is accompanied by changes in spectral activities and shifts of certain normal modes. The only high-frequency shifts observed were for the ν_7 a_{1g} and ν_6 b_{1g} fundamentals, the former being predicted to be due to

the release in steric hindrance of the ortho hydrogens on twisting for the β_{C-H} deformations. The lowest a_{1g} mode exhibited a decrease of 15 cm^{-1} from solid to melt and a further 9 cm^{-1} from melt to the gas phase. These shifts are consistent with a lowering of bond order of the central C-C inter-ring bond and predict a greater change in the gaseous phase.

The modes which are predicted and seen to move, namely the ν_{10} b_{1g}, ν_5 b_{1u}, ν_6 b_{2g} and ν_{10} b_{2u} fundamentals give an estimate of the dihedral angle which lies between 35° and 60°. Details of how the accuracy of this estimate can be improved are given in Chapter 4.

CHAPTER 3

The Vibrational Analysis of the 4-4'Dihalogeno Biphenyls

3.1 Introduction

It seemed a logical consequence of the work described above to examine the vibrational properties of the 4-4'dihalogeno biphenyls in order to estimate the conformations in different physical states. In marked contrast to the biphenyl history there is little detailed analysis of the spectra for these molecules. Recently Nanni et al (41) concluded that 4-4'-dichlorobiphenyl had a planar conformation in both solid and dissolved states. Whilst the spectra of difluorobiphenyl are very similar to those of biphenyl and can be interpreted accordingly, those of dichloro- and dibromobiphenyl have some very different features which cannot be explained as a simple mass effect.

3.2 Experimental

4-4'difluorobiphenyl was purchased from Koch-Lights Ltd., 4-4'dichlorobiphenyl from Pfaltz and Bauer Inc. and 4-4'dibromobiphenyl was synthesised according to Buckles and Wheeler (42). The bond lengths and masses used in the construction of the G matrix were taken as $r_{C-F} = 1.30$ Å, $r_{C-Cl} = 1.70$ Å, $r_{C-Br} = 1.865$ Å, $m_F = 19.000$ amu, $m_{Cl} = 35.457$ amu and $m_{Br} = 79.916$ amu.

3.3 Interpretation and assignments for 4-4'difluorobiphenyl

The principal infrared and Raman bands at frequencies below 1700 cm^{-1} are listed in Table III(1) and the features below 1000 cm^{-1} are illustrated in Fig. III(i). Calculated fundamentals for various dihedral angles with their corresponding assignment are seen in Table III(2). The force fields used in the calculations were transferred from work on mono- and di-substituted halogeno benzenes (12, 32).

A Species

As with biphenyl no frequency shifts with dihedral angle change are predicted and ν_{3} a_{2g}, the highest frequency ring mode, is again calculated about 60 cm^{-1} too high. This time, however, ν_7 is not observed to move but ν_{11} appears at 277 cm^{-1},

Fig. III(i)

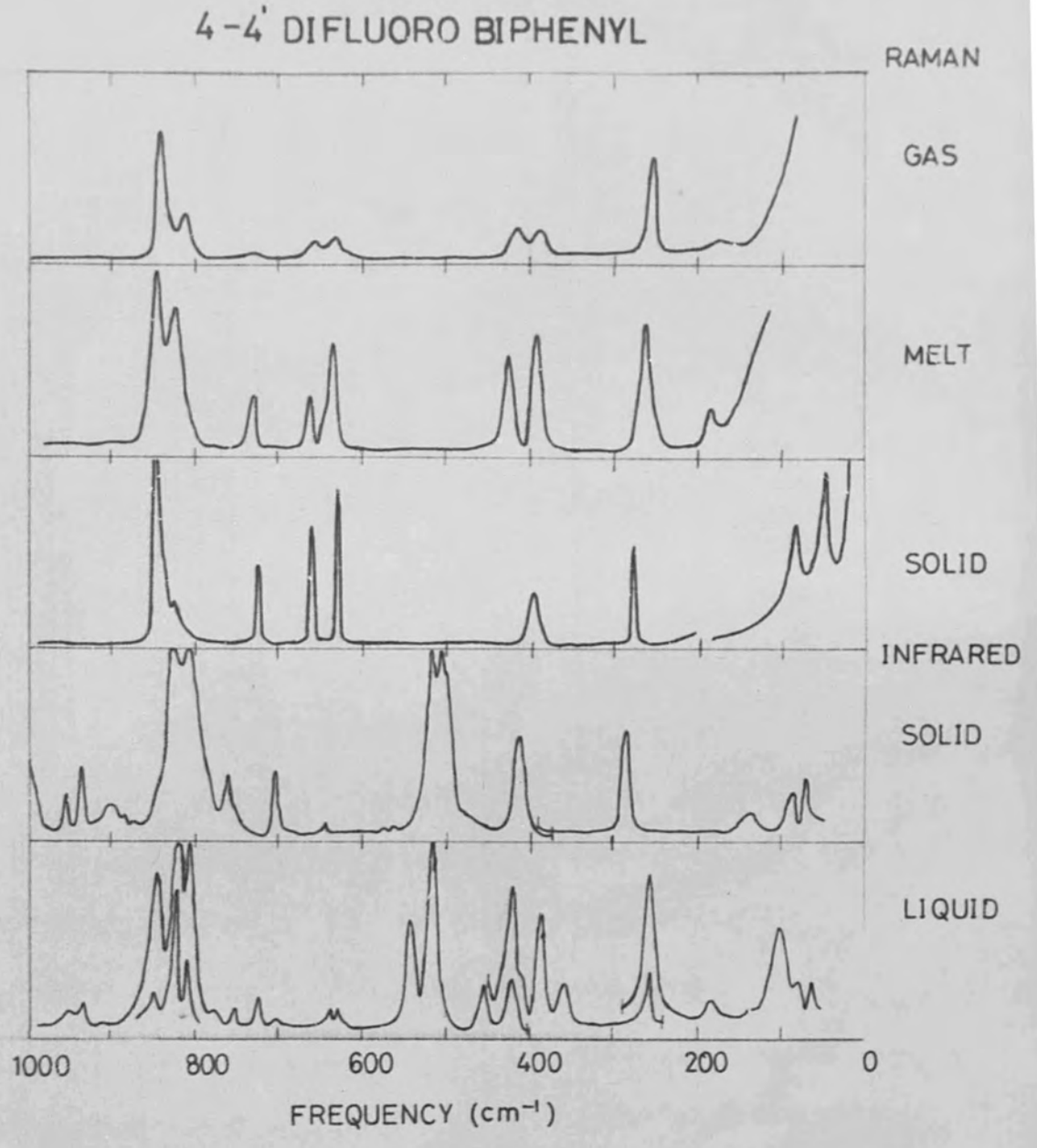
4-4' DIFLUORO BIPHENYL
RAMAN
GAS
MELT
SOLID
INFRARED
SOLID
LIQUID
1000
800
600
400
200
0
FREQUENCY (cm⁻¹)

264 cm^{-1} and 255 cm^{-1} in the solid, molten and vapour phases respectively. From the P.E.D. in Appendix 4 much of the energy of this fundamental is derived from inter-ring stretching deformation reflecting a change in bond order due to twist. Again all these symmetric modes give very strong ~~times~~ bands in the Raman and are readily identified by the band polarisations and the sharpness of the bands in the vapour phase.

The highest a_u mode cannot be located but the other two become active at 824 cm^{-1} and 423 cm^{-1} in the molten state. The latter is identifiable from its polarisation.

B3 Species

The higher frequency b_{3u} fundamentals exhibit the same kind of dichroism as observed for biphenyl, where their intensity rapidly diminishes on comparing the infrared spectrum of the solidified melt with that of the randomly orientated KBr disc. This suggests that the crystal structure is very similar to that of biphenyl in that the molecular axes along which the b_{3u} transition dipole moments are orientated are all parallel, and are perpendicular to the plate.

The three b_{3g} modes are doubly assigned with the three a_u modes.

Table III(1)

The Principal Infrared and Raman bands of 4-4'difluorobiphenyl at frequencies below 1700 cm^{-1}.

Infrared		Raman			Assignment
Solid	Soln.	Solid	Liquid	Gas	
1687w					
1660m	1660w				
1645m					
		1626m	1638w	1636w	
		1603vs	1607vs (0.44)	1604	a_g
1600vs	1600vs				b_{3u}
1585s	1586m				b_{2u}
		1554w	1553w		b_{1g}
		1529m	1524m (0.39)		a_g
	1516w				
1495vs	1496vs				b_{3u}
	1476m				
1450m	1458w				
1393m	1394m				b_{2u}
1343w	1350w				
		1323w	1320w		a_g
1317s	1302s				b_{2u}
1286w	1283vw				b_{2u}

Table III(1)(continued)

I Infrared		Raman			Assignment
Solid	Soln.	Solid	Liquid	Gas	
		1273vs	1283vs (0.27)	1284vs	a_g
		1257m	1257sh	1257sh	b_{1g}
		1245vw	1239w	1242w	b_{1g}
1235vs	1230vs				b_{3u}
		1176m			
		1169vs	1167m (0.12)	1163	a_g
1158	1153s				b_{3u}
		1113w			
1124s)) 1108))	1095s				b_{2u}
		1098m	1100w		b_{1g}
		1017w	1018w		a_g
1016s	1018s				b_{3u}
1007s	1008s				b_{3u}
		966vw			b_{3g}
956m	952vw				)) b_{1u})
935m	932vw				
		938vw			b_{2g}
		846vs	843vs (0.09)	840vs	a_g
	847s				b_{2g}
823vs	821vs				b_{1u}

Table III(1)(continued)

Infrared		Raman			Assignment
Solid	Soln.	Solid	Liquid	Gas	
		823w	824s		)
			812m		)a_u, b_{3g}
804vs	806s		808sh		b_{3u}
761m	755w				
	726m	722s	728m (0.90)	728w	b_{2g}
702m	704w				b_{1u}
		660s	661m (0.74)	658w	a_g
642w	638w				b_{2u}
	630w	627s	632m (0.94)	633w	b_{1g}
	542m	540vw			b_{2g}
518s					b_{3u}
498))vs 505)					b_{1u}
	454m	464vw			b_{1g}
	420m	-	423m (0.68)	415w	b_{3g}/a_u
412m	414w				b_{2u}
	390s	395s	392m (0.81)	389w	b_{2g}
	358m	340vw			b_{1g}
283m	255m				b_{1u}
		277vs	264s (0.22)	255vs	a_g

Table III(1)(continued)

Infrared		Raman			Assignment
Solid	Soln.	Solid	Liquid	Gas	
-	182vw	180vw	183m	178vw	b_{2g}
145w					
	101w				
96vw	81w				b_{2u}
72vw	68w				b_{1u}

* denotes double assignment

\+ mass sensitive modes

Table III(2)

Calculated and Observed Frequencies (cm^{-1}) for 4-4'difluorobiphenyl for various dihedral angles.

A Species (D_{2h} - A_g, A_u)

	Calculated frequencies for all	Observed frequencies				
		Raman			Infrared	
		Solid	Liquid	Gas	Solid	Liquid
A_g	3073					
	3072					
	1664	1603	1607	1604	-	-
	1535	1529	1524	1519	-	-
	1346	1323	1320		-	-
	1241	1277	1283	1284	-	-
	1143	1169	1167	1163	-	-
	1022	1017	1017		-	-
	835+	846	843	840	-	-
	653+	660	661	658	-	-
	229+	277	264	255	-	-
A_u	958	-	-	-		
	829	-	824	812		
	409	-	423	415		

* denotes double assignment

+ mass sensitive modes

Table III(2)(continued)

B_3 Species (D_{2h} - B_{3u}, B_{3g})

	Calculated frequencies for all θ	Observed frequencies				
		Raman			Infrared	
		Solid	Liquid	Gas	Solid	Liquid
B_{3u}	3073	-	-	-	-	-
	3072	-	-	-	-	-
	1586				1600	1600
	1494				1495	1496
	1245				1235	1230
	1144				1158	1153
	1032				1016	1018
	1016				1007	1008
	800+		808		804	806
	525+				518	515
B_{3g}	958	966				
	829	-	824*	812*		
	409	-	423*	415*		

Table III(2)(continued)

B_1 Species (D_{2h} - B_{1g}, B_{1u})

	Calculated frequencies for θ =				Observed frequencies				
					Raman			Infrared	
	0°	30°	60°	90°	Solid	Liquid	Gas	Solid	Liquid
B_{1g}	3070	3070	3070	3070					
	3069	3069	3069	3069					
	1583	1582	1581	1581	1554	1553	-		1555
	1391	1388	1381	1373	-	-	-		
	1293	1292	1291	1288	1257	1259	1267		
	1274	1275	1278	1281	1245	1239	1242		
	1095	1094	1092	1091	1098	1100	-		
	610	610	611	613	627	632	633	-	630
	444+	441	435	428	464	-	-		454
	301+	325	349	365	340	-	-		358
B_{1u}	945	945	945	946				935 or 956	932 or 952
	820	821	822	826				822	821
	709	712	720	729				702	704
	494	500	511	520				499/505	515*
	280+	254	233	196				283	255
	55+	56	58	61				71	72

Table III(2)(continued)

B_2 Species (D_{2h} - B_{2u}, B_{2g})

	Calculated frequencies for θ =				Observed frequencies				
					Raman			Infrared	
	0°	30°	60°	90°	Solid	Liquid	Gas	Solid	Liquid
B_{2u}	3070	3070	3070	3070				-	-
	3069	3069	3069	3069				-	-
	1586	1585	1583	1581				1585	1586
	1361	1362	1366	1373				1393	1394
	1291	1290	1288	1288				1317	1302
	1279	1280	1282	1281				1288	1283
	1088	1088	1089	1091				1124/1108	1095
	619	618	616	613		641		642	638
	417^+	418	423	428				414	415
	75^+	72	66	61				84	96
B_{2g}	949	947	947	946	938	-			
	838	834	830	826	847*	843*			847
	727	727	729	729	722	728	728		726
	520	522	522	520	540	-			542
	382^+	381	376	365	395	392	389		390
	150^+	157	173	196	180	183	178		182

B1 Species

The intensity of the b_{1g} Raman bands is again very weak. The two lowest fundamentals, ν_9 and ν_{10} are predicted to shift but unfortunately their Raman assignment is very uncertain because their signal to noise ratio is very low. Fairly strong infrared bands do appear in the solution state at 358 cm^{-1}, 454 cm^{-1} and 630 cm^{-1} and these are assigned as the three formerly lowest b_{1g} modes. If, indeed, 340 cm^{-1} of ν_{10} is valid for the solid state a dihedral angle change of approximately 25° is predicted.

All six b_{1u} fundamentals appear in the infrared, the only uncertainty lying with the ambiguity of ν_1. Since a strong band corresponding to 2 x 956 cm^{-1} appears in the overtone and combination γ_{C-H} region at 1900 cm^{-1}, the higher value is favoured. The lowest three bands are predicted to shift, the largest corresponding to ν_5 at 283 cm^{-1} in the solid state and 255 cm^{-1} in solution. This shift leads to an estimate of the change in dihedral angle of 32°. It is interesting to compare the ν_{10} b_{1g}/ν_5 b_{1u} splitting with biphenyl where the shifts occur in the opposite sense. It is difficult to observe any change in ν_6 from the interferogram transforms because the background energy is cut by the beam-splitter transmission characteristic. ν_4 is split as a doublet (presumably by crystal

effects) in the solid state but appears as one band (in fact doubly assigned) at 515 cm^{-1} in solution.

B2 Species

Although the calculations show no significant shifts in the b_{2u} fundamentals for change in dihedral angle, a change of 15 cm^{-1} is observed for ν_5. This decrease, from solid to solution, has been predicted as a relaxation in steric hindrance due to the ortho β_{C-H} deformations.

Five of the b_{2g} modes are characterised by their appearance in the solution infrared indicating a relaxation of the spectral activities from D_{2h} to D_2. The measureable depolarisation ratios for ν_3 and ν_5 are consistent with a non-symmetric vibration. Although ν_6 is predicted to shift no significant change can be observed for the weak Raman line at 180 cm^{-1} indicating that the dihedral angle change will be small and less than 30°.

3.4 Conclusion

It has been clearly demonstrated that the first order force field taken gives an excellent fit with the observable frequencies. Again a weak band in the solid far-infrared at 137 cm^{-1} which disappears on dissolution cannot be accounted for. Lim and Li (35)

suggest that the "butterfly" torsion (ν_4 a_u) forms a progression at 626 cm^{-1} in the luminescence spectra, but this has been assigned to the ν_8 b_{1g} fundamental in the Raman. The shifts observed for 4-4'difluorobiphenyl suggest an angle in solution of approximately 30°, a value which embraces a high degree of uncertainty. The further change in ν_{11} a_g Raman band from melt to gas suggest that the dihedral angle is greater in the gas phase. Unfortunately no infrared gas phase data was obtained to check this and no variable temperature solution data is available to investigate the temperature dependence of the dihedral angle.

3.5 Interpretation and assignments of 4-4'dichloro- and dibromobiphenyl

In contrast to biphenyl and its 4-4'difluoro derivative the other two halogeno derivatives show no significant frequency or intensity variations with change of state. The spectra can be fairly readily interpreted by comparison with the solution or molten state spectra of difluorobiphenyl on making allowance for the heavier masses of the substituents. A glance at the spectra in Figs. III(ii) and (iii) show that there are far more bands to assign in the solid state than the corresponding spectra of biphenyl itself. Apart from the a fundamentals all the infrared and Raman bands are coincident

Fig. III(ii)

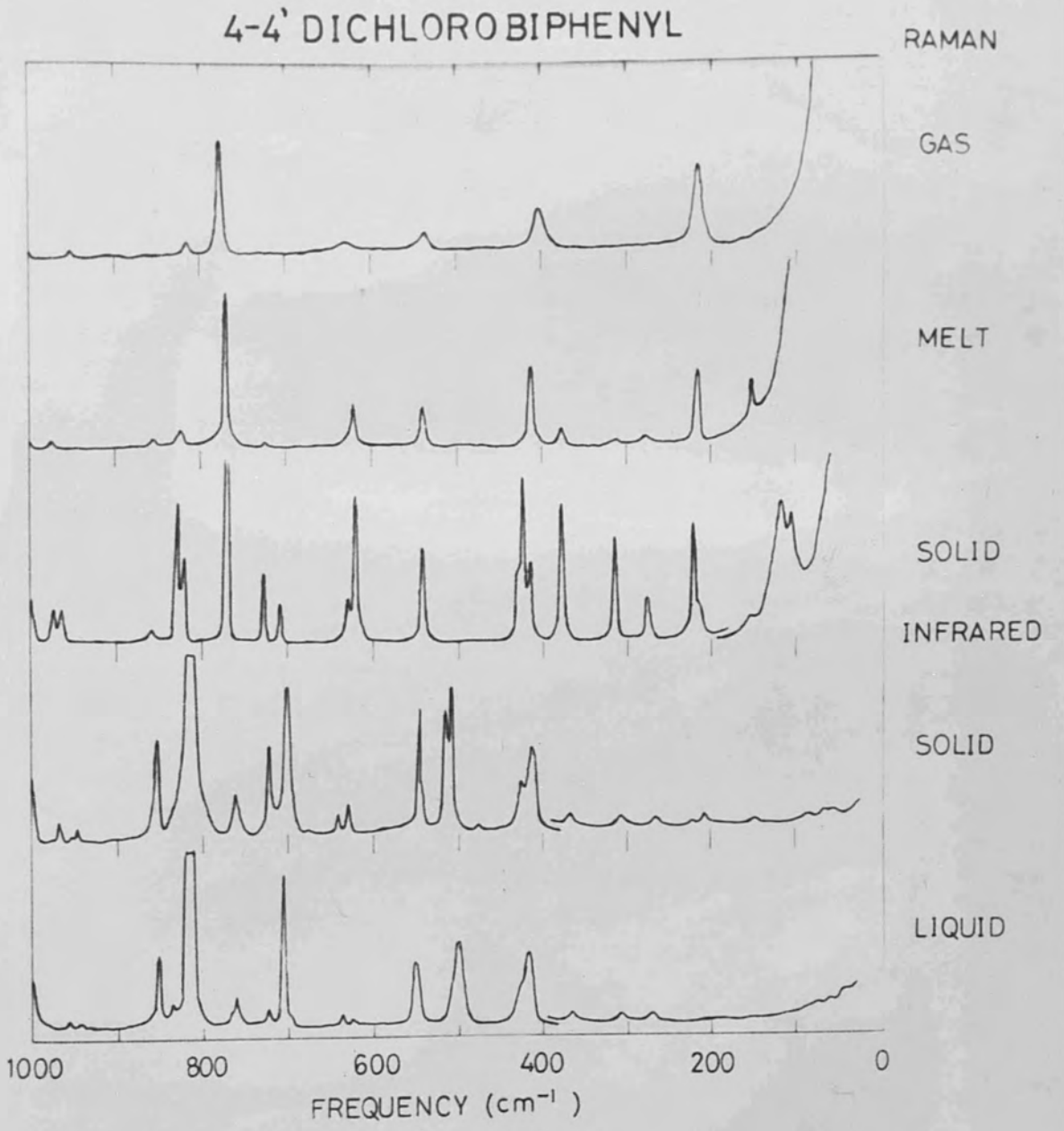
4-4' DICHLOROBIPHENYL
RAMAN
GAS
MELT
SOLID
INFRARED
SOLID
LIQUID
1000
800
600
400
200
0
FREQUENCY (cm⁻¹)

FIG(III) iii

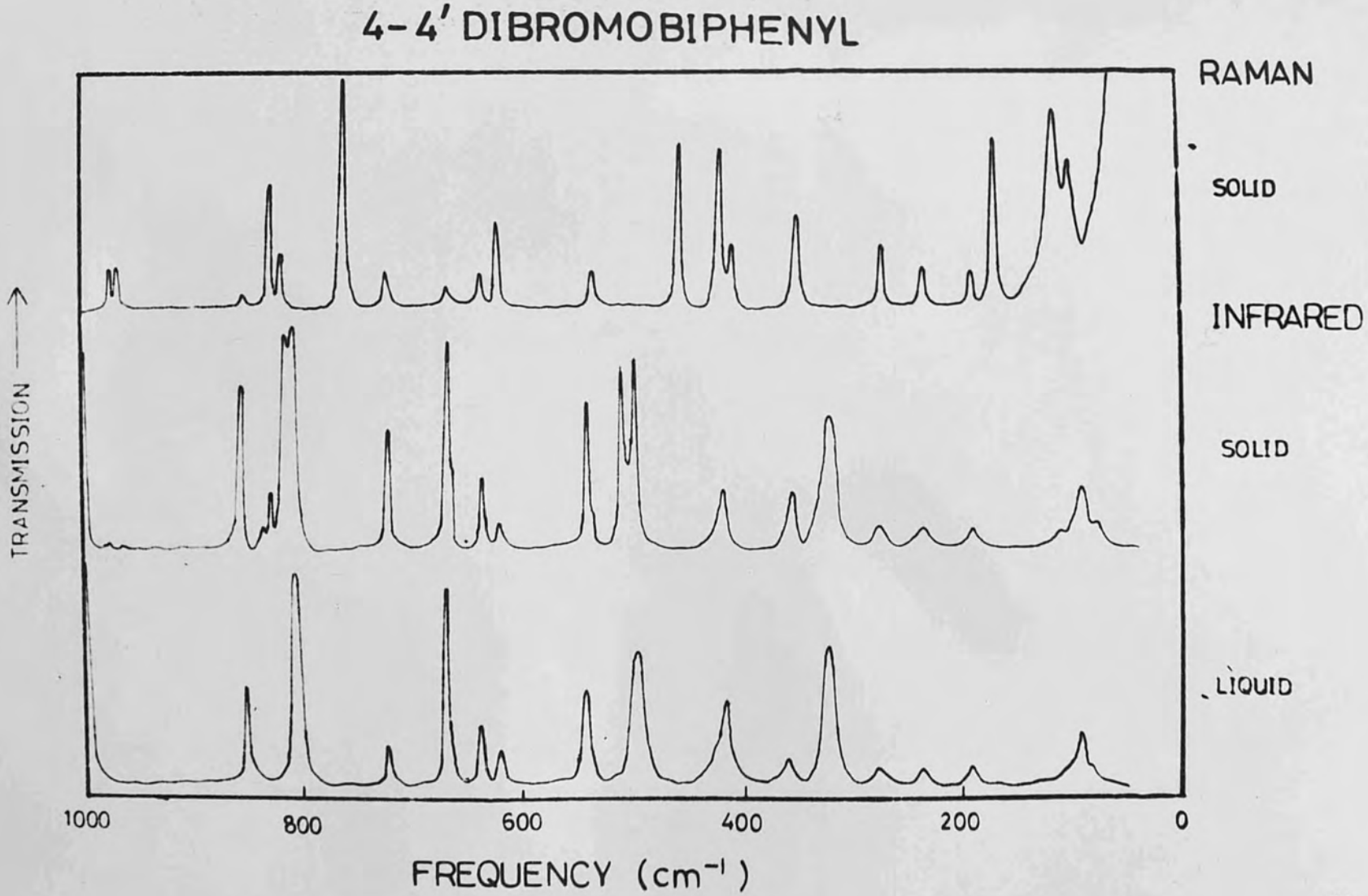
4-4′ DIBROMOBIPHENYL
RAMAN
SOLID
INFRARED
SOLID
LIQUID
TRANSMISSION
1000
800
600
400
200
0
FREQUENCY (cm⁻¹)

indicating that the Rule of Mutual Exclusion does not now apply and the molecules do not possess a centre of symmetry. This contradicts the conclusion deduced by Nanni et al (41) who assigned the spectra on the basis of D_{2h} symmetry.

The principle bands for dichloro-and dibromo-biphenyl are listed in Tables III(3) and (5), and the assignments together with the calculated normal modés are given in Tables III(4) and (6). The calculations were repeated for 4-4'difluorobiphenyl substituting the masses of the two fluorine atoms for $m_{Cl} = 35.5$ and $m_{Br} = 80.0$. In this way the fundamentals involving a large cartesian displacement (C.D.) of the carbon atoms, i.e. the modes sensitive to substitution were identified. These vibrations are marked with a cross (+) in Table III(2). It turns out that nearly all the low frequency fundamentals are mass sensitive.

Just as for difluorobiphenyl and biphenyl there are considerable intensity changes of bands between aKBr disc and a solidified melt spectrum. The greatest changes occur for those bands which are certainly b_3 fundamentals where the bands become weaker in the solidified melt. On the other hand, not all bands which exhibit this intensity decrease can arise from b_3 transitions. The principle deduction must be that the long axes are once more orientated almost perpendicular

Table III(3)

The principle infrared and Raman bands of 4-4'dichlorobiphenyl at frequencies below 1700 cm^{-1}.

Infrared		Raman			Assignment
Solid	Soln.	Solid	Liquid	Gas	
1675w	1667w				
1640w	1635w				
		1633w			
		1597vs	1597vs	1595vs	a
1595m	1593m				b_2
1588m					b_3
1556w		1549m			b_1
		1516m	1513vw		
		1503) d) 1495)		1505vw	a
1488m	1484s				
1474vs	1474s				b_3
1455m	1450vw	1453vw			
1410w	1411vw	1417vw			
1387m	1389m	1394vw			b_2
		1380vw			b_1
1300d-w	1300	1307sh			b_2
		1287vs	1284vs	1275vs	a
1271w					b_2
		1242w			b_1
		1224vw			

Table III(3)(continued)

Infrared		Raman			Assignment
Solid	Soln.	Solid	Liquid	Gas	
		1184vs	1191m	1186m	a
1186w)) 1172)	1180w				b_3
1116w	1114w	1123m	1124m	1123m	b_1
1100s	1100sh-w				b_2
		1098vs	1098s (0.13)	1096m	a
1087vs	1092vs	1078m	1077m	1070sh	b_3
		1016s	1018m (0.20)	1013w	a
1018vs	1019m	1019sh-w			b_3
1003vs	1004s	1000vw			b_3
971vw		973) d))		953vw	a
962w	957w				b_3
949vw					b_2
943w	941w				b_1
850s	843m	853w	847w		b_2
832w	829w	828) d) m	824m	817w	a/b_3
822sh-w		822)			
814vs	812vs				b_1
		773s	773m (0.04)	768s	a
762m	757m				
723m	722w	727m			b_2
702s	704s	706w			b_3
698sh-m	696				b_1

Table III(3)(continued)

Infrared		Raman			Assignment
Solid	Soln.	Solid	Liquid	Gas	
637w	637w	638w	639w		b_2
624w	626w	628m	629m (0.78)	627w	b_1
540sh		545s	543m (0.37)	536w	a
545s	538m				b_2
510/504 d-s	501s				b_1
420m	423w	424sh-m			b_3
410s	414s	421) d)m	413m (0.41)	406m	a
		414)			b_3
369w	368m	368m	370w		b_1
306w	306m	306m	309w		b_2
270w	270m	270m			b_1
227vw	-	227s	226w (0.09)	219s	a
215w	-	219w-sh			b_1
157w		150vw			b_2?
		116) d)vs			
		104)			
88-98m					b_2?
63w					b_1?
		56m			?
		42m			?

Table III(4)

Calculated and observed frequencies (cm^{-1}) for 4-4'dichlorobiphenyl for various dihedral angles.

A Species (D_{2h} - A_g, A_u)

	Calculated frequencies for all θ	Observed frequencies				
		Raman			Infrared	
		Solid	Liquid	Gas	Solid	Liquid
A_g	3072					
	3072					
	1653	1597	1597	1595		
	1503	1495	-	1505		
	1334	1287	1284	1275		
	1174	1184	1191	1186		
	1088	1098	1098	1096		
	1012	1016	1018	1013		
	788	773	773	768		
	521	542*	-	536	540	
	198	227	226	219	227	
A_u	964	973	-	953	971	
	832	822	-	817	822	824*
	408	421	413*	406	-	414*

Table III(4)(continued)

B_3 Species (D_{2h} - B_{3u}, B_{3g})

	Calculated frequencies for all θ	Observed frequencies				
		Raman			Infrared	
		Solid	Liquid	Gas	Solid	Liquid
B_{3u}	3072					
	3072					
	1563				1588	
	1468				1474	1474
	1174				1172/ 1186	1180
	1097	1078	1077		1087	1092
	1025				1019	1019
	997	1000			1003	1004
	712	706			702	704
	420	424	423		-	423
B_{3g}	964	966			962	957
	832	828	824*		832	829
	408	414	413*		-	414

Table III(4)(continued)

B_1 Species (D_{2h} - B_{1g}, B_{1u})

	Calculated frequencies for θ =				Observed frequencies				
					Raman			Infrared	
	0°	30°	60°	90°	Solid	Liquid	Gas	Solid	Liquid
B_{1g}	3070	3070	3070	3072					
	3070	3070	3070	3072					
	1566	1565	1564	1564	1549			1556	
	1387	1385	1380	1375	1380				
	1287	1287	1287	1290	1275				
	1284	1285	1285	1283	1242				
	1106	1105	1103	1100	1123	1124	1123	1117	1114
	621	621	622	624	628	629	627	624	626
	387	383	373	363	373	370		372	369
	242	261	277	289	274			271	270
B_{1u}	940	940	941	941				943	941
	809	810	813	820				814	812
	695	698	705	712				698	696
	472	481	498	512				504/ 510	501
	233	211	185	161	219	-	-	215	-
	42	43	45	48				63	-

Table III(4)(continued)

B_2 Species (D_{2h} - B_{2u}, B_{2g})

	Raman							Infrared	
	0°	30°	60°	90°	Solid	Liquid	Gas	Solid	Liquid
B_{2u}	3070	3070	3070	3070					
	3070	3070	3070	3070					
	1569	1568	1566	1564				1595	1593
	1368	1368	1370	1375	1394			1387	1389
	1296	1295	1293	1290	1307			1300	1300
	1279	1279	1281	1283				1271	-
	1095	1095	1097	1100				1100	1100
	630	629	627	624	639	639		637	637
	306	303	297	289	-	-		-	-
	63	59	54	48				87-95	
B_{2g}	944	943	942	941				949	
	832	831	826	820	853	847		850	843
	707	708	711	712	727			723	722
	518	518	517	512	542*	543		545	538
	345	348	355	363	309	309		306	306
	119	126	141	161	116/ 150	154		157	-

to the plane of major crystal development. A good example is afforded in dichlorobiphenyl by the complex region around 1100 cm^{-1}. In the crystallised melt spectrum a band at 1087 cm^{-1} is strongly reduced in intensity relative to its neighbouring bands. From this it is deduced that the associated transition is of a different species to that of its neighbours and is to be identified as b_3. However, a band assigned as b_3, either at 1186 or 1172 cm^{-1} and the only fundamental expected in this region besides an a mode, shows no dichroic effect at all.

Doublets near 960, 830 and 415 cm^{-1} are clearly assigned to the formerly 'a_u and b_{3g} out-of-plane' double assignments. That such doublets exist (average separation ~ 8 cm^{-1}) is further support for the D_2 conformation.

In difluorobiphenyl the Raman ν_8 b_{1g} mode appeared in the infrared solution spectrum and the infrared active ν_8 b_{2u} mode appeared in the Raman molten spectrum both around 630 cm^{-1}. Now in both dichloro-and dibromo- biphenyl a mass-insensitive doublet appears in both Raman and infrared spectra. Likewise the mass-insensitive ν_4 b_{1u} fundamental is split in the infrared for difluorobiphenyl and appears split around 500 cm^{-1} in the other two molecules. The ν_5 b_{2u} mode of difluorobiphenyl which was observed to shift from 1317 cm^{-1} in the solid state to 1302 cm^{-1} in solution due to steric relaxation now appears as

Table III(5)

The principle infrared and Raman bands of 4-4' dibromobiphenyl at frequencies below 1700 cm^{-1}

Infrared		Raman	Assignment
Solid	Liquid	Solid	
1670w			
1635w			
		1628w	
		1587vs	a
1590w	1588w		b_2
1584m			b_3
		1538vw	b_1
		1498m	a
1485s	1485) d)m 1480))	1490m	
1471vs	1470s		b_3
1452w			
1382s	1383m		b_2
1300d-w	1300w	1302vw	b_2
		1271w-sh	
		1263w-sh	b_1
		1235vw	
		1224w	b_1
		1201sh-vw	
		1184s	a
1166vw			b_3
1117w	1114vw		

Table III(5)(continued)

Infrared		Raman	Assignment
Solid	Liquid	Solid	
1100m	1100w	1103vw	b_2
1076s	1079m	1083m	b_1
1067vs	1071s		b_3
		1069s	a
1016vs	1016m	1015sh-w	b_3
		1010s	a
1000vs	1001s		b_3
970vw		969m	a
962w		962	b_3
949vw			b_2
944vw			b_1
848m	841m	844w	b_2
822w		824m	a
814sh-m		818m	b_3
810vs	807vs		b_1
		757s	a
720m	718w	720w	b_2
672s	672s	671w	b_3
668m-sh	668w-sh		b_1
635w	635w	632w	b_2
623w	624vw	623m	b_1
542m		540w	b_2
	537m		
538sh-w			

Table III(5)(continued)

Infrared		Raman	Assignment
Solid	Liquid	Solid	
506) d)m 500)	497s		b_1
		415s	a
410m	412s	408m	b_3
356w	355w	354w	b_1
315vs	316vs		b_3
271w		270w	b_2
237w		237w	b_1
190vw		192w	b_1
		167s	a
144vw			b_2?
108vw			
		112vs	b_2?
86w		98vs	b_2
74w			b_1

Table III(6)

Calculated and observed frequencies (cm^{-1}) for 4-4'dibromo biphenyl for various dihedral angles

A Species (D_{2h} - A_g, A_u)

	Calculated frequencies for all θ	Observed frequencies				
		Raman			Infrared	
		Solid	Liquid	Gas	Solid	Liquid
A_g	3072					
	3072					
	1651	1587				
	1496	1498				
	1339	1282				
	1168	1184				
	1066	1069				
	1016	1010				
B_{3g}	771	757				
	443	463				
	147	167				
A_u	972	969			970	
	827	818			814*	
	411	408				

Table III(6)(continued)

B_3 Species (D_{2h} - B_{3u}, B_{3g})

	Calculated frequencies for all θ	Observed frequencies				
		Raman			Infrared	
		Solid	Liquid	Gas	Solid	Liquid
B_{3u}	3072					
	3072					
	1560				1584	
	1462				1471	1470
	1169				1166	-
	1077				1067	1071
	1028				1016	1016
	1001				1001	1000
	679	671			672	673
	321				315	316
B_{3g}	972	962			962	
	827	824			822	
	411	415			410	412

Table III(6)(continued)

B_1 Species (D_{2h} - B_{1g}, B_{1u})

	Calculated frequencies for all θ				Observed frequencies				
					Raman			Infrared	
	0°	30°	60°	90°	Solid	Liquid	Gas	Solid	Liquid
B_{1g}	3070	3070	3070	2070					
	3069	3069	3069	3069					
	1546	1546	1548	1552	1538				
	1375	1374	1370	1367	-				
	1285	1284	1283	1281	1263				
	1234	1235	1238	1242	1224				
	1095	1094	1092	1090	1083			1076	
	616	616	617	618	623			623	624
	361	357	349	340	354			356	355
	182	176	161	144	237			237	
B_{1u}	925	925	925	926				944	
	816	817	820	827				810	808
	696	698	704	710				668	
	460	471	492	509				500/506	497
	220	220	221	222	192			190	-
	33	34	35	39				73	

Table III(6)(continued)

B_2 Species (D_{2h} - B_{2u}, B_{2g})

Calculated frequencies for all θ				Observed frequencies				
				Raman			Infrared	
	0°	30°	60°	90°	Solid	Liquid	Gas	Solid	Liquid
B_{2u}	3070	3070	3070	3069					
	3069	3069	3069	3069					
	1564	1562	1556	1552				1590	
	1364	1364	1365	1367				1382	1383
	1279	1279	1280	1281				1300	1300
	1248	1247	1245	1242					
	1087	1087	1088	1090				1100	1100
	625	624	622	618	632			635	635
	223	223	223	222	-	-	-	-	-
	50	48	43	39				89	
B_{2g}	928	928	927	926				949	
	839	837	833	827	844			848	841
	703	705	708	710	720			720	718
	519	518	516	509	540			542	537
	328	330	335	340	270			271	
	108	113	127	144	112/-			/145	

a finely split band centred at 1300 cm^{-1} in dichloro and dibromobiphenyl. This provides further evidence for a D_2 conformation in the solid state. The major evidence against a D_{2d} conformation is that there are too many bands assigned to the B_1 and B_2 species (greater than 16) even though some of the assignments are weak, missing or unsatisfactory. The Raman band at 413 cm^{-1} for dichlorobiphenyl is polarised (the lowest 'a_u - b_{3g}' pair) with a dipolarisation ratio of 0.41 indicating that D_{2d} symmetry does not occur even in the molten state.

A comparison of the spectra of 4-4'dichloro and dibromobiphenyl below 1000 cm^{-1} in Figs. III(i) and (ii) show that they possess identical features, the lower frequency fundamentals shifted slightly in the dibromo spectra because of the mass effect. Difficulty was experienced in obtaining a uniform crystallised melt spectrum for dibromobiphenyl because the material tended to form globules on the surface. The melt also tended to decompose, such that molten Raman data was not obtained.

3.6 Conclusion

The conformations of 4-4'dichloro and dibromobiphenyl have been shown to be D_2 irrespective of phase. The estimation of the angle, here, is more difficult because there are no shifts and the frequency fit is not as good. The very poor solubilities

of dichloro- and dibromo-biphenyl in common organic solvents compared with biphenyl and difluorobiphenyl indicate a difference in physical properties which may be related to structure.

A preliminary study, without calculations, was carried out on other 4-4'di-substituted biphenyls to investigate the effect of other common organic groups. 4-4'dimethyl, dicyano and dinitro biphenyl gave infrared and Raman spectra similar to dichloro and dibromo-biphenyl and had very poor solubilities. Since no shifts or changes in spectral activities occurred, it was deduced that they possess a D_2 conformation in all phases.

A study of 4-fluoro- and bromo-biphenyl, however, gave similar spectral changes experienced with biphenyl and 4-4'difluoro-biphenyl (43). Calculations were performed for 4-bromobiphenyl using the simple biphenyl model above and making the appropriate changes in symmetry (C_{2v}) and the bromine atom. A b_2 mode was calculated at 440 cm^{-1} and it was predicted to increase in frequency with dihedral angle. A band at 464 cm^{-1} in the infrared spectrum for the solid state shifted to 492 cm^{-1} in solution. The corresponding change in the B_1 symmetry block was predicted for a band to decrease in frequency at 353 cm^{-1}. In fact a Raman and infrared active band at 258 cm^{-1} was observed to move to 238 cm^{-1} in the molten and solution phase.

A study of the vibrational spectra of decafluorobiphenyl (44,45) by Steele et al suggested that the molecule existed in a D_2 conformation in all phases. It was thus decided to examine the vibrational spectra of 1,2,3,4,5-pentafluorobiphenyl (kindly donated by Professor G. Williams of Bedford College) to examine the effect of the strong dipole across the inter-ring bond. Again a D_2 conformation in all phases was confirmed.

It appears that any inductive or mesomeric effects of the groups, whether directed into or away from the ring, have little effect in determining the overall conformation. The change observed for 4-bromobiphenyl suggests that the planar conformation can only be realised when the substituents are either small or few in number, i.e. the determining factor is crystal packing.

CHAPTER 4

The Vibrational Analysis of Deuterated Biphenyls

4.1 Introduction

The estimate of the dihedral angle obtained in Chapter 2 for biphenyl and in Chapter 3 for difluorobiphenyl had a large degree of uncertainty associated with it. This error is to be expected because the first-order calculated frequencies have not been exactly aligned with the observed fundamentals. A perturbational analysis was thus carried out (33) using the solid-state data of biphenyl, perdeuterobiphenyl and biphenyl d-2 so as to refine the force field for the planar conformation. This time, however, inter-ring interaction constants were introduced to improve the large deviation associated with some of the higher frequency ring modes.

The use of deuterated data in the refinement of force fields is very common practice because the number of adjustable parameters always exceeds the number of observables for a large molecule. It is always assumed that the quadratic force-field, which is independent of anharmonic terms, is unaffected by the large mass change. Although deuteration refines the force constants for

deformations involving vibrations of the hydrogen atom to a high degree of accuracy, large uncertainties still arise for motions associated with the ring. Mills has recently pointed out (46) that other isotopic data, involving carbon and nitrogen, can be more useful even though the shifts are much smaller.

Teller and Redlich independently developed the general theory from which all isotopic rules can be derived. If $\lambda_1, \lambda_2 \ldots \lambda_k$ are the roots in a particular symmetry species of the secular equation

$$|G_s F_s - E\lambda| = 0$$

then

$$|F_s G_s| = |F_s| \cdot \mu_1 \cdot \mu_2 \ldots \mu_k$$

$$= \lambda_1 \cdot \lambda_2 \ldots \lambda_k$$

Since F_s will be the same for an isotopic species and $\lambda_k = 4\pi^2 c^2 \nu_k^2$ it follows that

$$\prod \frac{\nu_k'}{\nu_k} = \left(\prod \frac{\mu_k'}{\mu_k} \right)^{\frac{1}{2}}$$

where the prime signifies the isotopic species.

This result is only valid if the symmetry species contains no translation or rotation. If these degrees of freedom are involved the roots will vanish such that the product ratio is

indeterminate. This difficulty is overcome, however, by considering the result of applying weak forces which convert the motions of translation and rotation into low frequency oscillatory motions. In the limit of these vanishing forces (i.e. the coupling is negligible) the ratio of the translatory frequencies is

$$\frac{\nu_T'}{\nu_T} = \left(\frac{M}{M'}\right)^{\frac{1}{2}}$$

where M is the total mass of the molecule, and the rotational ratio is

$$\frac{\nu_R'}{\nu_R} = \left(\frac{I}{I'}\right)^{\frac{1}{2}}$$

where I is the moment of inertia with respect to the appropriate principle axes.

The product rule now takes the form

$$\prod_{k=1}^{3N-6} \frac{\nu_k'}{\nu_k} = \prod_{k=1}^{3N} \left(\frac{m_k}{m_k'}\right)^{\frac{1}{2}} \left(\frac{M'}{M}\right)^{\frac{3}{2}} \left(\frac{I_x' I_y' I_z'}{I_x I_y I_z}\right)^{\frac{1}{2}}$$

The calculated isotopic shifts are useful in assigning some of the more dubious bands.

4.2 Experimental

Biphenyl d-10 was purchased from Merck Sharp and Dohme of Canada Limited. Biphenyl d-2 was synthesised in these laboratories by R. J. W. Pulham and D. P. Sewell as part of a supervised third-year project.

4-4' dibromobiphenyl was prepared as described above (42). n-Butyl lithium reagent was prepared (47) at -10°C in dry ethyl ether by the action of n-butyl bromide on freshly-cut lithium metal. The reaction was carried out in an atmosphere of dry nitrogen and the final product was filtered free of reaction precipitate. The freshly-prepared n-butyl lithium reagent was then rapidly added to an ether solution of dibromobiphenyl and left overnight to stir (48). The mixture was then treated with 99.8% deuterium oxide. The ether phase was washed and dried and the solvent removed by roterary evaporation. The product was sublimed, twice to yield white crystals with a melting point of 66°C.

The purity of these isotopes was assessed by means of their mass spectra kindly run by Dr. W. Wheatley with an A.E.I. MS 12 double-focussing spectrometer using a direct-insertion sample probe. By reducing the operating ionising voltage from 70 eV, to about 10 eV, fragmentation of the molecular ion (M^+) does

not occur. The low-voltage spectra hence record the relative abundance of the deuterated molecular ions. Carbon-13 isotopic abundance of the partially deuterated species will have a negligible effect on the peak heights. Spectra were run at four ionising voltages (12, 11, 10 and 9 eV) and the mean compositions calculated as shown in Table IV(i). The table also shows that the extent of deuteration is 97.6% for biphenyl d-2 and 99.2% for biphenyl d-10.

Table IV(i)

Isotopic Composition of Deuterated Biphenyls

Compound	Percentage composition	Theoretical maximum purity
Biphenyl d-2	$C_{12}H_8D_2$ - 96.5%	99.6%
	$C_{12}H_9D$ - 2.3%	
	$C_{12}H_{10}$ - 1.2%	
Biphenyl d-10	$C_{12}D_{10}$ - 93.3%	98.0%
	$C_{12}H\ D_9$ - 5.6%	
	$C_{12}H_2D_8$ - 1.1%	

4.7 Results and Discussion

The observed Raman and infrared bands are listed in Tables IV(2) and (4) for biphenyl d-2 and d-10 respectively and the corresponding assignments are compiled in Tables IV(3) and (5). Zerbi and Sandroni have recently (49) used their modified UBFF to assign the in-plane fundamentals of most of the symmetrically deuterated biphenyls. The most striking observation in Zerbi's data is the number of bands which have not been assigned simply because they have not been seen, especially in the B_{1g} symmetry block. Difficulty in assignment also arises because of the severe overcrowding of fundamentals expected in the 800 - 860 cm^{-1} region (10 bands) for biphenyl d-10 and in the 600 - 620 cm^{-1} region (5 bands) for biphenyl d-2.

The majority of the fundamentals are assigned as previously described above for biphenyl h-10, but for the areas of ambiguity two lines of approach are adopted. The first is based on the assumption that the intensities of the bands (both Raman and infrared) throughout the series should be roughly comparable. Secondly, the ratio of the calculated data for the isotopic species and that of biphenyl h-10 is compared with the suspected observable ratios to find the best fit. This is admirably

Table IV(2)

Principle infrared and Raman bands of 4-4' dideuterobiphenyl below 2300 cm^{-1}

Infrared		Raman		Assignment
Solid	Liquid	Solid	Liquid(ρ)	
2290w		2294w	2297m	b_{3u}
2270w	2272w	2272m	2272w	a_g
1920s				(2x954)
1790m				
1685m				
		1611w-sh		
		1600vs	1606vs*	a_g
1596w or 1587w		1581w-sh	1583w-sh	b_{3u}
		1593vs	1606vs*	b_{1g}
1555w				b_{2u}
		1509w	1501m	a_g
		1491vw	1491sh-w	
1471s				b_{3u}
1394s	1394s			b_{2u}
	1375m			
	1355m			
1322m	1308m			b_{2u}
		1313w		a_g
	1283w	1288w-sh	1285vs	b_{1g}
		1274vs	1288vs	a_g

Table IV(2)(continued)

Infrared		Raman		Assignment
Solid	Liquid	Solid	Liquid(ρ)	
1262m	1263m	1263w-sh		b_{2u}
		1242vw	1242vw	
		1209w	1187m	a_g
1180m	1178m			b_{3u}
1130 } m				
1115 }	1110s			b_{2u}
		1117 } w	1107w	b_{1g}
		1110 }		
		1027m	1027m	a_g
1034m	1038s			b_{3u}
1007m	1007s			b_{3u}
		988s	990vs	a_g
	978m			b_{3u}
		975w-sh	967sh-m	b_{2g} ?
	964vw			b_{3g}
954vw	953*vw			b_{1u}/b_{2g} ?
	874vw sh	876m	869m	b_{1g}
	868vw-sh	865w		b_{2g}
862m	859s			b_{2u}
	838vs	845vw	838m	b_{3g}/a_u
841s	843vs			b_{1u}
767w	764m			

Table IV(2)(continued)

Infrared Solid	Infrared Liquid	Raman Solid	Raman Liquid(ρ)	Assignment
		743 m	744m	b_{2g}
	736m	738		
		734m	735s	a_g
716m	720s			b_{1u}
	697m			
610vs d	610*vs		617sh-m	b_{1u}/b_{2u}
604vs	602*vs	605m	603*s	$b_{3u}/b_{1g}/b_{2g}$
		597w	603s*	b_{2g}
	535m	538w	535w	b_{2g}
449m	477s			b_{1u}
	403vs	408vvw	405s	b_{3g}/a_u
	359w			b_{1g}
	305w	324m	309s	a_g
	259w	241m	262m	b_{2g}
		93m		Lattice modes
		55m		
		43m		
		25m		

Table IV(3)

Calculated and observed frequencies (cm^{-1}) for 4-4' dideutero-biphenyl for various dihedral angles

A Species (D_{2h} - A_g, A_u)

	Calculated frequencies for all θ	Observed frequencies			
		Raman		Infrared	
		Solid	Liquid(ρ)	Solid	Liquid
A_{gu}	3072				
	3072				
	2282	2276	2277(0.25)		
	1689	1600	1607*(0.25)		
	1516	1509	1501(0.24)		
	1338	1274	1281(0.22)		
	1192	1209	1187(0.15)		
	1024	1031	1027(0.07)		
	978	988	990(0.10)		
	738	734	735(0.10)		
	269	324	309(0.31)		305
Au	963		967*(0.11)		
	833		838*(0.31)		
	409		403*(0.35)		

Table IV(3)(continued)

B3 Species (D_{2h} - B_{3u}, B_{3g})

Calculated frequencies for all θ		Observed frequencies			
		Raman		Infrared	
		Solid	Liquid(ρ)	Solid	Liquid
B_{3u}	3072				
	3072				
	2282			2296	2297
	1603			1596/1587	
	1478			1471	
	1193			1180	1178
	1035			1034*	1038
	1019			1007	1008
	976				978
	604			604	602*
B_{3g}	963	975	967*(0.11)		964
	833	845	838*(0.31)		838
	409	408	403*		403

Table IV(3)(continued)

B1 Species (D_{2h} - B_{1g}, B_{1u})

	Calculated frequencies for θ =				Observed frequencies			
					Raman		Infrared	
	0°	30°	60°	90°	Solid	Liquid(ρ)	Solid	Liquid
B_{1g}	3070	3070	3070	3070	No measurements due to complexity			
	3069	3069	3069	3069	of overtone and combination bands			
	1608	1606	1604	1603	1593	1607*		
	1404	1401	1395	1388				
	1320	1319	1317	1315	1313			
	1280	1281	1283	1286	1288			1283
	1095	1094	1093	1091	1110/ 1117	1107		
	868	868	868	868	876	869*(0.79)		874
	604	605	605	606	605	603		610*
	340	322	293	267				359
B_{1u}	955	955	955	956			954	953*
	837	837	839	843			841	843
	714	716	723	731			716	720
	613	614	615	616		617*	610*	610*
	413	434	466	490			449	477
	88	88	88	89				

Table IV(3)(continued)

B3 Species (D_{2h} - B_{2u}, B_{2g})

	Calculated frequencies for θ =				Observed frequencies			
					Raman		Infrared	
	0°	30°	60°	90°	Solid	Liquid(ρ)	Solid	Liquid
B_{2u}	3070	3070	3070	3070				
	3069	3069	3069	3069				
	1605	1604	1603	1603			1555	
	1377	1378	1381	1388			1393	1394
	1312	1312	1313	1315			1322	1308
	1290	1290	1289	1286			1262	1263
	1088	1088	1089	1091			1131/ 1115	1110
	865	866	867	868			862	859
	619	618	617	616		617*	610*	610*
	95	94	91	89				
B_{2g}	958	957	957	956				953*
	854	852	848	843	865	869*(0.79)		868
	730	731	732	731	738/ 743	744(0.76)		736
	608	608	607	606	597	603		602*
	505	504	501	490	538	535		535
	229	234	248	267	241	255		259

Table IV(4)

Principle infrared and Raman bands of biphenyl D-10 below 1700 cm^{-1}

Infrared		Raman		Assignment
Solid	Liquid	Solid	Liquid(ρ)	
1620w	1614w			
1607w	1600w			
		1576m		
		1563vs	1571vs	a_{1g}
1566m	1565s			b_{3u}
1534w	1545w			
		1533w	1537vw	b_{1g}
1522w	1525w			b_{2u}
1440w	1438w			
1412w	1412w			
		1411m	1415s	a_{1g}
1400w	1400w			
		1398w	1401w	
	1370w			
		1347w	1343vw	b_{1g}
1343vs	1344vs			b_{3u}
	1325w			
1317m	1314m			b_{2u}
	1295w			
		1280w	1278vw	b_{1g}
1260m	1263m			b_{2u}

Table IV(4)(continued)

Infrared		Raman		Assignment
Solid	Liquid	Solid	Liquid(ρ)	
		1231vw		
		1216vw	1221vw	
1200w	1195m			
		1186s	1190vs	a_{1g}
1116w	1117m			
	1092w			
1024w	1024w			b_{2u}
	1007m		1006vw	b_{1g}
981w	981m			b_{3u}
		965s	962vs	a_{1g}
950vw	950w			b_{3u}
		880m	872m	a_{1g}
854s	860w			b_{3u}
844m	843m	850m	842m	b_{1g}, b_{2u}
		846m		a_{1g}
	830w-sh	831w	828ww	b_{1g}
818vw	825m			b_{2u}
	815vs*	816w		b_{2g}
813s				b_{3u}
			786w	a_u
	782*			b_{2g}, b_{3g}
742m	744s			b_{1u}

Table (IV(4)(continued)

Infrared		Raman		Assignment
Solid	Liquid	Solid	Liquid(ρ)	
		690m	691m	a_{1g}
		657m		
	652m*	658m d	652m**	a_u, b_{3g}
		651m		b_{2g}
620m	624s			b_{1u}
			597sh	(2x299)
594vw	596w			b_{2u}
588m	585s*			b_{3u}, b_{1g}
		583m	588m	b_{1g}
560w	564w			
	550m-sh	539w	551w	b_{2g}
538vs	542vs			b_{1u}
	464s	459vw		b_{2g}
410m	437s			b_{1u}
	352m	354vw	348m	a_u, b_{3g}
	334s			b_{1g}
	300w	312m	299m	a_{1g}
	248w	225m	243m	b_{2g}
165vw				
112vs	105vs			b_{2u}
	79vw			
83vw	73vw			b_{1u}
	61vw			

Table IV(5)

Calculated and observed frequencies (cm^{-1}) for biphenyl D-10 for various dihedral angles

A Species (D_{2h} - Ag, Au)

	Calculated frequencies for all θ	Observed frequencies			
		Raman		Infrared	
		Solid	Liquid(ρ)	Solid	Liquid
Ag	2287				
	2285				
	2280				
	1678	1563	1571(0.36)		
	1457	1411	1415(0.16)		
	1198	1186	1190(0.11)		
	951	965	962(0.06)		
	862	880	872(0.04)		
	840	846	842(0.34)		
	699	690	691(0.04)		
	261	312	299(0.12)		300
Au	780		786(0.25)		
	648		652*(0.48)		
	358		348(0.40)		

Table IV(5)(continued)

B3 Species (D_{2h} - B_{3u}, B_{3g})

	Calculated frequencies for all θ	Observed frequencies			
		Raman		Infrared	
		Solid	Liquid(ρ)	Solid	Liquid
B_{3u}	2287				
	2285				
	2280				
	1591			1566	
	1320			1343	1344*
	988			981	981
	947			950	950
	855			854	860
	823			813	815*
	590			588	586*
B_{3g}	780		786*		782**
	648	655/657	652*		652*
	358	354			352

Table IV(5)(continued)

B1 Species

	Calculated frequencies for θ = 0°	30°	60°	90°	Observed frequencies Raman Solid	Raman Liquid(ρ)	Infrared Solid	Infrared Liquid
B_{1g}	2281	2281	2281					
	2279	2279	2279	2279				
	1584	1583	1581	1581	1533	1537		
	1304	1301	1294	1289	1347	1343		1344*
	1277	1277	1279	1278	1280	1278		
	1038	1037	1033	1028		1006		1007
	840	840	840	840	850	842*		843*
	822	822	822	821	831	828		825
	583	583	585	587	583	588		585*
	319	302	276	254				334
B_{1u}	820	820	821	821			818	815*
	729	731	737	746			742	744
	613	616	623	631			620	624
	539	539	542	545			538	542
	387	404	430	446			410	437
	85	85	85	85			83	61(?)

Table IV(5)(continued)

B2 Species

	Calculated frequencies for θ =				Observed frequencies			
					Raman		Infrared	
	0°	30°	60°	90°	Solid	Liquid(ρ)	Solid	Liquid
B_{2u}	2281	2281	2281	2281				
	2278	2278	2278	2279				
	1582	1581	1580	1580			1522	
	1297	1296	1292	1289			1317	1314
	1262	1264	1269	1278			1260	1263
	1015	1018	1022	1028			1024	1024
	841	841	841	840			844	843
	822	822	821	821			818	815*
	596	594	591	587			594	596
	89	88	87	85			112	105
B_{2g}	826	826	825	822	816			815*
	759	758	753	746				782
	629	630	632	631	651	652*		652*
	549	548	547	543	539	551		550
	450	450	451	446	459	465		464
	221	226	237	254	225	243(0.65)		248

illustrated by the assignment of the ν_8 and ν_9 a_{1g} modes of biphenyl d-10. Using the data of biphenyl itself ν_8 and ν_9 are estimated to occur at 872 cm^{-1} and 843 cm^{-1} respectively. They in fact appear in the Raman solid state at 880 cm^{-1} and 846 cm^{-1}.

The same trends concerning spectral shifts also occur in the deuterated species. The ν_{10} b_{1g} modes are again inactive in the Raman but occur in the solution infrared as broad bands at 359 cm^{-1} for biphenyl d-2 and 334 cm^{-1} for biphenyl d-10. The infrared active ν_5 b_{1u} band moves from 449 cm^{-1} in the solid state to 477 cm^{-1} in solution for biphenyl d-2 and from 410 cm^{-1} to 437 cm^{-1} for biphenyl d-10, a shift of 28 cm^{-1} in both cases similar to biphenyl itself. Unfortunately interferometric work was not done with biphenyl d-2 but the ν_{10} b_{2u} mode of d-10 moved from 112 cm^{-1} to 105 cm^{-1}. The Raman active ν_6 b_{2g} modes were observed to shift from 241 cm^{-1} in the solid state to 255 cm^{-1} in solution for d-2 and from 225 cm^{-1} to 243 cm^{-1} for d-10.

Biphenyl d-2 exhibits the ortho-β_{C-H} steric effect with a shift of 22 cm^{-1} is ν_7 a_{1g} and 14 cm^{-1} in ν_5 b_{2u}. The corresponding high frequency shifts are not observed in biphenyl d-10 but both molecules show the characteristic shift in the lowest a_{1g} mode (324 cm^{-1} to 307 cm^{-1} for d-2 and 312 cm^{-1} to 299 cm^{-1} for d-10).

4.4 Perturbational Analysis

The solid state data for the three biphenyl species were used to refine the force field of the planar molecule using an iterative program written by Mr. R. A. R. Pearce. A preliminary perturbational analysis involved a refinement of the diagonal

Table IV(6)

1. 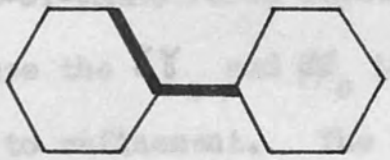 $f_{R.R} = 0.301$ mdyne/Å

2.  $f_{R} = -0.887$ mdyne/Å

3. 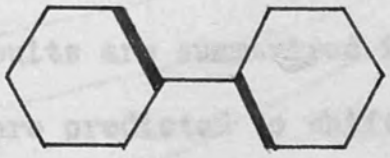 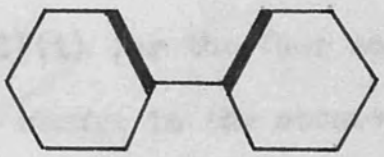 $f_{R.R} = 0.256$ mdyne/Å

4. $\gamma_{ring} - \gamma_{ring} = -0.010$ mdyne/Å

and then the off-diagonal constants but no improvement was observed for the high-frequency ring modes. However, when the inter-ring in-plane interaction constants of Table IV(6) were introduced and allowed to find their own values the fit was

dramatically improved. The numerical values and signs of these force constants are consistent with those of benzene-type interaction constants. Especially striking is the value and sign of f.c.2 which is predicted from the qualitative reasoning in Chapter 1. An increase in the inter-ring C-C bond length will result in a decrease in p-character in the ring and favour an opening of the adjacent angle.

The out-of-plane force constants proved more difficult to refine because the $\gamma\gamma_{o_1}$ and $\phi\phi_o$ interaction constants were insensitive to refinement. The fit, however, was improved by the introduction of f.c.4.

The final force field was then used to calculate the variation of the fundamental frequencies with dihedral angle. The results are summarised in Fig. IV(i) for the four modes which are predicted to shift. The change in the observed fundamentals was then plotted to give a more accurate estimate of the dihedral angle. This estimate lies within the range $30^\circ \pm 5^\circ$ for the ν_5 b_{1u}, ν_{10} b_{2u} and ν_6 b_{2g} modes. A value near 40° is predicted for the ν_{10} b_{1g} mode but this is probably an overestimate because the band is inactive in the solid state and the observed change in frequency cannot be calculated. The introduction of the force constants in Table IV(6) no longer make the A1 and B3 species invariant

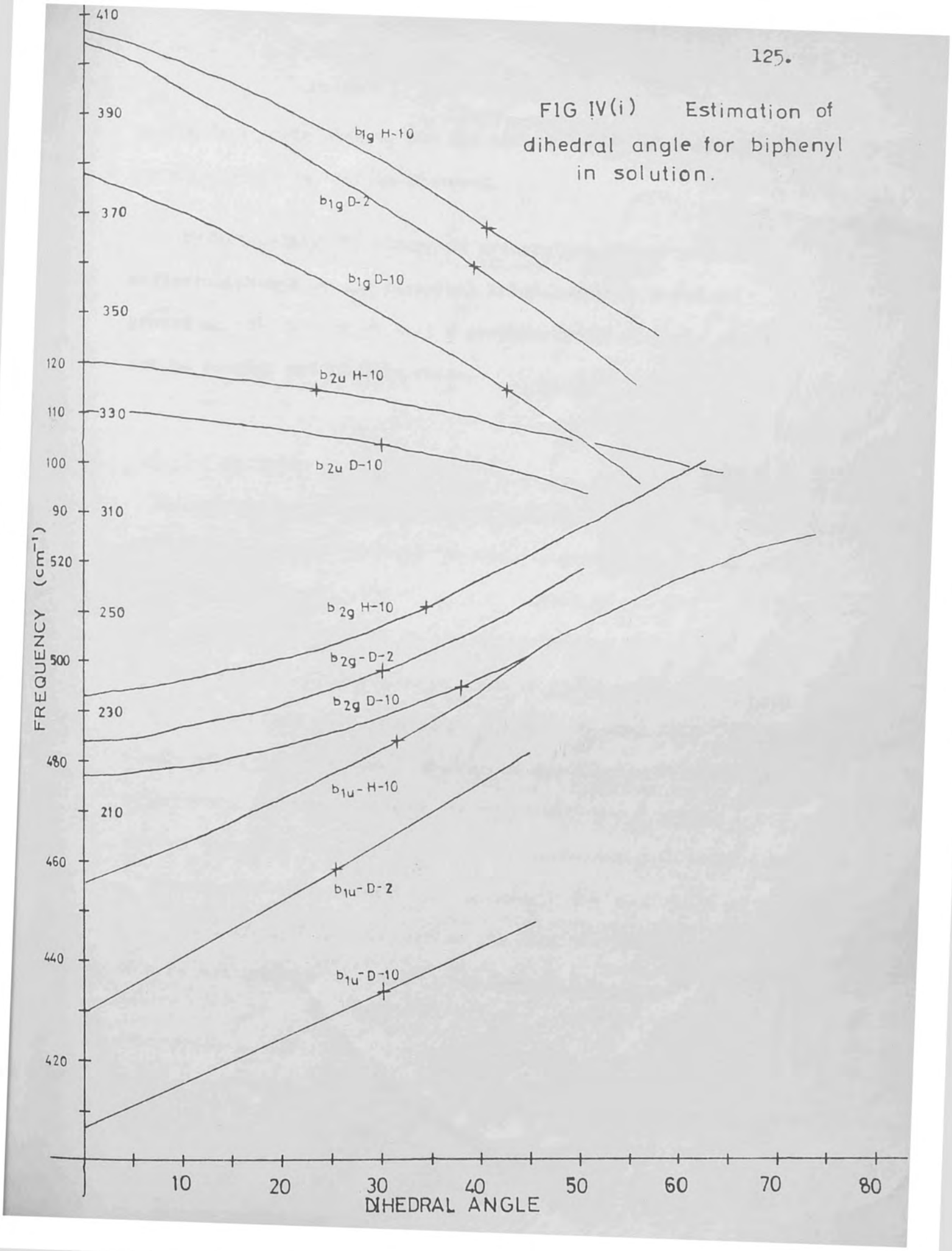

FIG IV(i) Estimation of dihedral angle for biphenyl in solution.

to dihedral angle change, but the very small changes calculated cannot explain the shifts observed.

Unfortunately the attempted preparation of perdeutero-difluorobiphenyl by the classical Friedel-Crafts technique proved unsatisfactory so that a perturbational analysis could not be carried out at this stage.

CHAPTER 5

Conformational Studies of Some Monohalogeno Tetrahydropyrans

SECTION A: Infrared and Raman Studies

5.1 Introduction

Cyclohexane and substituted cyclohexanes have been studied extensively by many physical techniques, partly, no doubt, because of the easy accessibility of many cyclohexanes and partly because such studies are of value in the understanding of the spectra of the many natural products which contain cyclohexane systems. Many reviews have ably summarised the work to date (50, 51, 52). Little work, however, has been done on the six-membered oxygen-heterocycle analogues, namely the tetrahydropyrans and this chapter presents the spectroscopic and conformational properties of some 4-monohalogeno tetrahydropyrans. The preference of a functional group X for the equatorial over the axial conformation is measured by the equilibrium constant K.

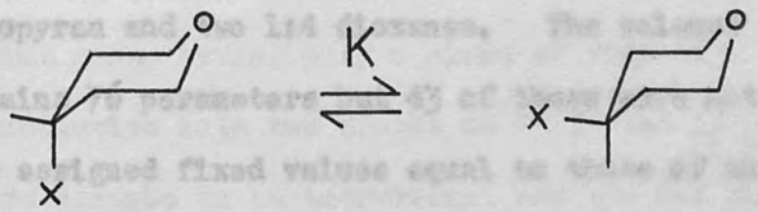

The free energy change ΔG is then readily calculated from the relationship

$$\Delta G = -RT \ln K$$

If desired the other thermodynamic parameters, ΔH and ΔS, can be found from measurements at two or more temperatures.

In the past, detailed vibrational analyses have not been performed on such molecules and an empirical approach for the assignment of bands has been adopted. Consequently there has been much uncertainty and discussion over the original ν (C-X) assignments of Larnaudic (53). More recently, however, Hallam and Ray (54) have established a linear relationship between the $\Delta\nu$ (C-X) shifts in various solvents and the corresponding shifts of a reference compound, cis-dichloro ethylene. Table V (1) summarises the ν (C-X) assignments for the monohalogeno cyclohexanes and tetrahydropyrans.

Normal coordinate calculations have been made possible owing to the availability of a force field derived for ten simple aliphatic ethers by Snyder and Zerbi (57), which included tetrahydropyran and two 1:4 dioxanes. The valence force field contains 76 parameters but 43 of these were not adjusted but were assigned fixed values equal to those of analogous force constants determined from earlier studies on the paraffins (16). These values appear in parentheses in Table V (2).

Table V (1)

Compound	Equatorial(cm^{-1})	axial(cm^{-1})	Ref.
Cyclohexyl fluoride	1129	1062	53
	1053	1020	51
Cyclohexyl chloride	742	688	53
Cyclohexyl bromide	687	658	53
Cyclohexyl iodide	654	638	53
	672		55
	653.9	652.8	56
4-Chloro tetrahydropyran	757	718	this work
4-Bromo tetrahydropyran	717	694	this work

The force field was modified for the halogeno part of the molecule by assuming a transferability of force constants from studies by Snyder of the n-alkyl chlorides (58) and bromo substituted alkanes (59).

5.2 Experimental

The molecular model under consideration belongs to the C_s point group having only a plane of symmetry. The 42 normal modes symmeterise into two blocks as 23 A' and 19 A''. All bond angles were assumed to be tetrahedral and the C-O bond distance was assumed to be equivalent to the C-C bond distance of 1.54 Å. Other bond

lengths were taken as follows: C-H 1.096 Å, C-Cl 1.767 Å and C-Br 1.94 Å. Calculations were only performed for the equatorial chair conformation. Atomic masses (60) were taken as follows: H - 1.00797, C - 12.01115, O - 15.9994, Cl - 35.453, Br - 79.916 and a calculation involving both isotopes of chlorine showed that only the ν (C-Cl) fundamental was affected by 2 cm^{-1}. The force field of tetrahydropyran (THP) is tabulated in Table V (2) with the additional force constants of 4-chloro-THP in Table V (3) and 4-bromo-THP in Table V (4). The observed bands are listed in Tables V (5), (7) and (9) and illustrated in Fig. V (i).

Preparations

The preparation of the 4-halogeno tetrahydropyrans requires 3-butene-1-ol as starting material.

Preparation of 3-butene-1-ol Allyl carbinol was prepared following the method of Nystrom and Brown (61) by the selective reduction of vinyl acetic acid (3-butenoic acid) in anhydrous ether. A solution of 45 g (1.17 mole) of lithium aluminium hydride in 600 ml. of sodium-dried ether was placed in a two litre three-necked flask equipped with reflux condenser, dropping funnel and mechanical stirrer, and protected from atmospheric moisture by a calcium chloride tube. Through the dropping funnel a solution of 80 g

(0.93 mole) of vinyl acetic acid (B.D.H.) in 400 ml. of ether was added at such a rate to produce a gentle reflux. After the addition was completed water was added cautiously to decompose excess hydride. 500 ml. of 10% sulphuric acid was then added with cooling under ice and the contents were extracted many times with ether. The extracts were dried with anhydrous magnesium sulphate. A crude product was obtained on rotary evaporation which was distilled under vacuum to give 3-butene-1-ol. (b.pt. 113°C (760 mm), yield 47.7%)

$$CH_2 = CH\ CH_2CO_2H \xrightarrow[\text{dry ether}]{LiAlH_4} CH_2 = CH\ CH_2CH_2OH$$

<u>Preparation of tetrahydropyran 4-ol.</u> T.H.P.-4-ol was prepared by a Prin's cyclisation outlined by Hanachke (62). 30 g (0.42 mole) of 3-butene-1-ol and 40 ml. of a freshly-prepared saturated paraformaldehyde solution (prepared by heating paraformaldehyde and distilled water overnight) are added to a 500 ml. 3-necked flask equipped with a condenser, dropping funnel and mechanical stirrer. 6 ml. concentrated sulphuric acid was then added dropwise to the mixture at 80°C at such a rate that charing did not occur. The mixture was heated for a further four hours and then neutralised with a sodium hydroxide solution. The product was extracted with ether and the extracts dried over anhydrous magnesium sulphate. After rotary evaporation the

crude product was distilled under vacuum to give a 74.4% yield of tetrahydropyran-4-ol (b.pt 86°C (11 mm)). Vapour phase chromatography showed the presence of two higher-boiling impurities (3%) which could not be separated on further distillation.

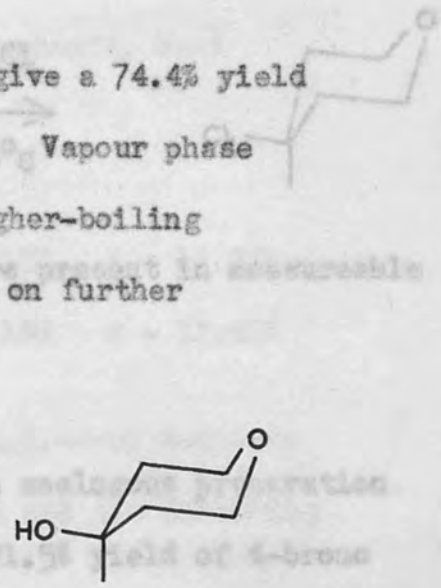

<u>Preparation of 4-chloro tetrahydropyran.</u> 50 g (0.71 mole) of 3-butene-1-ol was placed in a 500 ml. 3-necked flask equipped with a condenser, mechanical stirrer and bleed together with 100 ml. saturated formaldehyde solution in the presence of excess paraformaldehyde powder. Hydrogen chloride from a small lecture bottle was bubbled via a tap through the contents of the flask, cooled in an ice-bath, at a steady rate until the solution was saturated (i.e. all the paraformaldehyde had dissolved) care being taken to avoid sudden suck back. The solution was then neutralised with sodium hydroxide at 0°C and the aqueous solution extracted with diethyl ether. The ether extracts were dried with anhydrous magnesium sulphate and rotary evaporation yielded crude 4-chloro tetrahydropyran. Distillation under vacuum gave a colourless liquid (b.pt 42° at 12 mm of Hg) in 44.5% yield.

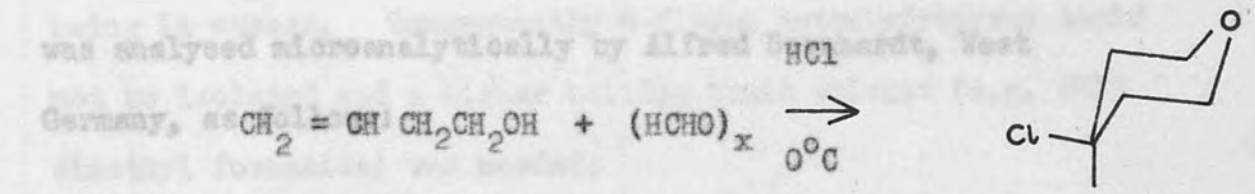

G.L.C. analysis indicated no impurities were present in measureable quantity.

Preparation of 4-bromo tetrahydropyran. An analogous preparation to the above with hydrogen bromide gave a 21.5% yield of 4-bromo tetrahydropyran (b.pt 65° at 19 mm). G.L.C. analysis indicated two higher-boiling impurities which could not be separated on further distillation.

Preparation of toluene-p-sulphonate derivative of T.H.P.-4-ol.

10 g (0.1 mole) of T.H.P.-4-ol was dissolved in 90 ml. of dry (NaOH) pyridine and cooled to -5^oC in an ice-salt bath. 20 g of tosyl chloride (B.D.H. m.pt 68^oC) was added in one portion to the mixture and swirled until dissolved. After allowing to cool for 2 hrs. at 0^oC a small amount (5 ml.) of water was added with shaking and the mixture quickly poured into 100 ml. of distilled water.

White crystals immediately precipitated out which were recrystallised to constant melting point in ethanol to give a yield of 86.4%. The previously unreportedcoompound (m.pt 54.5^oC)

was analysed microanalytically by Alfred Bernhardt, West Germany, as follows:

RMB1 C - 56.15% H - 6.35% O - 25.11% S - 12.37%

RMB2 C - 56.11% H - 6.18% O - 25.16% S - 12.42%

A compound with the composition of T.H.P.-4-ol tosylate would have a molecular formula of $C_{12}H_{16}O_4S$ and the following percentage composition:

C - 56.25% H - 6.25% O - 25.00% S - 12.50%

$$Me - C_6H_5 - SO_2Cl + T.H.P.-4-ol \xrightarrow[0^\circ C]{Py} Me-C_6H_5SO_2.OC_5H_9O + HCl$$

<u>Preparation of 4-fluoro tetrahydropyran</u>. An attempt to prepare this compound, previously unreported, was made by the action of the carbohydrate fluorinating agent tetra n-butyl ammonium fluoride (kindly supplied by Dr. J.H. Westwood, Chester Beatty Research Institute, London), 10 g (0.04 mole) on the tosylate of T.H.P.-4-ol dissolved in 100 ml. pure dry acetonitrile (B.D.H. b.pt 81°C). A slight excess of tetra n-butyl ammonium fluoride 15 g (0.06 mole) was added and the mixture refluxed for approximately 3 hours. After leaving overnight the solution was distilled under vacuum leaving a treacle coloured compound as residue. G.L.C. analysis indicated the presence of two components in the distillate with almost the same boiling points, the solvent

being in excess. Consequently 4-fluoro tetrahydropyran could not be isolated and a higher boiling ionic solvent (e.g. DMF dimethyl formamide) was needed.

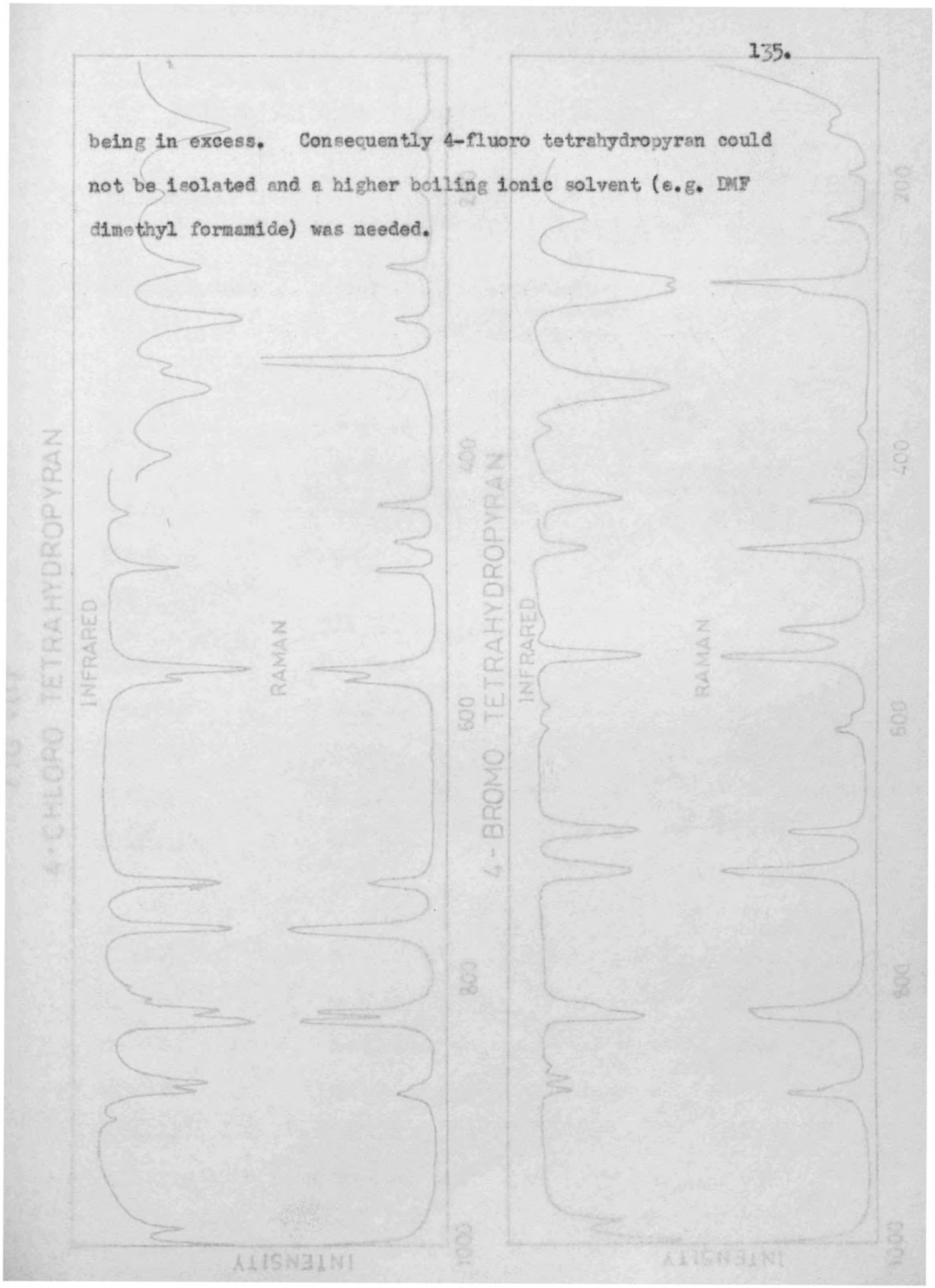

FIG V(1)

4-CHLORO TETRAHYDROPYRAN

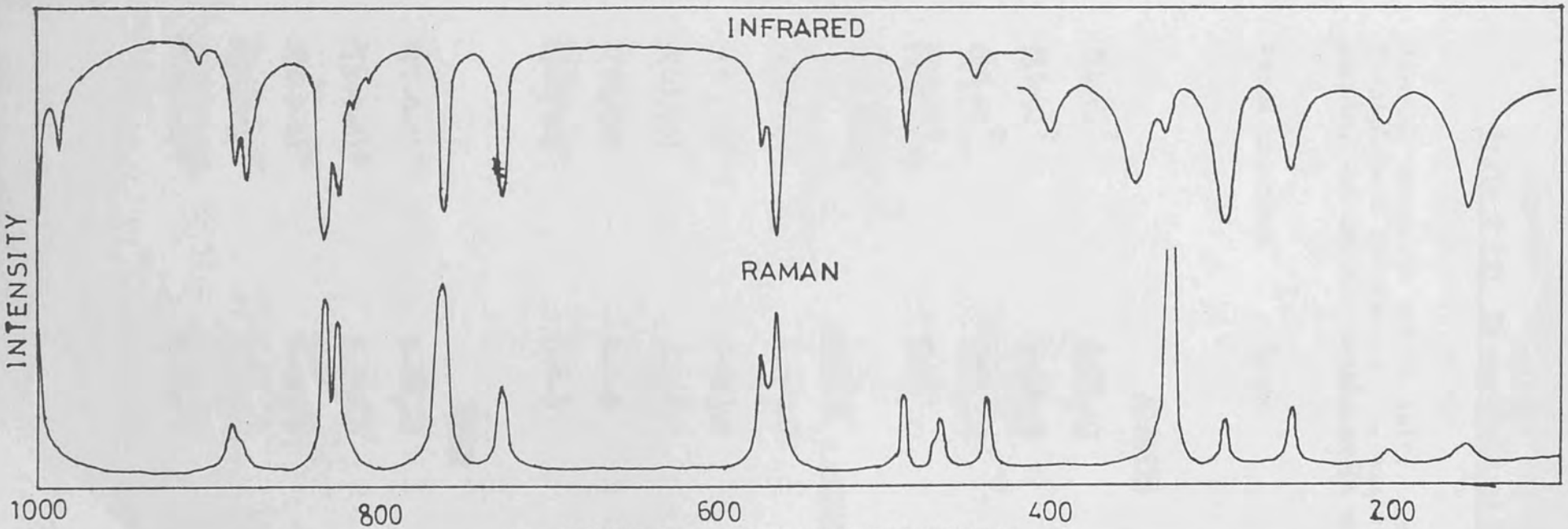

4-BROMO TETRAHYDROPYRAN

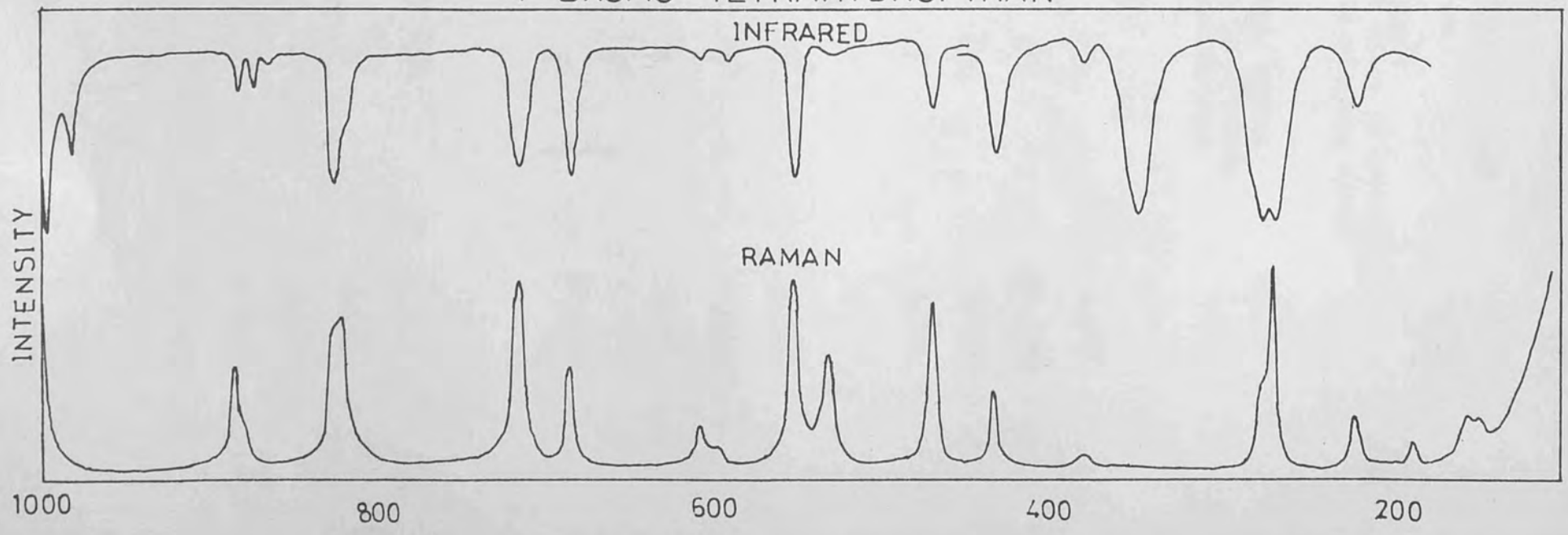

Table V (2) Force Field of Tetrahydropyran

Stretch constants are in units of mdyne/Å
Stretch-bend interaction constants in units of mdyne/rad.
Bending and torsion constants in units of mdyne Å/rad^2

Force constant	Group	Atoms common to interacting co-ordinates	Value
	STRETCH		
$f(C-H)^2$	$C-CH_2-O$	-	4.626
$f(C-H)^2$	$C-CH_2-C$	-	(4.554)
$f(C-O)^2$	C-O	-	5.090
$f(C-C)^2$	C-C	-	4.261
	STRETCH - STRETCH		
f(CH/CH)	$C-CH_2-O$	C	-0.046
f(CH/CH)	$C-CH_2-C$	C	(0.006)
f(CO/CO)	C-O-C	O	0.288
f(CC/CO)	C-C-O	C)	
		)	(0.101)
f(CC/CC)	C-C-C	C)	
	BEND		
$f(H-C-H)^2$	$C-CH_2-O$	-	0.471
$f(H-C-C)^2$	$C-CH_2-O$	-	0.752
$f(H-C-O)^2$	$C-CH_2-O$	-	0.901
$f(H-C-H)^2$	$C-CH_2-C$	-	(0.550)
$f(H-C-C)^2$	$C-CH_2-C$	-	(0.656)

Force constant	Group	Atoms common to interacting co-ordinates	Value
$f(C-O-C)^2$	C-O-C	-	1.313
$f(C-C-O)^2$	C-C-O	-	1.182
$f(C-C-C)^2$	C-C-C	-	1.071
	STRETCH - BEND		
f(CO/HCO)	$C-CH_2-O$	C-O	0.387
f(CC/HCC)	$C-CH_2-O$	C-C	0.478
f(CC/HCC)	$C-CH_2-C$	C-C	(0.328)
f(CO/HCC)	$C-CH_2-O$	C	0
f(CC/HCO)	$C-CH_2-O$	C	0
f(CC/HCC)	$C-CH_2-C$	C	0.079
f(CO/COC)	C-O-C	C-O	0.483
f(CO/CCO)	C-C-O	C-C	0.618
f(CC/CCO)	C-C-O	C-C	0.403
f(CC/CCC)	C-C-C	C-C	(0.417)
	BEND - BEND		
f(HCO/HCO)	$C-CH_2-O$	C-O	-0.005
f(HCC/HCC)	$C-CH_2-O$	C-C	0.105
f(HCO/HCC)	$C-CH_2-O$	C-H	0.115
f(HCC/HCC)	$C-CH_2-C$	C-C	(-0.021)
f(HCC/HCC)	$C-CH_2-C$	C-H	(0.012)

Force constant	Group	Atoms common to interacting co-ordinates	Value
$f(H_aCC/H_bCC)$	(O or C)-CH_2-CH_2-C	H_aC-CH_b gauche	(-0.005)
$f(H_aCC/H_bCC)$	(O or C)-CH_2-CH_2-C	H_aC-CH_b trans	(0.127)
$f(H_aCC^1/H_bC^1C^2)$	(O or C)-CH_2-C^1H_2-	C^* gauche	(0.009)
$f(H_aCC^1/H_bC^1C^2)$	(O or C)-CH_2-C^1H_2-	C^* trans	(0.002)

* If the plane formed by atoms H_aCC^1 bisects the angle formed by atoms $H_bC^1C^2$ then f is designated as gauche; otherwise it is trans.

f(HCO/CCO)	C-CH_2-O	C-O	)
f(HCC/CCO)	C-CH_2-O	C-C	) (-0.031)
f(HCC/CCC)	C-CH_2-C	C-C	)
f(HCO/COC)	CH-O-C	gauche H-C-O-C	0.004
f(HCO/COC)	CH-O-C	trans H-C-O-C	-0.112
f(HCC/CCO)	CH-C-O	gauche H-C-C-O	-0.113
f(HCC/CCO)	CH-C-O	trans H-C-C-O	0.028
f(HCC/CCC)	(O or C)-CH-C-C	gauche H-C-C-H	(-0.052)
f(HCC/CCC)	(O or C)-CH-C-C	trans (H)C-C(H)	(0.049)
f(COC/OCC)	C-O-C-C	gauche (C)-O-C-(C)	)
f(CCC/CCO)	C-C-C-O	gauche (C)C-C(O)	) (0.011)
f(CCC/CCC)	C-C-C-C	gauche (C)C-C(C)	)

Force constant	Group	Atoms common to interacting co-ordinates	Value
f(COC/OCC)	C-O-C-C	trans (C)-O-C-(C)	
f(CCC/CCO)	C-C-C-O	trans (C)-C-C-(O)	(-0.011)
f(CCC/CCC)	C-C-C-C	trans (C)C-C(C)	

TORSION

Torsion about $C_m - O_n$

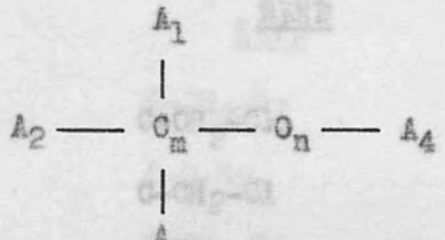

$$T_{mh} = 3^{-\frac{1}{2}} \sum_{i}^{3} T_{imn\,4}$$

Torsion about $C_m - C_n$

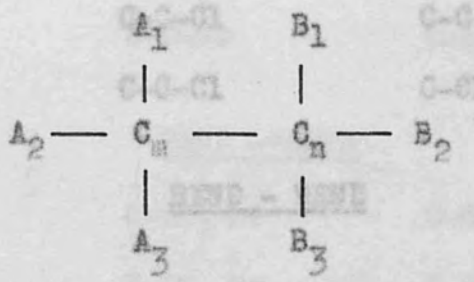

$$T_{mn} = 3^{-\frac{1}{2}} \sum_{i,j}^{3} T_{imnj}$$ where A_i and B_j are trans across $C_m - C_n$

T(C-O)	C-O	-	0.026
T(C-C)	C-C	-	(0.024)

Table V (3) Additional valence force constants for the n-alkyl chlorides

Force constant	Group	Atoms common to interacting co-ordinates	Value
	STRETCH		
$f(C-H)^2$	$C-CH_2-Cl$	-	(4.846)
$f(C-Cl)^2$	C-Cl	-	3.231
	STRETCH - STRETCH		
f(C-C/C-Cl)	C-C-Cl	C	(0.730)
	BEND		
$f(H-C-C)^2$	$C-CH_2-Cl$	-	0.692
$f(H-C-Cl)^2$	$C-CH_2-Cl$	-	0.879
$f(C-C-Cl)^2$	C-C-Cl	-	0.936
	STRETCH - BEND		
f(CCl/HCCl)	$C-CH_2-Cl$	Cl-Cl	(0.333)
f(CC/CCCl)	C-C-Cl	C-C	0.084
f(CCl/CCCl)	C-C-Cl	C-Cl	(0.550)
	BEND - BEND		
f(HCC/HCCl)	$C-CH_2-Cl$	H-C	0.087
f(HCC/CCCl)	$Cl-C-CH_2$	gauche (H)C-C(Cl)	(-0.037)
f(CCC/CCCl)	C-C-C-Cl	trans (C)C-C(Cl)	0.026

Table V (4)

Additional valence force constants for some branched alkyl bromides

Force constant	Group	Atoms common to interacting co-ordinates	Value
	STRETCH		
$f(C-H)^2$	$C-CH_2-Br$	-	4.588
$f(C-Br)^2$	C-Br	-	2.312
	STRETCH - STRETCH		
f(CC/CBr)	C-C-Br	C	0.347
	BEND		
$f(H-C-Br)^2$	$C-CH_2-Br$	-	0.736
$f(C-C-Br)^2$	C-C-Br	-	1.052
$f(H-C-C)^2$	$C-CH_2-Br$	-	0.657
	STRETCH - BEND		
f(CBr/HCBr)	$C-CH_2-Br$	C-Br	0.226
f(CC/CCBr)	C-C-Br	C-C	0.121
f(CBr/CCBr)	C-C-Br	C-Br	0.421
	BEND -=BEND		
f(HCC/HCBr)	$C-CH_2-Br$	C-H	0.088
f(HCC/CCBr)	$C-CH_2-Br$	C-C	-0.030
f(HCBr/CCBr)	$C-CH_2-Br$	C-Br	-0.031
f(CCBr/CCBr)	C-CHBr-C	C-Br	-0.041

Force constant	Group	Atoms common to interacting co-ordinates	Value
f(CCC/CCBr)	C-CHBr-C	C-Br	-0.041
f(HCC/CCBr)	CH_2-CHBr	gauche (H)C-C(Br)	-0.030
f(CCBr/CCC)	C-C-C-Br	trans (C)C-C(Br)	0.093

Table V (5)

The infrared and Raman bands of tetrahydropyran and their assignment

I.R.	Raman (ρ)	Assignment
254 s	253 w (0.84)	A"
	404 m (0.13)	A'
430 vw	434 m (0.90)	A"
	459 m	A'
565 m	565 vvw	A'
810 sh-w		A"
816 m	818 vs (0.05)	A'
855 m	856 w	A'
873 vs	873 vw	A"
968 m	971 vvw	A"
1010 m	1011 s (0.73)	A'
1030 m	1032 s (0.64)	A'
1047 s	1049 vs (0.82)	A"
1090 vs		A"
1155 w	1158 m	A'
	1172 w	A"
1196 s	1198 w	A"
1255 m	1258 m	A'
1272 m	1274 s	A'
1298 m	1301 s	A'
1350 w	1350 w	A"
1360 w		A"

I.R.		Raman (ρ)		Assignment
1382 m	A'	1385 vw	A"	A'
1433 m		1438 s		A"
1440 m		1442 sh-s		A"
1453 m		1456 s		A'
1467 m		1468 w-sh		A'

Table V (6)

Calculated frequencies and assignments for tetrahydropyran

A'		A"		
2969		2967		
2932		2927		
2926		2861		
2862		2855		
2856		1459	1442	
2854		1452	1438	
1465	1467	1389	1360	
1456	1456	1368	1350	
1448	-	1319	-	
1391	1385	1254	-	
1324	1301	1222	1198	dp
1246	1274	1168	1174	
1234	1258	1105	1090	
1138	1158 p	1078	1049	dp
1077	1032 p	968	971	
979	1011 p	876	873	
889	-	814	810	
852	856	453	434	dp
806	818 p	232	253	dp
565	565			
450	459			
391	404 p			
242	-			

Table V (7)

The infrared and Raman bands of 4-chloro tetrahydropyran and their assignment

I.R.	Raman (ρ)	Assignment
157 s	156 w (0.67)	A'
205 w	206 w (0.89)	A"
258 m	258 w (0.74)	A"
300 m	300 w (0.16)	A'
338 m-sh	338 vs (0.27)	A'
355 s	-	(157 + 205) comb
402 w	-	-
443 w	445 w (0.11)	A"
-	475 w d (0.76)	A"
-	479	
492 m	492 w (0.25)	(338 + 156) comb
564 s	564 s (0.18)	A'
575 m	574 m (0.16)	
719 s	718 m (0.16)	A'
758 s	757 s (0.21)	
802 vw	-	A"
815 vw	-	
824 vs d	825 s d (0.14)	A'
832	835	
877 m d	-	A'
885	-	

I.R.	Raman (ρ)	Assignment
903 w	-	A"
981 m	-	A"
1001 s	1004 s (0.63)	A'
1020 s d 1026	1021 w d 1027	-
1068 s	1069 w	A'
1090 vs	1088 w (~1.0)	A"
1111 m	1111 m (0.14)	A'
1145 s	1147 vw (0.80)	A"
1167 m	1170 vw (0.20)	-
1185 m	1187 vw (0.76)	A"
1221 vs d 1227	1227 w-br (0.49)	A'
1242 sh		A"
1264 m	1266 w (0.54)	A'
1290 sh	-	A"
1299 m	1301 w (0.50)	A'
1344 m	1347 vw	A'
1382 m	1387 vw	A'
1419 w	1424 w	A"
1434 w	1438 w	A'
1446 m 1454 sh	1458 w	A"
1467 m	1469 w	A'

Table V (8)

Calculated frequencies and assignments for 4-chloro tetrahydropyran

A'		A"	
2984		2967	
2969		2927	
2929		2861	
2862		2855	
2856		1459	1458
1464	1469	1452	1424
1451	1438	1395	-
1390	1387	1379	-
1329	1347	1286	1290
1290	1301 p	1250	1242
1234	1266 p	1176	1187 dp
1232	1227 p	1153	1145 dp
1106	1111 p	1105	1090 dp
1057	1069	977	981
993	1004 p	924	903
875	877/885	816	815/802
821	825/835 p	458	475/479 dp
750	757/718 p	254	258 dp
576	574/564 p	223	206 dp
427	445 p		
351	338 p		
339	300 p		
134	156 p		

Table V (9)

The infrared and Raman bands of 4-bromo tetrahydropyran and their assignment

I.R.	Raman (ρ)	Assignment
	134 w, 146 w } d	A'
	193 w (0.78)	A"
220 m	222 m (0.83)	A"
261 s, 270 s } d	262 vs, 270 vs } (0.37)	A'
350 vs		(222 + 134) comb
386 w	388 w (0.64)	A'
438 m	440 m (0.24)	A'
468 m	471 s (0.35)	
531 w, 547 s } d	533 m, 549 m } d (0.33)	A'
598 m, 614 m } d	602 w, 618 w } d	
692 s	694 m (0.33)	A'
714 s	717 s (0.37)	
823 sh, 828 s } d	826 vs, 832 vs } d (0.30)	A'
863 w		
872 w, 880 w } d	874 sh, 883 m } d (0.52)	A'
-	915 w (0.95)	A"

I.R.	Raman (ρ)	Assignment
982 m	-	A"
998 m	1000 s (0.68)	A'
1018 m	1012 sh	
1023 m	1020 sh	
1037 w		A'
1067 s	1070 w (0.67)	A"
1086 s		A'
1110 w	1100 w (0.38)	A"
1142 s	1144 w (0.66)	A"
1067 w	1170 w	
1183 vw	1188 sh-w	A'
1200 s	1203 m (0.40)	
1220 m		A"
1232 m		A'
1252 m	1254 m (0.41)	A'
1296 s	1298 m (0.57)	A'
1337 m-br	1340 m (0.48)	
	1356 w	A'
1383 m	1388 w	A"
1418 w	1420 w	A'
1431 w	1436 w	
1445 m		A"
	1458 w	A'
1467	1469 w	

Table V (10)

Calculated frequencies and assignments for 4-bromo tetrahydropyran

A'		A"	
2969		2967	
2930		2927	
2902		2861	
2862		2855	
2856		1458	1458
1464	1469	1451	1420
1451	1436	1387	-
1390	1388	1372	-
1321	1340 p	1278	-
1255	1298 p	1249	1232
1233	1254 p	1171	1167
1198	1203 p	1155	1144
1087	1100 p	1104	1086
1057	1070 p	973	982
986	1000 p	927	915 dp
880	883/874 p	816	-
821	826/832 p	462	-
727	694/717 p	241	222 dp
554	533/549 p	218	193 dp
421	440/471 p		
338	388 p		
263	262/270 p		
123	134/146		

5.3 Results and Discussion

The assignments for tetrahydropyran, 4-chloro THP and 4-bromo THP are given in Tables V (6), (8) and (10) respectively. As can be seen from Fig. V (i) most of the bands are both infra-red and Raman active as anticipated for molecules with such low symmetry. Most of the bands are strong in the Raman spectrum and are readily assigned by their depolarisation ratios. Many of the bands below 900 cm^{-1} for 4-chloro THP and 4-bromo THP occur as doublets and this is attributed to the presence of two conformers at room temperature. The frequency fit is fairly good for a first-order force field for both molecules and would obviously be improved by a perturbational analysis of the transferred halogeno force constants. Even so, the ν (C-X) modes are predicted very near their experimental frequencies and the PED distribution indicates a correct assignment (ν_{18} A' for 4-chloro THP has a 49.1% contribution from f(C-Cl) and ν_{18} A' for 4-bromo THP has a 31.9% contribution from f(C-Br)). The equatorial vibration is almost always found at a higher frequency than is the axial and this has been assumed for the two molecules under study. It has been suggested that the reason for this consistent difference is that when the C-X bond is stretched there is a small restoring force acting on the carbon when X is axial, and the vibration is essentially

perpendicular to the plane of the ring. When X is equatorial, the motion of the carbon forces a ring expansion, the restoring force is greater and the frequency of the motion is therefore higher.

The ratio of the integrated infrared intensities of the axial and equatorial ν(C-X) components does not give a valid equilibrium constant. Indeed, it has been shown by Jensen and Gale (63) that the ratio of the equatorial and axial molecular extinction coefficients for cyclohexyl bromide is 1.85. This was accomplished by utilising the corresponding cis- and trans-methyl cyclohexyl compounds and assuming that the molecular extinction coefficients were the same as those for the two conformations of the cyclohexyl derivative. Previous work (64) using 4-t-butyl derivatives of cyclohexanols showed that a bulky grouping assumed an equatorial preference and its remoteness had little effect on the ν (C-X) vibrational mode. Unfortunately the unavailability of such compounds in the tetrahydropyran series precludes any reliable estimate of the equilibrium constant K by infrared measurements.

It is interesting to compare the infrared and Raman spectra molecules with conformational isomers in both solid and liquid states. In the solid phase substances are generally crystalline and a crystal usually contains only one conformation. On the

other hand additional bands often appear in the liquid state indicating the presence of a second conformation not present in the solid in equilibrium with the more stable conformation. Chlorocyclohexane (65, 66) freezes to a solid at one temperature but the infrared spectrum of this solid is essentially that of a liquid. At a still lower temperature there is a transition to another solid which is conformationally pure. Fluorocyclohexane, however, exhibited the same spectrum as the liquid even at very low temperatures. This led Lunde et al to the incorrect conclusion that the compound existed in one conformation only, even in the liquid state. N.M.R. evidence (67), however, proved the existence of both conformations in the liquid state. It was thus deduced that the two conformations are isomorphous in the solid state; that is they fit equally well into the crystal lattice. Such a situation is not unexpected since fluorine and hydrogen are so nearly the same in size.

Variable temperature studies were performed with 4-chloro THP. The vapour was sprayed under vacuo via a fine jet onto a KBr plate secured to a cold finger at liquid nitrogen temperature. Even after annealing the film no change in the resulting infrared spectrum was observed. Secondly a 10% carbon disulphide solution was cooled in the variable temperature Raman cell, described above, with cold nitrogen gas (approx. -100°C) in a manner similar to a N.M.R. variable temperature unit. The integrated areas,

however, remained constant within the limits of experimental error with a 66% ratio in favour of the equatorial conformer.

Chiurdoglu (68) calculated that the free energy difference for both chloro- and bromo- cyclohexane in the liquid state to be between -0.3 to -0.4 Kcal/mole (approx. 60% equatorial) for all solvents by infrared methods. More reliable work (63) indicated a value of -610 ± 20 cals/mole for bromo cyclohexane.

SECTION B: Nuclear Magnetic Resonance Studies

5.4 Introduction

Cyclohexane has been the subject of numerous investigations using N.M.R. spectroscopy. During a flip of the six-membered ring giving a chair-chair interconversion, each axial proton transforms to an equatorial environment and vice versa. However, when the rate of ring inversion is appreciably greater than the chemical shift difference ($\nu_a - \nu_e$) an averaged environment gives a sharp singlet at 8.56 (solvent CS_2). The inversion rate can be retarded using low temperatures and at -50°C the sharp singlet begins to broaden and eventually at -70°C it is seen as two very broad resonances each containing much fine structure. The coalescence temperature T_c, the temperature at which on warming the sample the doublet resonances have just merged to a single broad peak, is in the region -65°C to -67°C. Below -90°C the

spectrum is temperature independent. The chemical shift difference ($\nu_a - \nu_e$) of 0.48 ppm from the early measurements of Muller and Tosch (69) on the broad bands was later confirmed by the elegant work of Anet and co-workers (70) using undecadeutero cyclohexane. Here only a single proton was observed and since H-D couplings are only about 0.153 times as great as the corresponding H-H couplings, the signals were quite narrow. A further improvement was obtained by recording the spectra with simultaneous irradiation at the deuterium frequency (double resonance) thus removing the effects of H-D coupling.

The coalescence temperature is related to the rate constant for interconversion by

$$K = 2^{-\frac{1}{2}}\pi \left| \nu_a - \nu_e \right| \qquad 5.4.1$$

where ν_a and ν_e are the frequencies of the axial and equatorial protons at the coalescence temperature (71). For cyclohexane a rate constant of 52.5 sec^{-1} was obtained. From the Eyring equation

$$k = \left[(\alpha k_B T)/h\right] e^{-\Delta G^*/RT} \qquad 5.4.2$$

where α is the transmission coefficient (assumed to be unity) k_B the Boltzmann constant and h Planck's constant, the free

energy of activation ($\Delta G^{\ddagger}$) for chair-chair interconversion was calculated to be 10.1 kcal/mole (72).

Study of the monohalogeno cyclohexanes is facilitated by the observation that the α-proton is deshielded by the adjacent halogen atom and is found at very low field compared to the remaining ring protons. It can therefore be easily identified and studied.

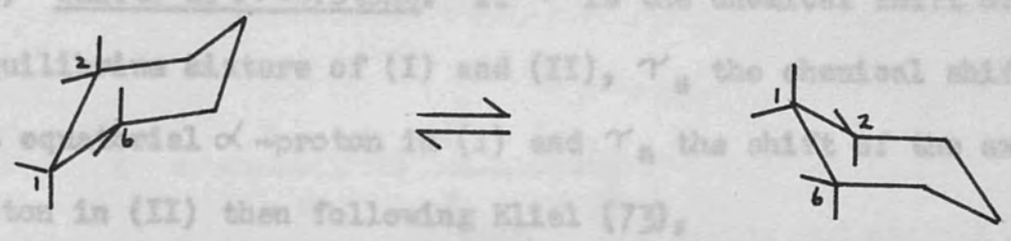

(I) axial (II) equatorial

The chemical shifts of the α-protons in conformations (I) and (II) will have different values but their assignment does not require a full analysis of the spectrum. Use is made of their signal widths. Thus for the equatorial proton H_1 in (I)

$$\tfrac{1}{4} \times \text{signal width} \sim 2Je_1a_2 + 2Je_1e_2$$

and for the axial proton in (II)

$$\tfrac{1}{4} \times \text{signal width} \sim 2Ja_1a_2 + 2Ja_1e_2$$

Since $J_{aa} \gg J_{ae} \sim J_{ee}$ it follows that the signal width of the axial proton is appreciably greater than the equatorial proton. It is always found that the equatorial α-proton in (I) resonates at lower field than the axial α-proton in (II). The value of the equilibrium constant can be determined by the following methods:

a) Direct integration. Accurate results will only be obtained if it is fortuitous that the signals are well separated.

b) Shifts of α-protons. If τ is the chemical shift of the equilibrium mixture of (I) and (II), τ_e the chemical shift of the equatorial α-proton in (I) and τ_a the shift of the axial α-proton in (II) then following Eliel (73),

$$\tau = x\tau_a + (1 - x)\tau_e$$

where x is the fraction of compound present in the more stable conformation.

$$\text{Hence } K = \frac{x}{1 - x} = \frac{\tau - \tau_e}{\tau_a - \tau}$$

c) Measurements of vicinal coupling constants (H-C-C-H)

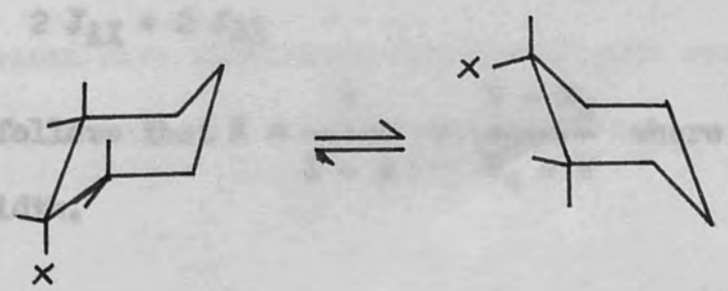

(I) (II)

In the rapidly interconverting mixture of (I) and (II) the observed vicinal coupling constants J and J^1 are weighted averages of the coupling constants in the separate conformations. Thus

$$J = \text{average } J_{AX} = x\, J_{2ela} + (1-X)\, J_{2ale}$$

$$J^1 = \text{average } J_{BX} = x\, J_{2ala} + (1 - x)\, J_{2ele}$$

whence

$$K = \frac{x}{1 - x} = \frac{J - J_{2ale}}{J_{2ela} - J}$$

and

$$K = \frac{x}{1 - x} = \frac{J^1 - J_{2ele}}{J_{2ala} - J^1}$$

Normally the first expression for K is not useful because J_{2ela} and J_{2ale} are almost equal and the numerator and denominator become comparable with experimental error.

d) <u>Signal widths.</u> For the X portion of an AA'BB'X spin system the distance between the outer lines is independent of $\nu_A - \nu_B$ and equals

$$2\, J_{AX} + 2\, J_{BX}$$

It follows that $K = \frac{x}{1 - x} = \frac{W - W_e}{W_a - W}$ where W corresponds to signal width.

The parameters contained in the above equations can be determined experimentally for the conformer pairs either by low temperature isolation or by using the 4-t-butyl cis and trans derivatives. Poor results are generally obtained for compounds with relatively large ΔG values, e.g. > 1.3 kcal mole^{-1} where the substituents are usually bulky and preferentially assume the equatorial position.

Table V(II) summarises the results of many workers using the area and shift N.M.R. techniques to obtain thermodynamic data for the mono-substituted halogeno cyclohexanes. The results indicate that the free energy change is dependent on technique of determination and worker to worker as well as solvent and temperature. More recently Jensen and Bushweller (79) succeeded in preparing equatorially-substituted chlorocyclohexane free from its conformational isomer. The compound was cooled through its melting-point range (-43.9°C) when the equatorial conformer crystallised preferentially. The crystals were immediately cooled to -151°C (solvent CD_2CDCl) and the N.M.R. spectrum showed the presence of only the axial α-proton. When the solution was warmed to -125°C the resonance of the equatorial α-proton of the other conformer began to appear and increased with time until the equilibrium was established with approximately 87% equatorial conformer.

Table V (11)

Compound	$-\Delta G$(cal mole^{-1})		Conditions	Reference
C_5H_{11}-X	Area	Shift	Temp/Solvent	
F	250	241		
Cl	513	478	$-81^{\circ}C/CS_2$	74
Br	480	439		
I	431	407		
Cl		417	4-t-butyl/ cis decalin	75
Br		393		
Cl		435	4-t-butyl/ o-dichlorobenzene	75
Br		421		
Br		200	RT/neat	76
Cl	406		$-100^{\circ}C/CS_2$	77
Br	511			
F		153	$^{19}F/CCl_3F/29^{\circ}C$	78
F	242		$^{19}F/CCl_3F/-55^{\circ}C$	

Very little systematic work to date has been published on the N.M.R. spectra of simple tetrahydropyrans compared to the vast interest in carbohydrates, which contain the THP skeleton. However, the work of Gatti et al (80) suggests that the conformational mobility of the THP ring in comparison with

100 MHz N.M.R. SPECTRA OF 4-CHLORO TETRAHYDROPYRAN

that of the cyclohexane ring is not sensibly affected by the presence of the oxygen atom.

The 60 MHz PMR spectrum obtained at room temperature shows two complex multiplets centred at 1.5 ppm and 3.5 ppm from TMS, having integrated intensities of 6 and 4 respectively. On the basis of the value of the chemical shift and peak intensity the upfield absorption is assigned to the β - and γ - protons, and the remaining downfield absorption to the CH_2- group linked to the oxygen atom. By double resonance at 1.5 ppm, the CH_2 multiplet transforms into a clear singlet at 3.45 ppm that, with decreasing temperature, broadens and finally aplits at -65°C into an AB quartet. This pattern remains unchanged below -85°C. At this temperature the spectral parameters are: $\nu_o \delta_{AB} = 55$ Hz and $J_{AB} = 12$ Hz which is consistent with geminal coupling. The rate constant at the coalescence temperature is calculated to be about 70 sec^{-1} from the relation (81)

$$K = \frac{\pi}{2\sqrt{2}} (\delta^2 + 6 J^2)^{\frac{1}{2}}$$

FIG V(ii) 100 MHz N.M.R. SPECTRA OF 4-CHLORO TETRAHYDROPYRAN

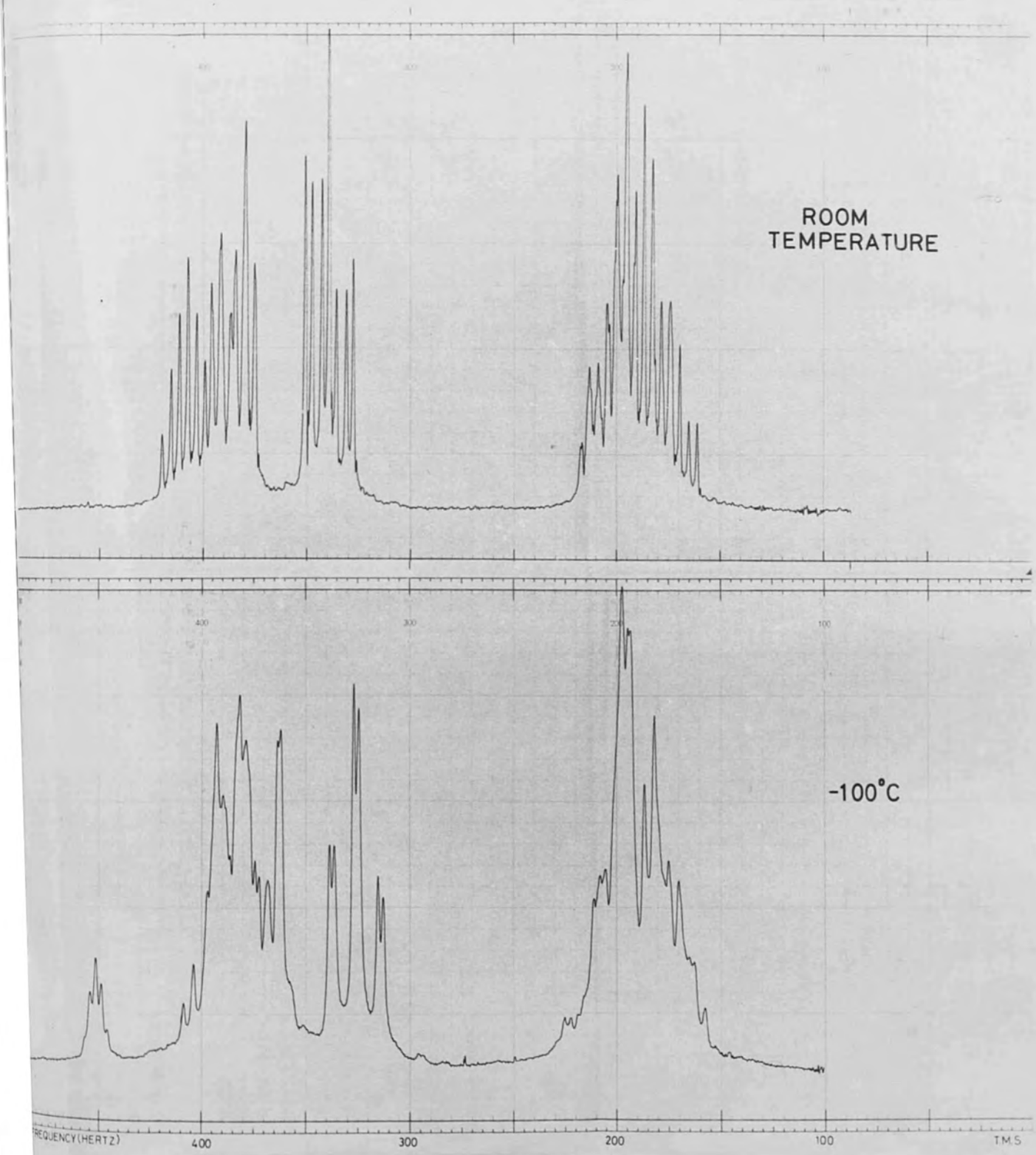

100 MHz SPECTRA OF 4-BROMO TETRAHYDROPYRAN FIG V(iii)

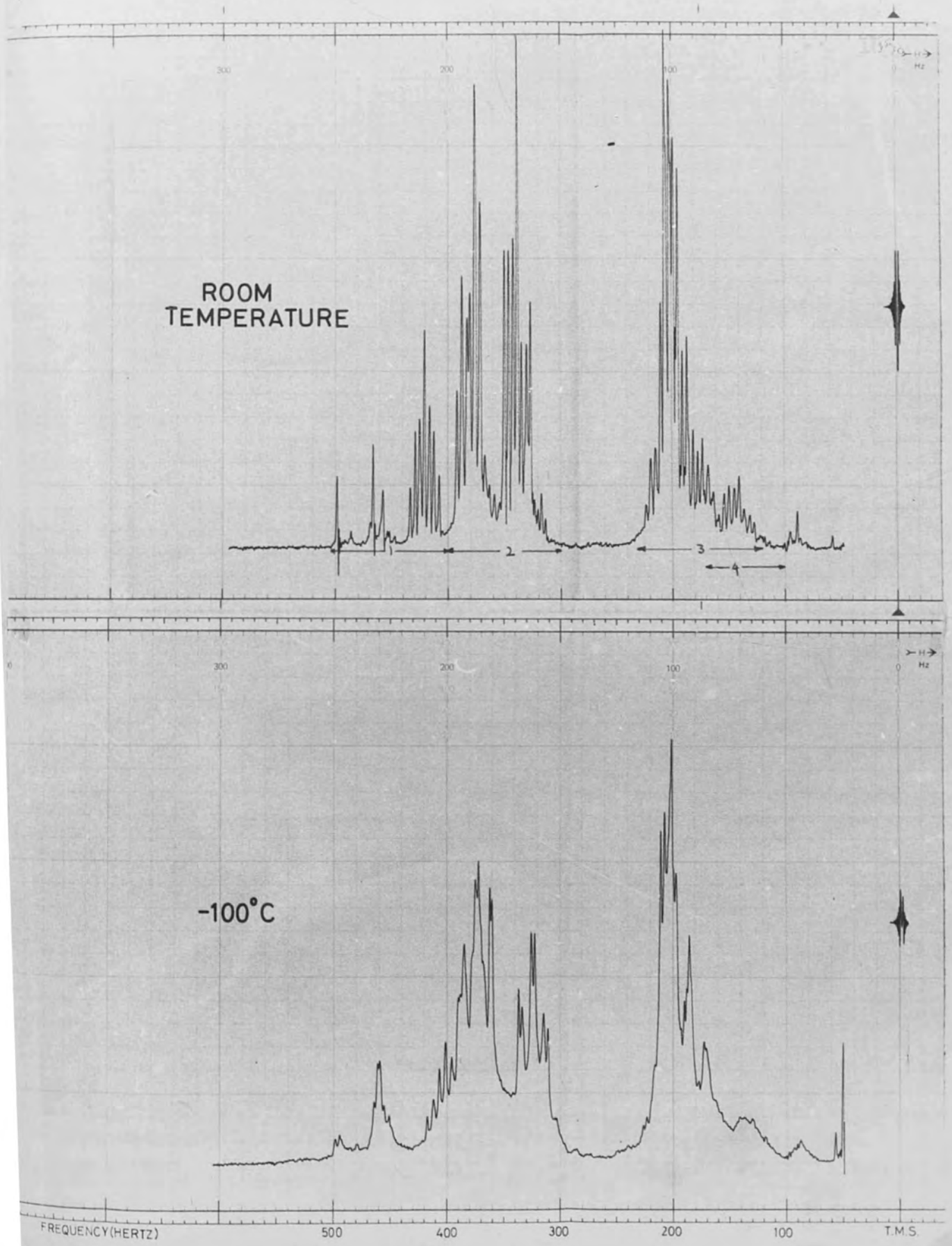

FIG V(iv) 220 MHz EXPANSION OF 4-CHLORO TETRAHYDROPYRAN

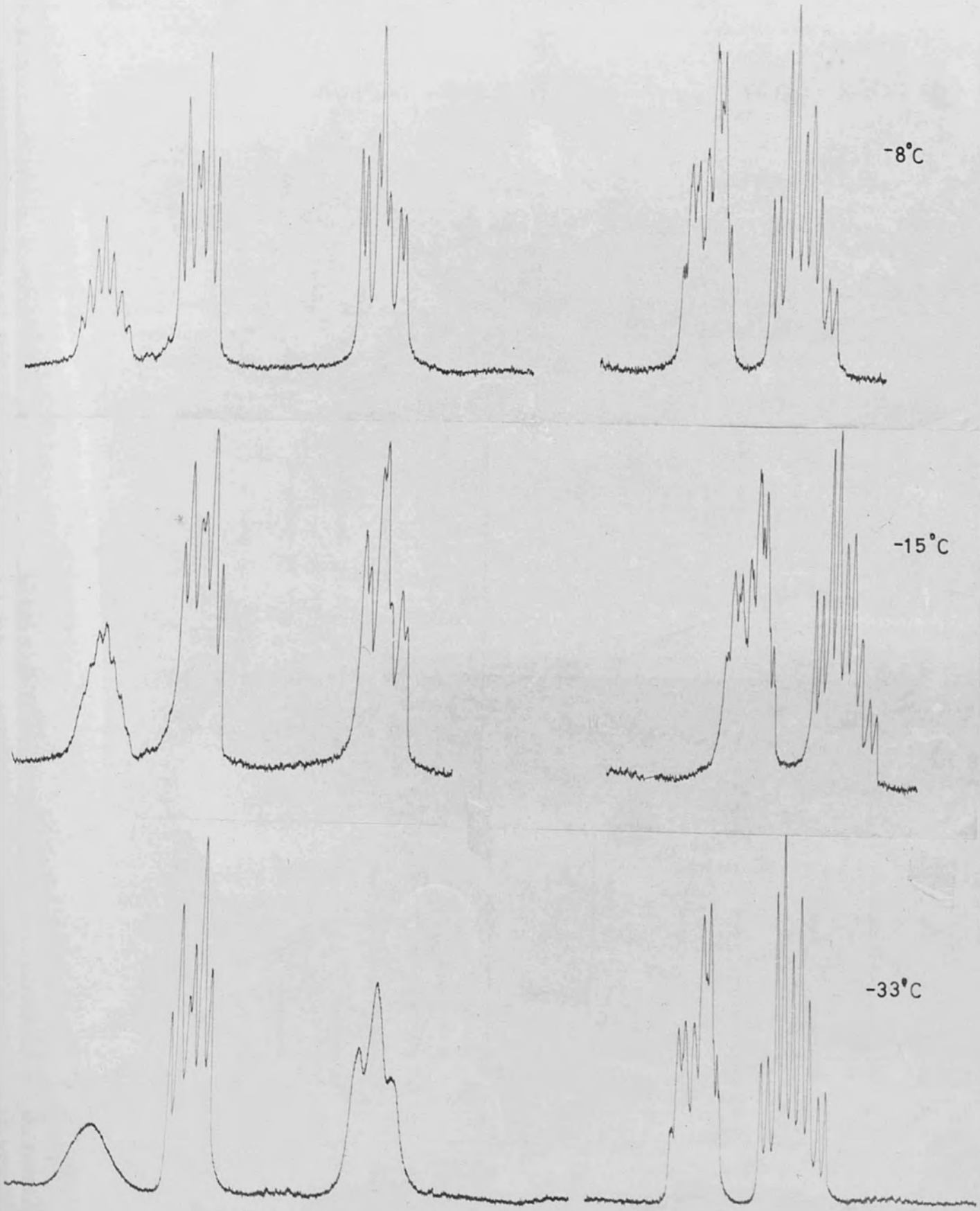

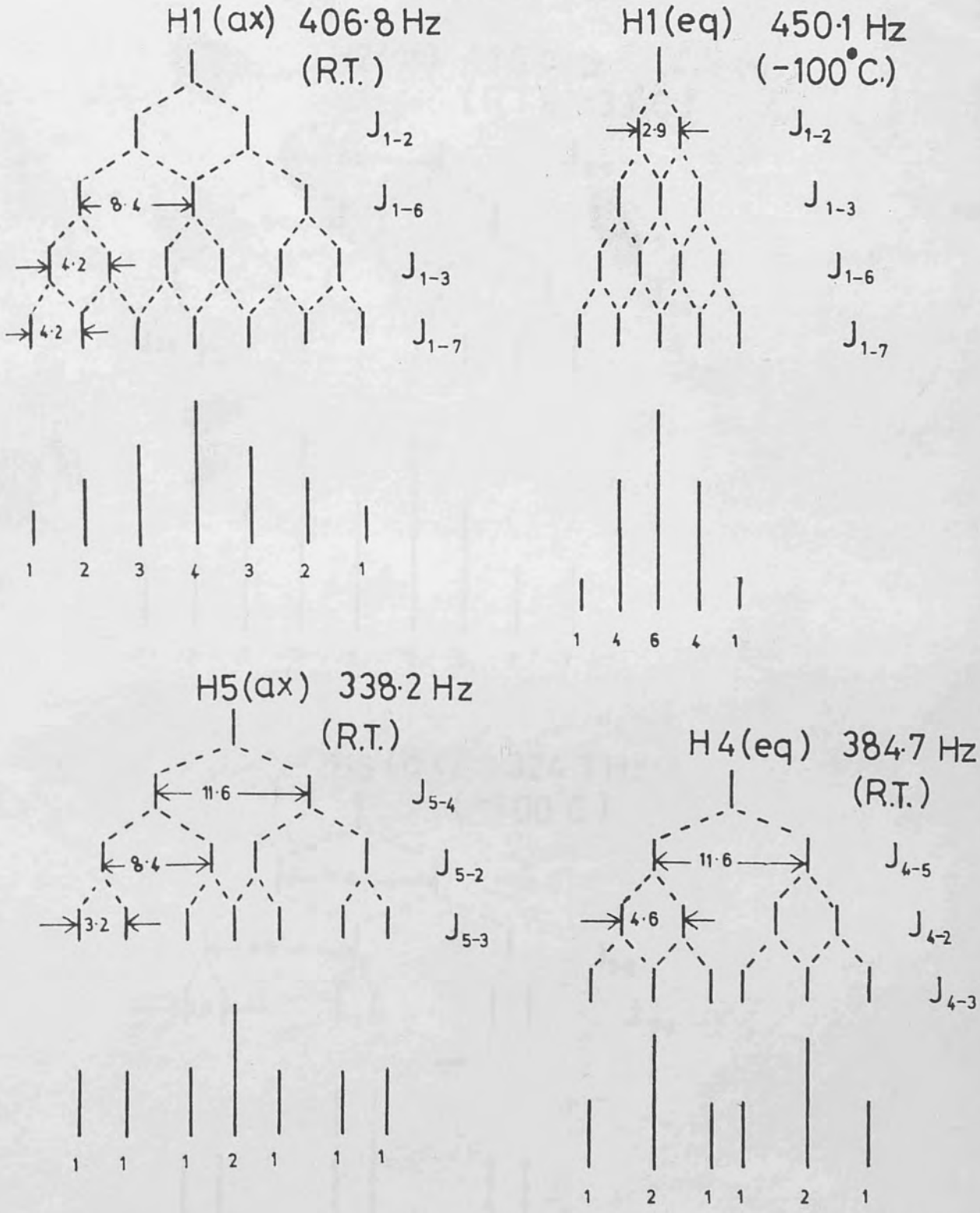

FIG V(v)

NMR Spectral features of 4-chloro tetrahydropyran

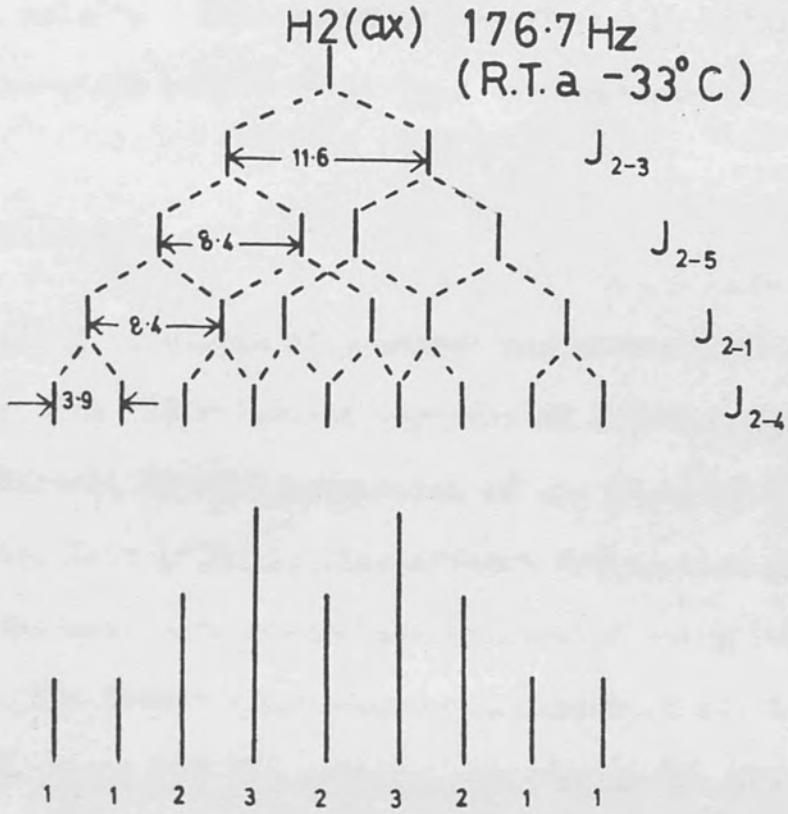
H2(ax) 176·7 Hz
(R.T. a -33°C)
11·6
J 2-3
8·4
J 2-5
8·4
J 2-1
3·9
J 2-4
1 1 2 3 2 3 2 1 1

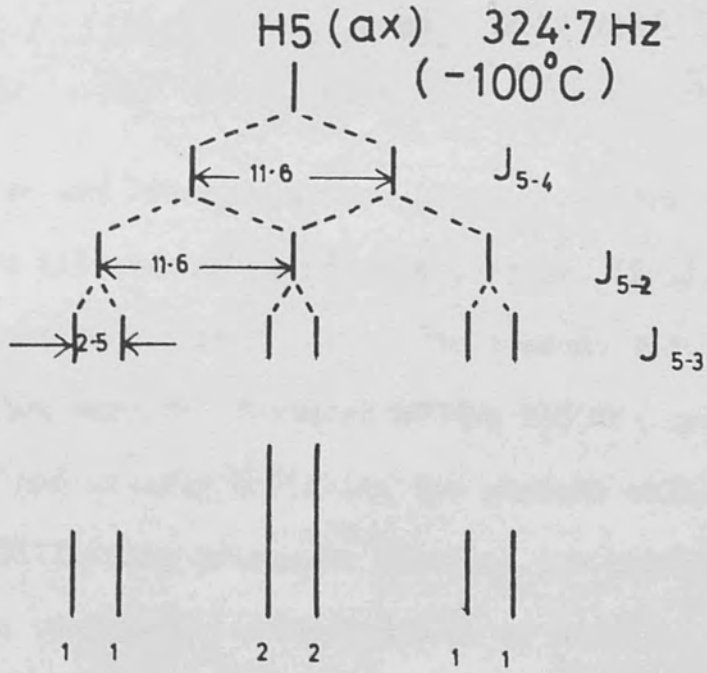
H5 (ax) 324·7 Hz
(-100°C)
11·6
J 5-4
11·6
J 5-2
2·5
J 5-3
1 1 2 2 1 1

FIG V(v) cont.

It corresponds to a free energy of activation (ΔG^{*}) of 10.2 Kcal mole^{-1}. This value was confirmed by obtaining K by the line-width method at various temperatures above T_c (82).

5.5 Experimental

10% ($^{v}/_{v}$) solutions of 4-chloro and 4-bromo THP in carbon disulphide with TMS reference were run on a Varian HA 100 spectrometer at Harwell by kind permission of the Physical Chemical Measurements Unit (PCMU). The off-set frequencies of the expanded features were accurately calibrated using the frequency counter. The lowest temperature obtainable at 100 MHz was -100 ± 5°C. All 220 MHz spectra were run by the SRC unit at Runcorn where the lowest temperature obtainable was -33°C.

5.6 Results

The room- and low-temperature 100 MHz spectra for the two compounds are illustrated in Figs. V (ii) and (iii). A small amount of impurity can be detected for 4-bromo THP. Fig. V (iv) illustrates the expanded features of the 220 MHz spectra for 4-chloro THP and clearly indicates the gradual collapse of two features. Difficulty arises in locating the centre of the septet in the room-temperature spectrum of 4-chloro THP due to overlap. It has been estimated by assuming that the lines of the septet are equally spaced. Table V (12) summarises the

values of the equilibrium constants and the corresponding free energy changes. The results indicate that the equilibrium favours the equatorially-substituted conformers - approximately 80% for 4-chloro THP and 68% for 4-bromo THP. Unfortunately, these values cannot be checked by direct integration of the low-temperature signals because the septet of the proton adjacent to the halogen atom merges with the low-field features of the protons next to the heterocyclic oxygen atom. The free energy change for 4-bromo THP is approximately the same as for its cyclohexane analogue (74) but that of 4-chloro THP is far greater than expected. The accuracy of these values depends on the extent of the equilibrium. A 50 - 50 equilibrium of conformers will give a more accurate estimate of the free energy change than an equilibrium involving one predominant conformer. As with the cyclohexane series the value of K is dependent on the method of argument.

Table V (12)

Compound	Equilibrium constant (K)		
C_5H_9O-X	Shift	Coupling	Signal width
Cl	3.26*/4.2	5.15*	4.2*
Br	2.19	2.36	1.7
Corresponding free energy change ($-\Delta G$ in cal $mole^{-1}$)			
Cl	704/855	977	855
Br	467	512	316

* values marked with an asterisk indicate that calculation has been performed by assuming a symmetric septet in the room-temperature spectrum of 4-chloro THP

5.7 Computer simulation of NMR spectra

A further glance at the low-field characteristics of the 100 MHz spectra reveals that the features can be interpreted on a first-order basis

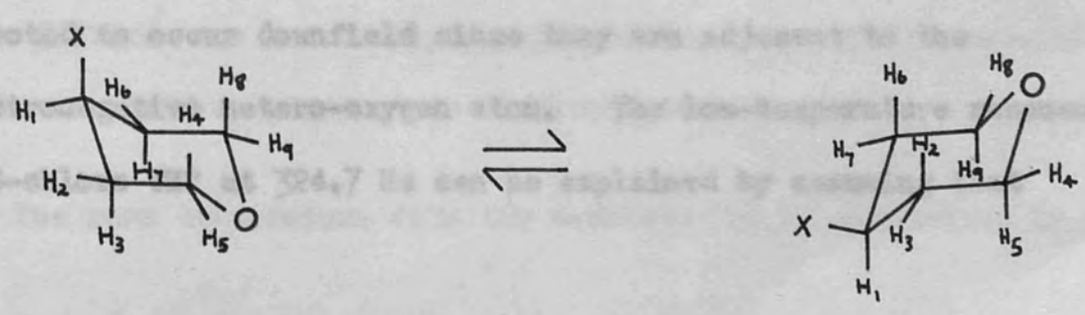

(I) (II)

Proton H1 Fig. V(v) shows that the symmetrical septuplet of H1 of both molecules can be explained by assuming that $J_{aa} = 2\ J_{ae} = 2\ J_{ee}$, and the low-temperature spectrum reveals the isolated shift of H1 in the equatorial conformation at 450.1 H_z for 4-chloro THP and 462.3 H_z for 4-bromo THP. The fine structure reveals a 1:4:6:4:1 quintet for 4-chloro THP made up by assuming that $J_{ae} \sim J_{ee}$. The corresponding fine structure of equatorial H1 for 4-bromo THP, namely a 1:5:10:10:5:1 sextet, remains to be explained in a satisfactory manner. The centre of the septet at higher field due to the axial proton H1 can be clearly seen for 4-bromo THP but becomes obscured, as remarked above, for 4-chloro THP from coincidence with another low field resonance. It is interesting to note that H1 resonates at 417.0 H_z when the spectrum of 4-chloro THP is run as a neat liquid, clearly showing the full septet. Hence the neat liquid favours a lower equilibrium constant and a corresponding lower free energy change than for a solution. This result agrees with data for the cyclohexane analogues in Table V(11).

Protons H4 and H5 The signals from these two protons would be expected to occur downfield since they are adjacent to the electronegative hetero-oxygen atom. The low-temperature resonance of 4-chloro THP at 324.7 Hz can be explained by assuming that

the vicinal coupling constant has the same value as the axial-axial coupling constant of 11.6 Hz. Hence the high-field component must belong to the axial environment. At room temperature, however, J_{5-2} becomes an averaged coupling constant and its value falls (8.4 Hz). Consequently the form of the resonance changes through the given temperature range and this can be clearly seen from the 220 MHz expanded features in Fig. V (iv). The room temperature resonance at 384.7 Hz comprises a predominant equatorial environment whose associated couplings have smaller values which will not vary to any extent over the two extremes of temperature. It is indeed observed that this resonance remains intact at 220 MHz (-33°C). At -100°C (100 MHz) this area becomes very complicated due to the presence of two equatorial protons from two conformational isomers.

Protons H2 and H3. The remaining alkyl proton resonances are expected to be found near the TMS reference signal. These are very close together and can only be separated at 220 MHz. The broader of the two signals obviously contains a large J_{aa} coupling constant and hence belongs to the axial environment. The first order features can be clearly deciphered from the 220 MHz expansion. The lower-field counterpart is difficult to interpret.

The room temperature data for 4-chloro THP is summarised in Table V (13) below:

Table V (13)

	Shift (Hz) at 100 MHz	Coupling constant (Hz)			
		J_{12}	J_{13}	J_{14}	J_{15}
H1	406.8	8.4	4.2	-	-
		J_{23}	J_{24}	J_{25}	
H2	176.7	-11.6	3.9	8.4	
		J_{34}	J_{35}		
H3	203.5	4.6	3.2		
		J_{45}			
H4	384.7				
H5	338.2	-11.6			

A program in Fortran II, namely UEA NMR BASIC was obtained from Dr. R. K. Harris of the University of East Anglia. This program comprises the original program LAOCOON of Castellano and Bothner-By with two modifications:

(a) the program automatically performs magnetic equivalence factoring (e.g. an X_3 group is treated as occupying a quartet state with a total spin of $\frac{3}{2}$, or a doublet state of spin $\frac{1}{2}$ and multiplying the calculated intensities by the appropriate weighting factor);

(b) factorisation of the total spin Hamiltonian is performed for different types of nuclei with large differences in resonant frequency.

* The mathematical treatment for the solution of frequencies and intensities for the simplest of spin systems has been outlined in various texts (83, 84). For the complex spin system under consideration a computational procedure has to be adopted.

The contents of this program were updated to Fortran IV for use on the CDC 6600. The capacity of the program is ultimately limited by the size of the largest matrix to be diagonalised after factorisation - namely 35 x 35. The program can therefore only handle a maximum of seven spins (since $^{7}C_{3} = 35$). Fortunately the molecule under consideration has a plane of symmetry thus reducing the size from nine to five spins.

The logic of the program can be summarised into a number of steps:

(i) use is made of a set of basis functions as appropriate linear combinations of the 2^n basic product functions.

$$\psi_n = \alpha\beta\alpha\ldots\ldots\ldots\beta(n)$$

$$\Phi_n = \sum^{n} a_n \psi_n$$

(2) The Hamiltonian (H) is made up of two components

$$H = H_o + H_1$$

H_o represents the energy of isolated nuclei of magnetogyric ratios γ_i acted on by fields B_i

$$H_o = (2\pi)^{-1} \sum_i \gamma_i B_i I_z(i)$$

B_i will differ from the external field B_o because of electronic screening

$$B_i = B_o (1 - \sigma_i)$$

The indirect spin coupling may be represented by a Hamiltonian involving the scalar products of the spin vectors of all pairs of magnetic nuclei.

$$H_1 = \sum_{i\ j} J_{ij}\, I(i).I(j)$$

(3) The matrix elements of the Hamiltonian H_o are

$$(\psi_m | H_o | \psi_m) = (2\pi)^{-1} \sum_i \gamma_i B_i \left[I_z(i) \right]_m$$

where $\left[I_z(i) \right]_m$ is $\frac{1}{2}$ if nucleus i has α spin in ψ_m and $-\frac{1}{2}$ if it has β spin. H_o contains diagonal elements only.

(4) The matrix elements of the spin-coupling Hamiltonian H_1 between product functions are

$$(\psi_m | H_1 | \psi_m) = \tfrac{1}{4} \sum_{i<j} J_{ij} T_{ij}$$

$$(\psi_m | H_1 | \psi_n) = \tfrac{1}{2} U J_{ij} \qquad m \neq n$$

where $T_{ij} = 1$ or -1 depending on whether spins i and j are parallel or antiparallel in ψ_m, and $U = 1$ if ψ_m differs from ψ_n by an interchange of spins i and j and is zero otherwise. Matrix elements between linear combinations of basic products are evaluated by expansion.

(5) The order of the complete secular equation can be reduced by using the rule that no mixing occurs between functions with different values of the total spin component F_z.

(6) If several species of nuclei A, B etc., are present, step (5) leads to a further simplification because to a high approximation, no mixing occurs between functions which differ in any of the total spin components F_z (A), F_z (B) etc. The same rule can be applied when there are several sets of nuclei of the same species if the chemical shift between them is large compared with the coupling constants.

(7) Diagonalisation of the submatrices of the total Hamiltonian and consecutive operations on unit matrices of similar dimensions leads to the computation of energies and wave functions.

(8) The number of possible transitions is limited by the selection rule $F_z = \pm 1$.

(9) The probability of a transition induced by the field in the x direction for a single isolated nucleus of spin $\frac{1}{2}$ between states m and m' is given by

$$P_{mm'} = \gamma^2 B_1^2 \left| (m' \,|I_x|\, m) \right|^2 g(\nu)$$

where g ( ) is a line-shape parameter.

For transitions between states of a set of coupled nuclei the perturbing Hamiltonian is

$$H' = -2B_1 M_x \cos 2\pi\nu t$$

where M_x is the component of the nuclear moment in the x direction:

$$M_x = \hbar \sum_i \gamma_i I_x(i)$$

Hence for the multi-nuclear problem the intensity arising from the transition $q \rightarrow q'$ will be proportional to the square of the modulus of the corresponding matrix element of the

nuclear-moment component M_x. This is

$$\hbar^2 \left| \left[q \left| \sum_i \gamma_i I_x(i) \right| q' \right] \right|^2$$

The data of Table V (13) gives an output of lines with the corresponding intensity. It is obvious that a visual representation of the calculated spectrum can be more easily compared with the actual spectrum. To enable this to be done NMR FIT (see Appendix 5) was written to make use of the Atlas Calcomp plotting facility. Basically this program fits a Lorentzian line shape, to the calculated intensities.

$$I(\nu) \propto \frac{I(\nu_o)}{1 + \left(\frac{2\Delta\nu}{\Delta\nu_{\frac{1}{2}}} \right)^2}$$

where $\Delta\nu_{\frac{1}{2}}$ is the half-band width and $I(\nu_o)$ the calculated intensity. The spectrum can be plotted in many forms and Figs V(vi) and (vii) illustrate two such examples. It is useful to note that the shifts of the spin system at one operating frequency can be multiplied by the appropriate scaling factor to predict the spectra at other operating frequencies (coupling constants are invariant to operating frequency). A comparison with the observed spectrum of 4-chloro THP shows a very good fit except for proton H1 where coupling has been restricted to one half of the molecule only.

The fit of the upfield features could have been improved by using the iterative version of the program, namely UEA NMR, ITERATIVE which incorporates a least squares procedure. A useful additional feature of this version is that the frequencies are listed indicating associated energy levels and connected transitions. Such information is useful when interpreting the results of double resonance and spin-tickling experiments. However, the refinement of the molecular parameters did not warrant the use of the vast storage required by the program on the CDC 6600.

Theoretically it would prove extremely elegant to choose a conformational problem whereby the molecular parameters could be determined for both conformers from the low temperature spectrum. The room temperature spectrum could then be predicted by the summation of the individual contributions in the calculated conformer ratio.

5.8 Conclusion

NMR measurements indicate an anomalous trend in the equilibrium constant in CS_2 for 4-chloro and 4-bromo THP. More work on the fluoro and iodo derivatives is needed to confirm this trend, together with supplementary information from the ^{19}F resonance of 4-fluoro THP.

Fig. V (vi) 100 MHz calculated spectrum for 4-chloro THP

NMR SPECTRUM OF
CHLORO TETRAHYDROPYRAN

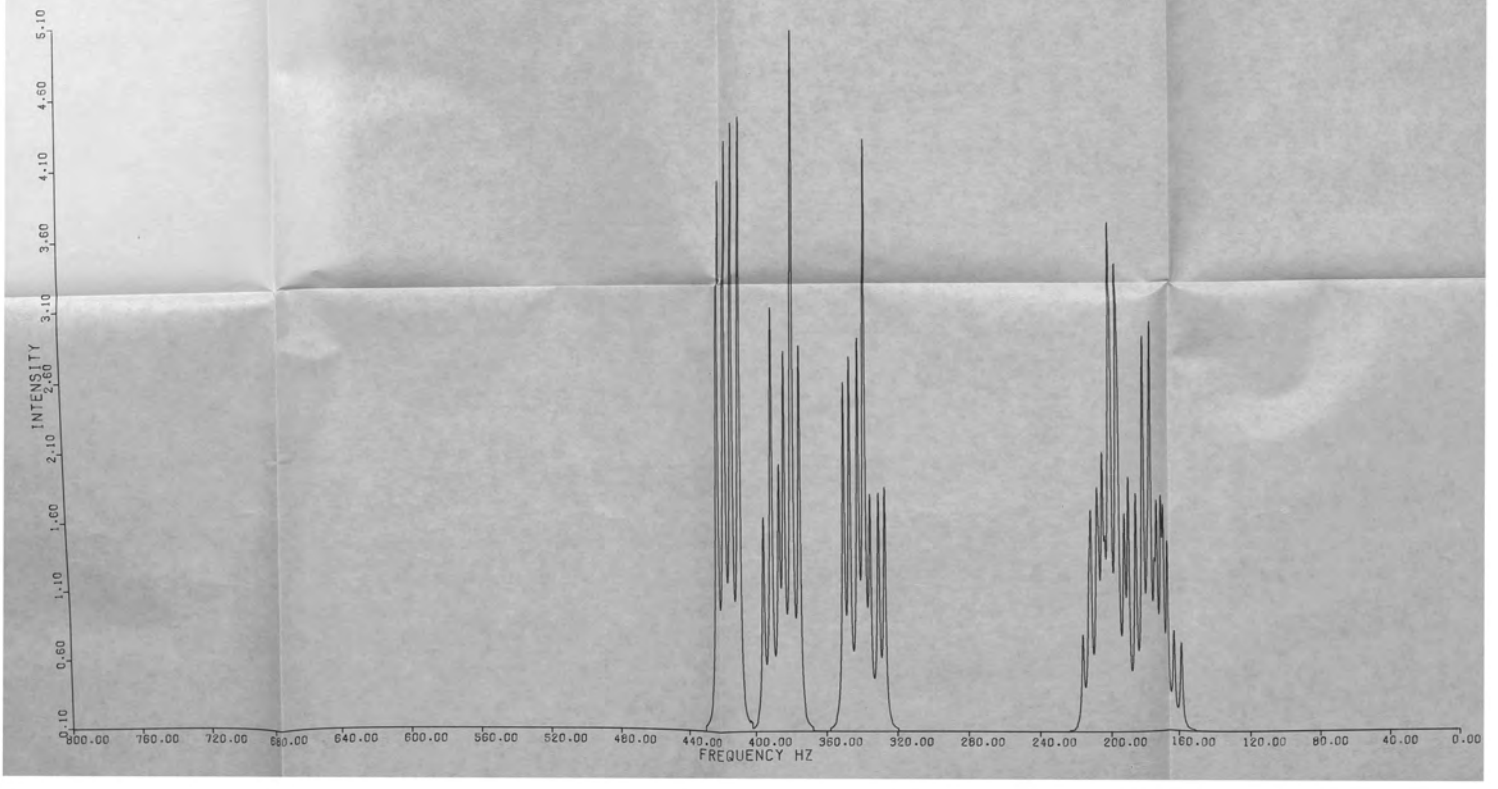

Fig. V (vii) 220 MHz calculated spectrum for 4-chloro THP

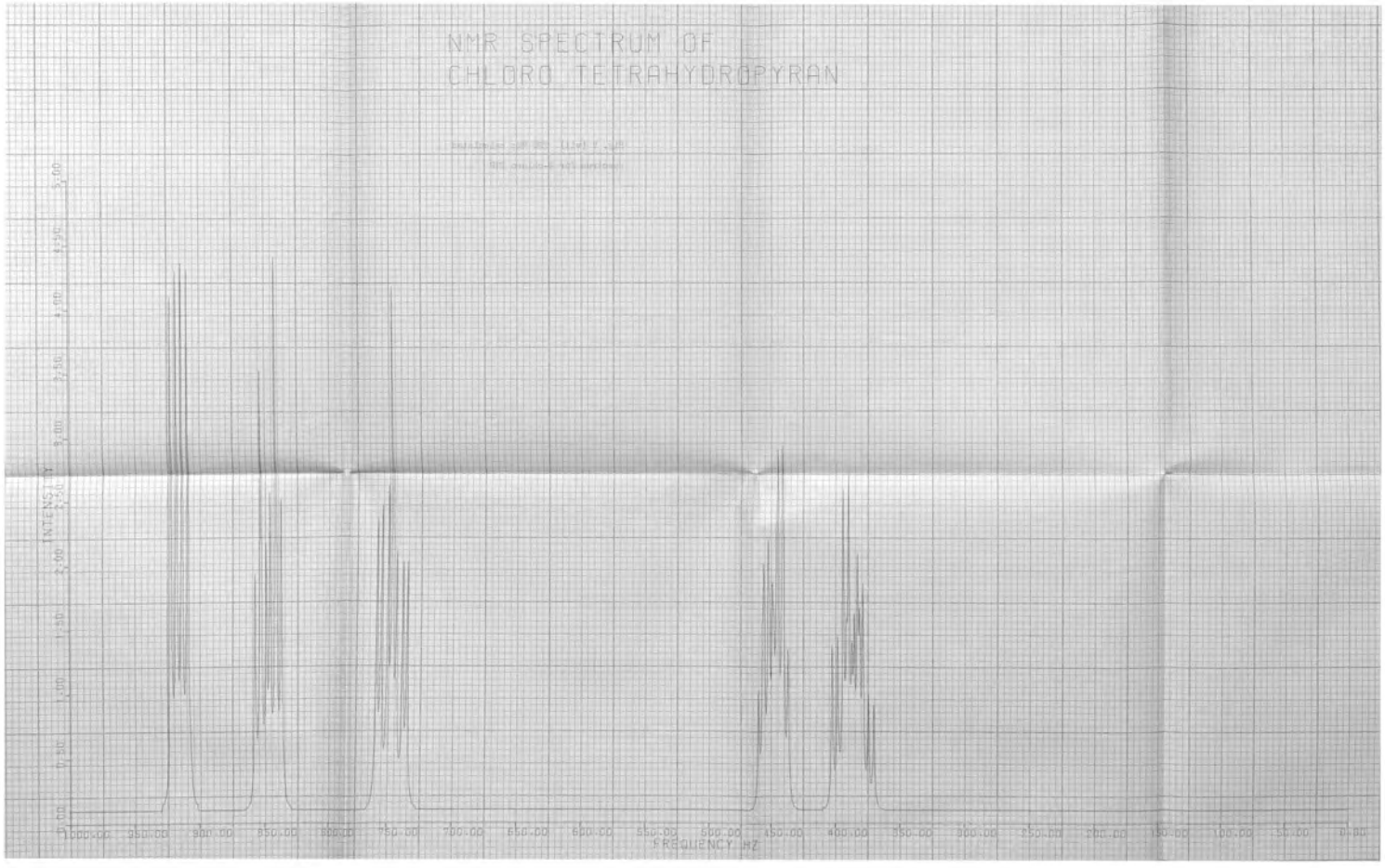
NMR SPECTRUM OF
CHLORO TETRAHYDROPYRAN
INTENSITY
FREQUENCY HZ

CHAPTER 6

Liquid Band Shape Analysis for the 215 cm^{-1} Mode of Hexafluorobenzene.

6.1 Introduction

It has been an embarrassing fact from a spectroscopic point of view that no direct evidence has been presented for the existence of the hexafluorobenzene complex in the solution state. Previous work has shown that hexafluorobenzene forms 1:1 molecular complexes with many aromatic hydrocarbons (85) in the solid state. Here it was suggested that the complexes are of the charge transfer type with the aromatic hydrocarbon acting as the donor and HFB (hexafluorobenzene) as the acceptor. Additional inferential evidence for the existence of a complex has been obtained from measurements of heat of mixing (86), vapour pressure in gas (87) and liquid states (88), excess volume (89), and dielectric constants/ refractive indices (90).

The characteristic spectral band which is associated with undoubted charge-transfer complexes, e.g. I_2 with benzene (200-260 nm) is not observed for the HFB-B system. Bauer et al (90) concluded that the HFB-B system has very little polar character with a permanent dipole moment not in excess of 0.1 D. The degree of mixing of the charge-transfer state into the ground state for such a complex is usually estimated to be in the order of 5-10% leading to complex dipole moments of approximately 1 D. Gaw and Swinton (88)

suggest a pure electrostatic interaction, the most probable being a dipole - quadrupole interaction, the C - F bond dipoles of HFB interacting with the π -electron quadrupole of the aromatic hydrocarbon. Such an interaction would produce a maximum attractive force when the planes of the two molecules were parallel, i.e. the configuration of the complex in the drystalline state (91). The assumption of this type of force can also account for the increase of stability of the complex as the electron-donating power of substituent groups on the aromatic ring is increased.

Vapour phase and solution phase infrared intensities of hexafluorobenzene were determined by Wheatley and Steele (92). Since the polarisability of HFB is small it was anticipated that the solution-phase intensities would be explained by the standard Debye-Onsager theory. This premise turned out to be true for all the bands measured, except the fundamental at 215 cm^{-1}. This was assigned by Steele and Whiffen to the out-of-plane γ_{C-F} mode of symmetry a_{2u} (93) although other work (94,95) suggests that it is the e_{1u} mode. In benzene solution the intensity of the a_{2u} mode was approximately 40% more than in cyclohexane and carbon disulphide. Furthermore the frequency of the band maximum increased by 4 cm^{-1} and in the opposite direction to the normal solvent effect. Wheatley then

proceeded to measure the absolute intensity of this band in a mixed solvent system extending from pure cyclohexane to pure benzene. The results showed that the intensity rose sharply below 20% w/w benzene-cyclohexane and then remained fairly constant above this composition. The intensity increase could be interpreted in terms of the appearance of the HFB-B complex. Bauer et al (90) estimated the HFB-B inter-molecular stretching frequency of the complex to be approximately 0.1 the total HFB-B bond energy. Assuming the latter to be a few kilojoules, the frequency should be on the order of 200 cm^{-1} and the equilibrium constant could be calculated from the intensity data as shown below. However, in recent years the infrared spectroscopist has shifted his attention from eigenvalues and eigenvectors of infrared bands to the actual band shapes of fundamentals in the solution phase because much information can be deduced concerning intermolecular interaction and molecular motion.

6.2 Experimental

Materials

Hexafluorobenzene was purchased from Imperial Smelting Co. Ltd. (B.pt. 80.1°C/760 mm). G.L.C. analysis showed no traces of impurity present and the sample was used without further purification. Benzene (B.pt. 80.1°C/760 mm) and

cyclohexane (B.pt. 80.7°C/760 mm) were purchased from B.D.H. (spectroscopic grade) and used without further purification.

Interferometric Recording

All spectra were recorded on a F.S. 720 manufactured by the Research and Industrial Instruments Company. An excellent review on interferometric spectroscopy in the far infrared has been written by Hurley (96) and only a short summary will be covered here. Essentially the interferogram function F(x) is related to the spectral distribution I (ν) by a Fourier transformation.

$$F(x) = \int_{-\infty}^{+\infty} I(\nu) \cos(2\pi\nu x)\, d\nu$$

Conversely,

$$I(\nu) = \int_{-\infty}^{+\infty} F(x) \cos(2\pi\nu x)\, dx$$

In practice F(x) can only be obtained over a finite interval on either side of the ZPD (zero path difference) say -X to +X so that the calculated spectrum is given by a truncated integral

$$I(\nu) = \int_{-x}^{+x} F(x) \cos(2\pi\nu x)\, dx$$

Since F(x) is symmetrical about the ZPD,

$$I(\nu) = \int_0^x F(x) \cos(2\pi\nu x)\, dx$$

In calculating spectra the Fourier cosine integral is approximated by a summation.

$$I(\nu) = 2 \sum_0^x F(x) \cos 2\pi\nu x \Delta x$$

It can be shown from information theory that in order to obtain all the information in a spectrum from $0 < \nu < \nu_{max}$ it is necessary to sample points from the interferograms at intervals of

$$\Delta x = \frac{1}{2\nu_{max}}$$

In our case ν_{max} is 400 cm^{-1} and hence the sampling interval must be at least 12.5μ. Because of the periodic sampling it can be shown that at the frequency ν the computed spectrum contains false energies of frequencies.

$$2n\nu_{max} - \nu \qquad \text{where n is an integer.}$$

This effect is called aliasing and a black polythene filter was used to cut off frequencies above 400 cm^{-1} to produce an unambiguous spectrum.

The resolution obtained is governed by the maximum path difference of the interfering beams by the following relationship

$$\Delta \nu = \frac{1}{x}$$

All the sample runs were performed with a mirror movement of 8 mm either side of the ZPD giving a resolution of 0.625 cm^{-1}. The signal from the Golay detector was sent through an analogue/digital converter such that the interferogram function was digitised and outputed on paper tape. A 25 gauge Mylar beam splitter effectively covered a range of 40-400 cm^{-1} giving maximum transmission near 200 cm^{-1}.

The background and sample interferograms were then transformed and ratioed using a programme written at King's College, London University, which incorporated interferogram symmeterisation and triangular apodisation. The output spectra were then plotted at 0.5 cm^{-1} intervals such that any change in band shape which occurred would be clearly visible.

Sample Handling

A suitable polythene far infrared cell was constructed having a cell thickness of approximately 2 mm with apparatus designed in these laboratories (31). A stock solution of hexafluorobenzene in cyclohexane was prepared from which a constant

volume was pipetted each time to make up a series of solutions containing the same concentration of hexafluorobenzene in a mixed solvent solution containing varying amounts of benzene and cyclohexane. The interferograms of a cyclohexane background plus the solutions were recorded and the ratioed spectra plotted. The polythene cell was filled with each sample by means of a syringe and annealed with a hot spatula. To prevent deformation under vacuum the cell was firmly clamped between the metal parts of a conventional liquid cell (R.I.I.C. F-01). The accurate cell thickness was determined when all the runs had been completed - the cell was clearly cut and an average taken of various positions under a travelling microscope.

6.3 Results

The absolute intensity of an infrared absorption band for a molecule in solution is given by

$$\Gamma = \frac{N \times 1000 \times 2.303}{N \times c \times l} \int^{\text{Band}} \log_{10}\left(\frac{I_o}{I}\right) \frac{d\nu}{\nu}$$

M - molecular weight of molecule

c - concentration in $g.l^{-1}$

N - Avogadro constant

l - path length in cm.

The units of Γ are $cm^2 mol^{-1}$

Intensities in some texts are expressed in terms of a quantity A which is related as follows

$$A = \Gamma c \nu_o$$

where ν_o is the frequency of the band origin in cm^{-1}, and c is the velocity of light. The units of A are therefore $mol^{-1} cm^2 sec^{-1}$.

The absolute intensities of the 215 cm^{-1} band of HFB are presented in Table VI (1).

Table VI (1)

% w/w benzene	ν_{max}	$\Delta\nu_{\frac{1}{2}}$	A x 10^{-8}	Γ x 10^{-21}
0.0	216	7.5	4.34	6.69
4.0	216.5	8.0	4.62	7.11
7.9	216.5	9.0	5.12	7.88
15.5	217	10.0	5.27	8.08
25.0	217.5	10.0	5.28	8.10
50.0	218	11.3	5.15	7.91

The band area required for the calculation of Γ or A was obtained by the Simpson's Rule summation. The main difference which readily distinguishes interferometric spectra from conventional grating spectra is the position of the background curve (I_o). Wheatley (92) took the background absorption from the spectrum of the empty cell since benzene and cyclohexane show no absorption in the spectral range concerned. In the case of the above interferometric spectra a linear background base line was computed from two points at either extremities of the band where the rate of change of intensity with frequency was minimal. To check the validity of this approximation five solutions of different concentrations of hexafluorobenzene in cyclohexane were made up from the stock solution. Using the same cell the interferometric spectra were recorded and the band areas calculated. Figure VI (i) shows a linear Beer's Law plot passing through the origin, indicating that band areas computed in this way have meaningful values. This approximation will, however, affect the accuracy of the band shape near the wings and this will lead to uncertainties in the calculation of the correlation function referred to in Section 6.4.

It can clearly be seen from Table VI (i) that the position of the band maximum shifts by 2 cm^{-1} for a 50% w/w mixed solvent. The absolute intensity and half-band width

Fig VI (i)

Beer's Law Plot of Band Intensity vs Concentration for Hexafluorobenzene in Cyclohexane

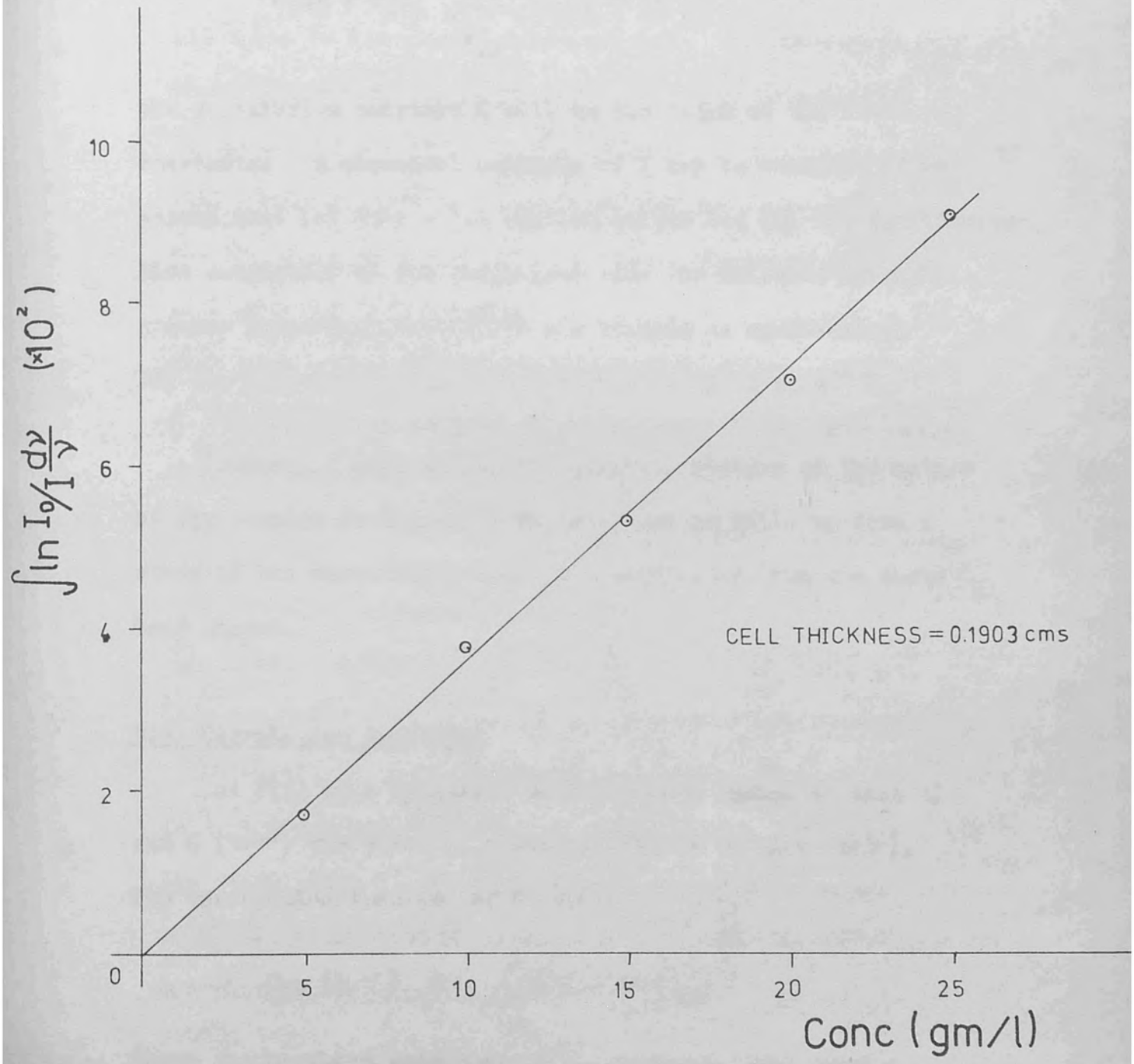

show a marked initial increase up to 15.5 % w/w mixed solvent and then remain fairly constant for greater proportions of benzene.

If we consider the equilibrium as follows,

$$C_6H_6 + C_6F_6 \underset{k_{-1}}{\overset{k_1}{\rightleftharpoons}} C_6H_6 = C_6F_6$$

the equilibrium constant K will be the ratio of the rate constants. A classical estimate of K can be obtained if we assume that (a) only a 1:1 complex exists and (b) the equilibrium lies completely to the right-hand side for solvents having a greater percentage than 15.5% w/w benzene to cyclohexane. For the 7.9% w/w solvent K has a value of 0.21 mole^{-1} l.

However, a more meaningful physical picture of the nature of the complex in the solution state can be built up from a study of the correlation functions calculated from the above band shapes.

6.4 Correlation Functions

Let F(t) be a dynamical variable of a system at time t, and G $(t+\tau)$ the value of another variable at time $(t+\tau)$. The correlation function of F and G is

$$C_{FG}(t,\tau) = \left\langle F(t)\, G(t+\tau) \right\rangle$$

where the brackets represent an average over some appropriate

statistical ensemble. If F and G are the same variable, $C(t,\tau)$ is known as the autocorrelation function, and if defined for an ensemble which is time independent we have

$$\left\langle G(t).G(t+\tau)\right\rangle = \left\langle G(0).G(\tau)\right\rangle = C_G(\tau)$$

Considering the motion of an individual molecule in a liquid, let $\mu_i(o)$ be its dipole moment at t=0. At subsequent times this moment $\mu_i(t)$ will follow a random behaviour covering positive and negative values. The product $\mu_i(0)\mu_i(t)$ will behave similarly. The summation of this product over all the molecules divided by the total number of molecules will give the dipole correlation function. At t=0, $c_\mu(t)$ will have a finite positive value and as t becomes large, $c_\mu(t)$ will converge towards zero. The dipole correlation function thus represents a qualitative measure of the loss of memory of the direction of the dipole after a certain time.

Correlation functions have great importance in non-equilibrium statistics because all transport phenomenon (e.g. diffusion and viscosity coefficients) may be expressed as integrals of the appropriate correlation function. In fact, whereas the knowledge of the partition function permits the calculation of all equilibrium properties of a system in equilibrium statistical mechanics, knowledge of the various time correlation functions permits the calculation of transport properties.

Time-dependent perturbation theory applied to the interaction of radiation with matter (97) gives the probability per unit time that a transition takes place between two quantum states. When calculating the band shape $I(\omega)$ using Heisenberg quantum mechanics, which stresses the time dependence of the system rather than the stationary levels of the Schrödinger model, an expression is obtained (98) involving a Fourier transform of the dipole correlation function

$$I(\omega) = \frac{1}{2\pi} \int_{-\infty}^{+\infty} d\,t\, e^{-i\omega t} \left\langle \mu(0) \cdot \mu(t) \right\rangle$$

Conversely, on inverting the Fourier analysis, an expression for the correlation function is obtained in terms of the band shape

$$C(t) = \int^{\text{band}} d\omega\, e^{i\omega t} I(\omega)$$

Considering only the real part of the correlation function

$$C(t) = \int^{\text{band}} I(\omega) \cos 2\pi\omega t \; d\omega$$

It is convenient to normalise the correlation function to unity at $t = 0$.

$$C(0) = \left\langle \mu^2(0) \right\rangle = \int^{\text{band}} I(\omega)\, d\omega$$

Hence $$C(t) = \frac{\int^{\text{band}} I(\omega)\cos 2\pi\omega t\, d\omega}{\int^{\text{band}} I(\omega)\, d\omega}$$

Gordon (99) plotted the correlation functions of carbon monoxide in various environments from previous experimental data. From Fig.VI(ii) the correlation function for a low pressure gas decays rapidly to assume negative values and then converges to zero. This indicates that the molecule is freely rotating such that after half a period of rotation its orientation is predominantly in the opposite direction. At higher pressures or in solution rotational relaxation is superseded by collisional reorientation and inter-molecular torques leading to an increase in the correlation function at a particular time.

A Fourier analysis of the band shape described above enables the short- and long-term motion to be considered separately. At short times the behaviour of the correlation function is best displayed by considering a power series in the time.

$$\langle \mu(0).\mu(t) \rangle = \sum_{n=0}^{\infty} \frac{t^n}{n!} \left(\frac{d^n}{dt^n} \langle \mu(0).\mu(t) \rangle \right)_{t=0}$$

Fig VI (ii)

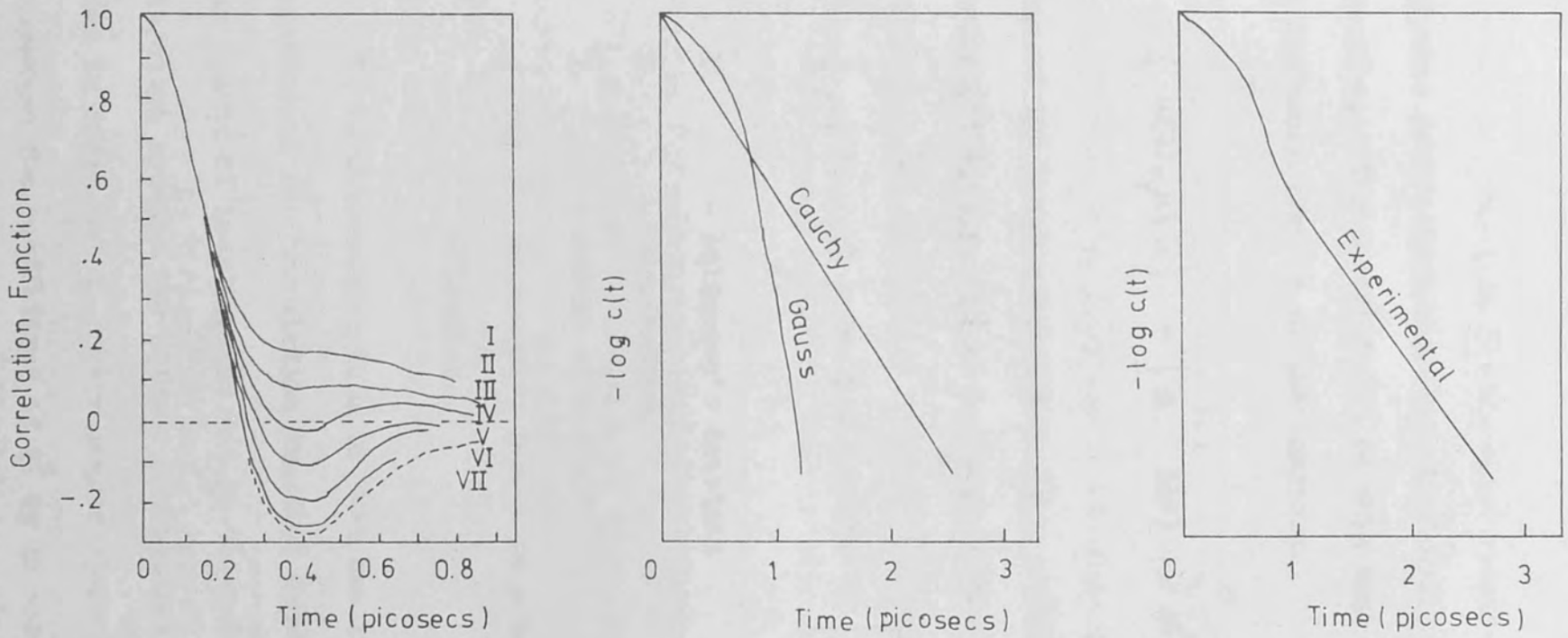

I – CO in $CHCl_3$ (liq)

II – CO in CCl_4 (liq)

III – CO in $n-C_7H_{16}$ (liq)

IV – CO in Ar (gas 510 amagat)

V – CO in Ar (gas 270 amagat)

VI – CO in Ar (gas 66 amagat)

VII – CO free (calculated)

Cauchy and Gauss absorption curves

Experimental curve

The time derivatives are determined using the time dependent wave equation. The coefficients in this time series are identified as frequency moments of the spectrum.

$$\left\langle \mu(0).\mu(t) \right\rangle = \int e^{i\omega t} I(\omega)\, d\omega = \sum_{n=0} \frac{(it)^n}{n!} \int \omega^n I(\omega) d\omega$$

Some of the lower moments have been computed previously by Gordon (100), e.g. for an infrared band of a linear molecule

$$\left\langle \mu(0).\mu(t) \right\rangle = 1 - (kT/I)t^2 + \left[\frac{1}{2}\left(\frac{kT}{I}\right)^2 + (24I^2)^{-1} \left\langle (OV)^2 \right\rangle \right] t^4$$

k - Boltzmann's constant

T - temperature,

I - moment of inertia

$\left\langle (OV)^2 \right\rangle$ - mean square torque on a molecule due to the other molecules.

It is interesting to note that the initial curvature (second moments) of the correlation function depends only on the temperature and moment of inertia, but not on the molecular forces. For classical systems the effects of intermolecular forces are first seen in terms for t^4. For longer times the hindering of rotation increases the coefficient of t^4 by an amount proportional to the mean-square torque. Hence the actual decay of the rotational

correlation function for hindered rotors is slower than the decay for free rotors. This can clearly be seen from a typical experimental decay curve in Fig. VI (ii).

For hexafluorobenzene M(2) can be calculated from molecular parameters and is found to be 28.92 cm^{-2}.

From an analysis of the band shape for hexafluorobenzene in cyclohexane with no benzene present the following moments were determined: $M(1) = -0.272\ cm^{-1}$, $M(2) = 11.09\ cm^{-2}$, $M(3) = -4.628\ cm^{-3}$, $M(4) = 416.2\ cm^{-4}$.

The second moment is thus considerably below its classical value and hence one may suspect that measurements were not carried far enough into the wings of the band. Slight assymmetry is indicated by the presence of finite values for odd moments. Hence during a brief initial period, free rotation, as in the gas, will determine the kinetics of the dipole rotation and the time correlation function should follow a Gauss decay rate.

At longer times the rotational motion has become so complicated by the intermolecular torques that the average correlation is indistinguishable from that of a stochastic (random averaged) exponential decay. The recent paper by Bratoz et al (101) describes a stochastic-type theory to explain the infrared spectra of inert solutions of diatomic molecules.

They discuss the relation between a given band form and the nature of the dominating relaxation process, which include translational diffusion, free rotation, rotational diffusion and an intermediate type reorientation. The characteristic narrowness of infrared and Raman bands in the solid state where rotational motion is suppressed indicate that in the solution state the reorientational relaxation function $G_R(t)$ is far greater in magnitude than the vibrational relaxation function $G_V(t)$. Rotational diffusion is, in fact, the most widely applied stochastic model for the behaviour of rotational correlation functions at long times, and the Lorentzian form generates a correlation function of the form

$$\ln G_R(t) = -\beta_R t$$

where β_R is taken as the rotational diffusion constant as calculated by Favro (102) which should have the same value for all vibrations of the same symmetry species.

6.5 Application to Hexafluorobenzene

The correlation functions of the band shapes recorded in Section 6.2 are plotted in Fig. VI(iii). It can be clearly seen that as the concentration of benzene increases, the correlation function relaxes faster. A collision-induced vibrational relaxation is probably taking place involving a

Fig VI (iii)

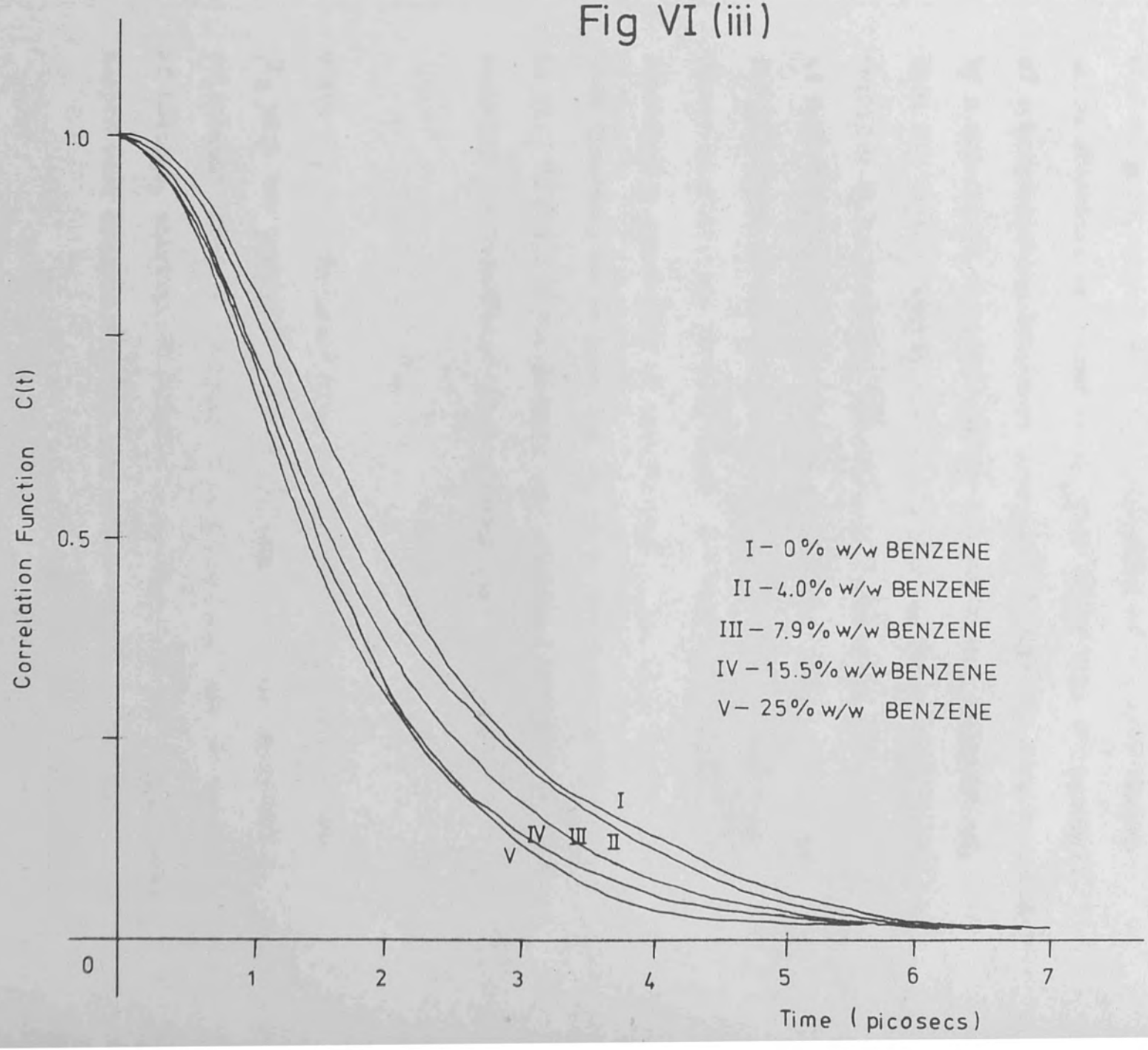
1.0
0.5
0
Correlation Function C(t)
1
2
3
4
5
6
7
Time (picosecs)
I
II
III
IV
V
I – 0% w/w BENZENE
II – 4.0% w/w BENZENE
III – 7.9% w/w BENZENE
IV – 15.5% w/w BENZENE
V – 25% w/w BENZENE

$\pi - \pi$ complex which involves bonding orbitals of the same symmetry as the out-of-plane a_{2u} mode of vibration. This mechanism is supported by the assymmetry of the band shapes which according to Bratoz et al (101) arise from the presence of a non-vanishing imaginary component of $G_V(t)$ in turn favoured by a one-to-one character in the solvent-solute interaction. When the complex splits the vibrational bond energy is presumably degraded to heat energy, a mechanism favoured by the fact that at room temperature, the photon energy $h\nu \sim kT$. A plot of the logarithm of the correlation functions versus time gave severe oscillations at long times such that the gradients exhibited a great deal of uncertainty. The band shapes were then symmeterised by hand and the plots recalculated as shown in Fig. VI (iv). The results are tabulated in Table VI (2). Assuming the Born-Oppenheimer approximation to hold

$$\beta_T = \beta_V + \beta_R$$

where β_V is associated with the vibrational relaxation and β_R with the reorientational diffusion. β_V can therefore be calculated for each solution if it is assumed that in the absence of benzene, vibrational relaxation is suppressed. The optimum slopes were calculated using the method of least squares.

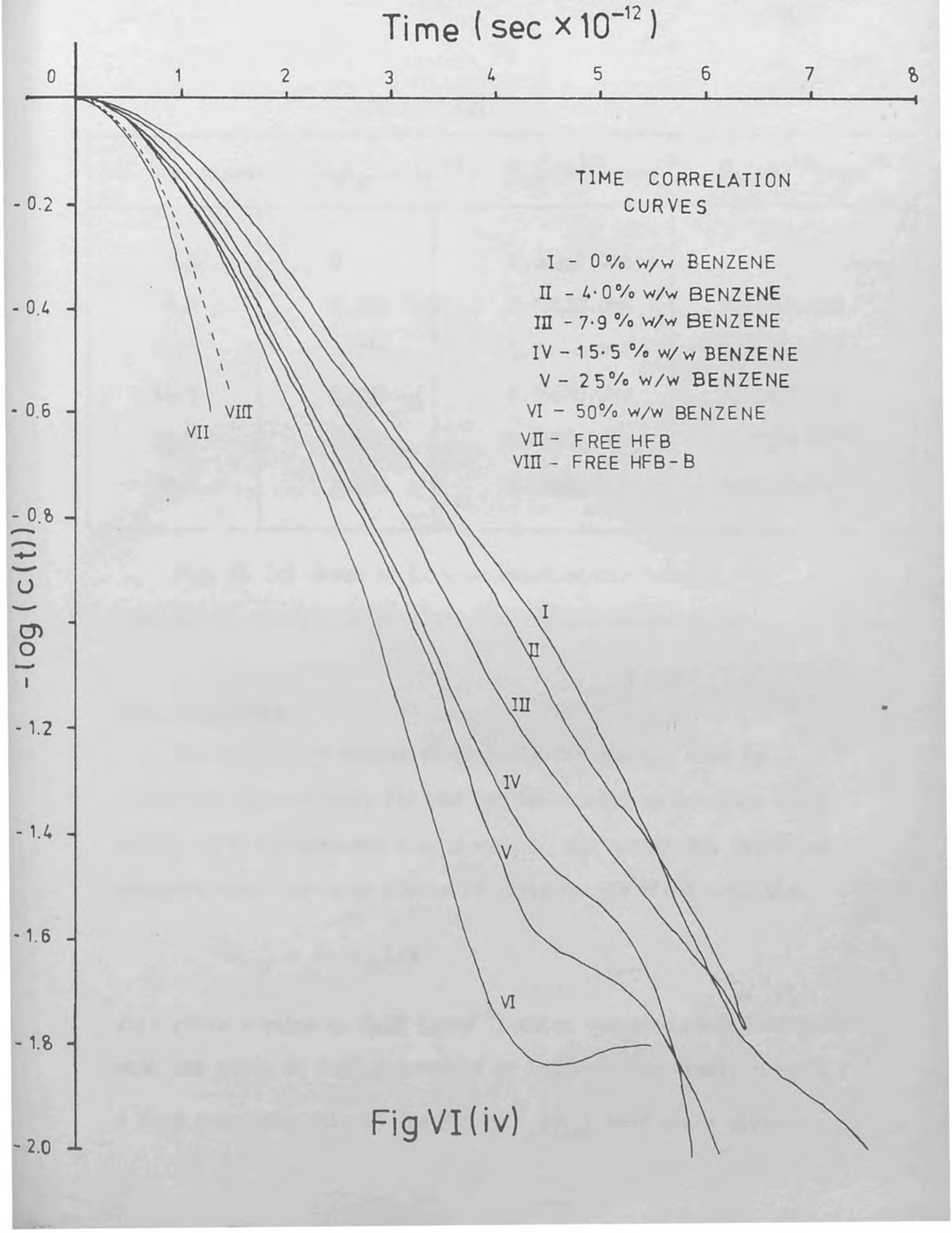
Time (sec × 10⁻¹²)
0
1
2
3
4
5
6
7
8
- 0.2
- 0.4
- 0.6
- 0.8
- 1.2
- 1.4
- 1.6
- 1.8
- 2.0
- log (c(t))
TIME CORRELATION CURVES
I - 0% w/w BENZENE
II - 4·0% w/w BENZENE
III - 7·9 % w/w BENZENE
IV - 15·5 % w/w BENZENE
V - 25% w/w BENZENE
VI - 50% w/w BENZENE
VII - FREE HFB
VIII - FREE HFB-B
I
II
III
IV
V
VI
VII
VIII

Fig VI (iv)

Table VI (2)

% w/w benzene	$[C_6H_6]$ mole.$^{-1}$	$\beta_T(\times 10^{12})$ psec^{-1}	$\beta_V(\times 10^{12})$ psec^{-1}
0.0	0	0.642±0.005	0
4.0	0.385	0.698±0.005	0.056±0.010
7.9	0.736	0.743±0.006	0.092±0.012
15.5	1.358	0.896±0.007	0.254±0.013
25.0	2.041	0.879±0.007	0.237±0.012
50.0	3.453	1.144±0.009	0.502±0.014

Fig. VI (v) shows an inverse relationship between the vibrational relaxation time and the benzene concentration.

6.6 Discussion

The transition moment responsible for the a_{2u} band is along the symmetry axis (z) and can be rotated by rotation about either of the equivalent x or y axes. The rotational diffusion constant about the x or y axis is given by the simple relation

$$D_{x,y} = \beta_R(a_{2u})/2$$

This gives a value of 0.32 (psec^{-1}) which compares very favourably with the value of 0.36 determined by Fujiyama and Grawford (95). A band shape analysis of the 315 cm^{-1} (e_{1u}) band would give an

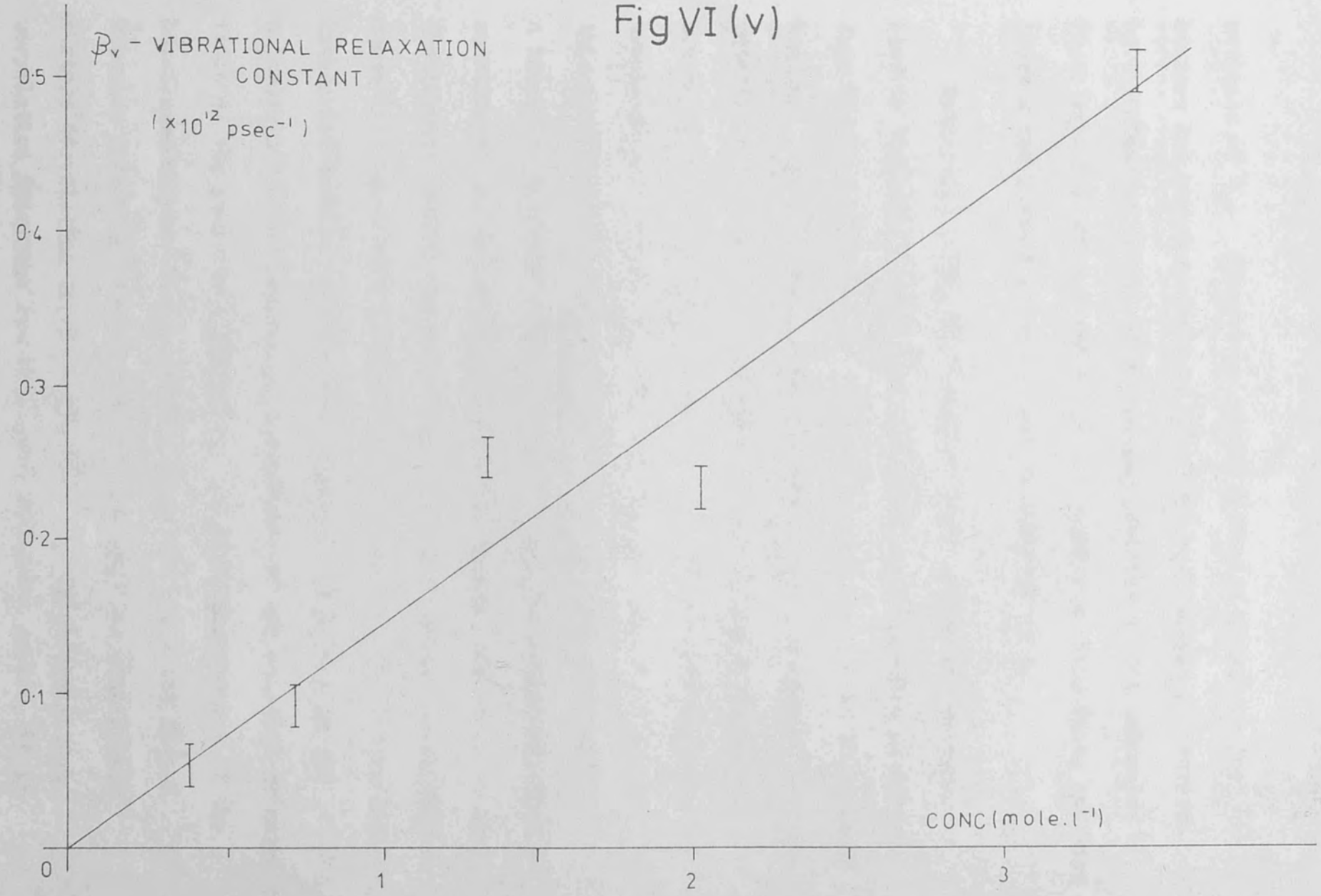
Fig VI (v)
β_v - VIBRATIONAL RELAXATION CONSTANT
($\times 10^{12}$ psec^{-1})
0·5
0·4
0·3
0·2
0·1
0
1
2
3
CONC (mole.l^{-1})

estimate of D_z. Comparison of the diffusion constants for benzene and hexafluorobenzene show that replacement of hydrogen by fluorine has little effect on the spinning of the molecules (i.e. rotation about z axis) but the ability to flip (i.e. rotation about x and y axes) is diminished by a factor of 3.

Rothschild (103), in a similar study of the chloroform-benzene complex, investigated the correlation function derived from the band shape of the 362 cm^{-1} (parallel) mode of $CDCl_3$ in benzene. He also calculated the correlation function of freely rotating $CDCl_3$ molecules and from a value of the equilibrium constant, the correlation function of an equilibrium mixture of complexed and uncomplexed $CDCl_3$ molecules. For short times this correlation function is, to a good approximation, given by a linear combination of two gaussians, each describing the free rotation of the corresponding molecular species and weighted by the correct equilibrium mole fraction. The actual correlation curve fell below that of the calculated equilibrium mixture and Rothschild deduced that the weak intermolecular bond in the chloroform-benzene complex is independent of the relative orientations of the individual molecules. A similar treatment of the hexafluorobenzene-benzene complex gives the solid and dashed Gaussian curves in Fig. VI (iv) for the free and equilibrium mixture correlation curves respectively. Since the actual correlation functions lie well above these two curves, it is

deduced that the HFB-B complex is held together by relatively strong anisotropic forces, i.e. rotation of the HFB molecule about the intermolecular bond (z axis) may be possible but not in a perpendicular direction (x and y axes). This deduction will be correct even if the estimate of the equilibrium constant K is wrong, because the moment of inertia of the complex is only fractionally larger than that of free HFB.

Fig. VI (iv) shows that the correlation curves of hexafluorobenzene start to disperse after 0.3 picosecs. Up to 0.2 picosecs all the curves are indistinguishable indicating that on the average HFB molecules and HFB-B complex initially experience free rotation. An estimate of the reverse rate constant (k_{-1}) for the HFB-B equilibrium will be

$$k_{-1} = \frac{1}{\tau_v} = \beta_v$$

This estimate assumes that vibrational energy transfer occurs in every dissociative act.

Since $K = 0.2 = {}^{k_1}/_{k_{-1}}$

then $k_1 \sim 1 \times 10^{11}$ litres mole^{-1} sec^{-1} (for 50% w/w solvent). This is of the order one might expect for diffusion controlled reactions.

Interesting aspects of molecular motion in the solution state for other simple molecules have been investigated from the dipole-correlation time curves. Fujiyama and Crawford (104) showed that an isotope effect operated when substitution of hydrogen by deuterium in methyl iodide affected the rotational diffusion constants. Rothschild (105) investigated most of the fundamentals of methylene chloride as well as summation, difference and overtone bands. The results showed that the anisotropy of the rotational motion in the liquid state is very similar to that found with freely-rotating CH_2Cl_2 molecules. In other words the rotational motion is insensitive to molecular association or weak hydrogen-bond formation.

6.7 Conclusion

Evidence for the existence of the HFB-B complex in the liquid state from a study of the dipole autocorrelation functions has been presented. The concept of the time correlation function is being applied to other measurements of the properties of liquids, particularly proton magnetic resonance, electron spin resonance and neutron diffraction spectroscopy. Whether one obtains the true kinetically significant band is difficult to assess. Infrared and Raman bands are influenced by weak dombination and difference bands, hot bands and displaced bands

arising from molecules containing isotopic species. Corrections arising from variable refractive index has been discussed by Crawford and co-workers (95, 104) using the method of attenuated total reflection. More recently, Konynenburg and Steele (106) have calculated the correlation functions for three simple molecules (chloroform, methyl iodide and methylene chloride) after correction had been made to the band shapes to eliminate these contributions. In the future more sophisticated models of the liquid state will be formulated for simple and complex molecules, but for the present the experimental difficulties of generating meaningful spectra are a more serious limitation.

Appendix 1.

All the programmes described in this thesis are available on magnetic tape (MARYLU No. UH0031) or permanent disc file on the London University CDC 6600. Programme LINDA whose flow diagram is given in Chapter 1 can be modified to give either Cartesian Displacements (CD) or Potential Energy Distribution (PED). The version outlined below in Fortran IV shows how the redundancies are removed to give the Cartesian Displacement coordinates for a typical large molecule.

```
      PROGRAM LINDA (INPUT,OUTPUT,TAPE2=INPUT,TAPE1=OUTPUT)
      DIMENSION G(72,72),F(72,72),GMAT(20,20),FMAT(20,20),
     ZX(3,22),EA(72),B(68,72)AMASS(22),U(72,20),MARY(5),DMAT
     Z(20,20),D(20,20),S(20),R(20),IH(8),JH(8),VAL(8),IB(9),
     ZJB(9),VALUE(9),Z(20),A(72,72)
      COMMON NOAT,NINT,NQ,NATOM1,NATOM2,NATOM3,NATOM4,NATOM5,
     ZNATOM6,NR,NDEF,RA
      READ(2,3)NPROB
    3 FORMAT(I1)
      DO 4 NCYC=1,NPROB
      READ(2,5)MARY
    5 FORMAT(5A8)
      WRITE(1,6)MARY
    6 FORMAT(1H1,50X,5A8,/,51X,10H**********,//)
      READ(2,7)NOAT,NR
    7 FORMAT(2I2)
      NQ=3*NOAT
      WRITE(1,8)NOAT,NR
    8 FORMAT(1H ,40X,10HNO. ATOMS=,I2,/,41X,16HNO. INT. COORDS=,I2,////)
      READ(2,12)((X(I,J),I=1,3),J=1,NOAT)
   12 FORMAT(9F8.5)
      WRITE(1,13)
   13 FORMAT(1H ,40X,1HX,20X,1HY,20X,1HZ)
      DO 14 J=1,NOAT
   14 WRITE(1,15)J,X(1,J),X(2,J),X(3,J)
   15 FORMAT(1H ,20X,I2,15X,F8.5,12X,F8.5,12X,F8.5)
      WRITE(1,16)
   16 FORMAT(1H ,////,54X,8HB MATRIX,/,54X,8H********,//)
      DO 17 IC=1,NR
      DO 18 I=1,NQ
   18 EA(I)=0.0
      READ(2,19)NINT,NDEF,NATOM1,NATOM2,NATOM3,NATOM4,NATOM5,NATOM6
   19 FORMAT(8I3)
      WRITE(1,20)NINT,NDEF,NATOM1,NATOM2,NATOM3,NATOM4,NATOM5,NATOM6
   20 FORMAT(1H ,5X,5HNINT=I2,5X,5HNDEF=I2,5X,7HNATOM1=I2,5X,7HNATOM2
     Z=I2,5X,7HNATOM3=I2,5X,7HNATOM4=,I2,5X,7HNATOM5=I2,5X,7HNATOM6
     Z=I2)
      GO TO (21,22,23,24,25,26)NDEF
   21 CALL STRET(X,EA)
      GO TO 127
   22 CALL ABEND(X,EA)
      GO TO 127
```

```
 23 CALL OPLAN(X,EA)
    GO TO 127
 24 CALL TORSN(X,EA)
    GO TO 127
 25 CALL IPLAN(X,EA)
    GO TO 127
 26 CALL SPECT(X,EA)
    GO TO 127
127 DO 27 J=1,NQ
 27 B(J,NINT)=EA(J)
 17 CONTINUE
    READ(2,28)(AMASS(I),I=1,NOAT)
 28 FORMAT(8F10.6)
    WRITE(1,29)
 29 FORMAT(1H ,////,50X,4HMASS/50X,4H****,/)
    DO 30 I=1,NOAT
 30 WRITE(1,31)I,AMASS(I)
 31 FORMAT(1H ,20X,I2,13X,F10.6)
    DO 32 J=1,NR
    DO 33 I=1,NR
    G(I,J)20.0
    DO 34 K1=1,NOAT
    DO 35 M=1,3
    K2=3*K1+M-3
    G(I,J)=G(I,J)+B(K2,I)*B(K2,J)/AMASS(K1)
 35 CONTINUE
 34 CONTINUE
 33 CONTINUE
 32 CONTINUE
    READ(2,133)NSYMB,MCDS
133 FORMAT(2I2)
    DO 51 I=1,NR
    DO 52 J=1,NR
    F(I,J)=0.0
 52 CONTINUE
 51 CONTINUE
    WRITE(1,56)
 56 FORMAT(1H ,///,30X,23HUNSYMMETERISED F MATRIX/30X,23H**********
   Z**********,////)
    DO 53 KD=1,MCDS
    READ(2,54)(IH(M),JH(M),VAL(M),M=1,8)
 54 FORMAT(8(2I2,F6.4))
    WRITE(1,58)(IH(M),JH(M),VAL(M),M=1,8)
```

```
 58 FORMAT(8(2HF(,I2,1H,I2,2H)=,F7.4,1X))
    DO 55 M=1,8
    IG=IH(M)
    JG=JH(M)
    F(IG,JG)=VAL(M)
 55 F(JG,IG)=VAL(M)
 53 CONTINUE
    WRITE(1,134)NSYMB
134 FORMAT(1H ,////,40X,17HNO. SYMM. BLOCKS=,I2)
    DO 135 JC=1,NSYMB
    READ(2,36)NDIM,NCDS,NRT
 36 FORMAT(3I2)
    WRITE(1,37)NDIM,NCDS,NRT
 37 FORMAT(1H ,///,20X,5HNDIM=I2,20X,5HNCDS=,I2,20X,4HNRT=,I2,/)
    DO 9 I=1,NR
    DO 10 J=1,NDIM
    U(I,J)=0.0
 10 CONTINUE
  9 CONTINUE
    DO 38 KC=1,NCDS
    READ(2,39)(IB(N),JB(N),VALUE(N),N=1,9)
 39 FORMAT(9(2I2,F4.0))
    DO 40 N=1,9
    ID=IB(N)
    JD=JB(N)
 40 U(JD,ID)=VALUE(N)
    WRITE(1,41)(IB(N),JB(N),VALUE(N),N=1,9)
 41 FORMAT(1H 9(2HU(I2,1H,I2,2H)=F4.1,1X))
 38 CONTINUE
    DO 42 JA=1,NDIM
    US=0.0
    DO 43 IA=1,NR
 43 US=US+U(IA,JA)*U(IA,JA)
    UN=SQRT(US)
    DO 44 IA=1,NR
 44 U(IA,JA)=U(IA,JA)/UN
 42 CONTINUE
    DO 145 I=1,NDIM
    DO 144 J=1,NDIM
    CMAT(I,J)=0.0
144 CONTINUE
145 CONTINUE
    DO 46 JA=1,NDIM
    DO 47 IA=1,NR
    EA(IA)=0.0
    DO 48 K=1,NR
 48 EA(IA)=EA(IA)+U(K,JA)*G(K,IA)
```

```
 47  CONTINUE
     DO 49 IA=1,NDIM
     DO 50 K=1,NR
 50  GMAT(IA,JA)=GMAT(IA,JA)+EA(K)*U(K,IA)
 49  CONTINUE
 46  CONTINUE
     WRITE(1,45)JC
 45  FORMAT(1H ,50X,14HSYMM G MATRIX(,I1,1H),/,50X,16H****************,
    Z///)
     WRITE(1,60)((I,J,GMAT(I,J),J=1,NDIM),I=1,NDIM)
 60  FORMAT(5(3H G(I2,1H,I2,2H)=F12.8,3X))
     DO 161 I=1,NDIM
     DO 162 J=1,NDIM
     FMAT(I,J)=0.0
162  CONTINUE
161  CONTINUE
     DO 62 JA=1,NDIM
     DO 63 IA=1,NR
     EA(IA)=0.0
     DO 64 K=1,NR
 64  EA(IA)=EA(IA)+U(K,JA)*F(K,IA)
 63  CONTINUE
     DO 65 IA=1,NDIM
     DO 66 K=1,NR
 66  FMAT(IA,JA)=FMAT(IA,JA)+EA(K)*U(K,IA)
 65  CONTINUE
 62  CONTINUE
     WRITE(1,61)JC
 61  FORMAT(1H ,///,50X,14HSYMM F MATRIX(,I1,1H),/,50X.16H*************
    Z***,///)
     WRITE(1,168)((I,J,FMAT(I,J),J=1,NDIM),I=1,DNIM)
168  FORMAT(1H ,5(2HF(,I2,1H,I2,2H)=,F12.8,3X))
     CALL EA03A(GMAT,DMAT,NDIM,20,1E-08)
     LY=0
     DO 67 I=1,NDIM
     R(I)=GMAT(I,I)
     IF(R(I).LE.0.001) GO TO 68
     JI=I-LY
     A(JI,JI)=SQRT(R(I))
     DO 69 J=1,NDIM
     D(J,JI)=DMAT(J,I)
 69  CONTINUE
     GO TO 67
 68  LY=LY+1
     WRITE(1,70)
 70  FORMAT(22H NEGATIVE ROOT WARNING)
 67  CONTINUE
```

```
      DO 72 I=1,NDIM
      DO 73 J=1,NRT
      GMAT(I,J)=0.0
      DO 74 K=1,NDIM
      GMAT(I,J)=GMAT(I,J)+FMAT(I,K)*D(K,J)
   74 CONTINUE
   73 CONTINUE
   72 CONTINUE
      DO 76 I=1,NRT
      DO 77 J=1,NRT
      DMAT(I,J)=0.0
      DO 78 K=1,NDIM
      DMAT(I,J)=DMAT(I,J)+D(K,I)*GMAT(K,J)
   78 CONTINUE
   77 CONTINUE
   76 CONTINUE
      DO 79 I=1,NRT
      DO 80 J=1,NRT
      FMAT(I,J)=0.0
      DO 81 K=1,NRT
      FMAT(I,J)=FMAT(I,J)+DMAT(I,K)*A(K,J)
   81 CONTINUE
   80 CONTINUE
   79 CONTINUE
      DO 179 I=1,NRT
      DO 180 J=1,NRT
      DMAT(I,J)=0.0
      DO 181 K=1,NRT
      DMAT(I,J)=DMAT(I,J)+A(I,K)*FMAT(K,J)
  181 CONTINUE
  180 CONTINUE
  179 CONTINUE
      CALL EA03A(DMAT,FMAT,NRT,20,1E-08)
      DO 183 I=1,NRT
      S(I)=0.0
  183 CONTINUE
      DO 184 I=1,NRT
      S(I)=1302.9*SQRT(DMAT(I,I))
      WRITE(1,185)I,S(I)
  185 FORMAT(7H OMEGA(I2,2H)=F10.1)
  184 CONTINUE
      DO 201 I=1,NRT
      DO 202 J=1,NRT
      DMAT(I,J)=0.0
```

```
      DO 203 K=1,NRT
      DMAT(J,I)=DMAT(J,I)+A(J,K)*FMAT(K,I)
  203 CONTINUE
  202 CONTINUE
      WRITE(1,186)I,(DMAT(J,I),J=1,NRT)
  186 FORMAT(23H EIGENVECTOR FOR OMEGA(I2,1H),/10(2X,F9.5))
  201 CONTINUE
      DO 190 I=1,NRT
      DO 190 J=1,NRT
      GMAT(I,J)=0.0
  190 CONTINUE
      DO 191 I=1,NRT
      DO 192 J=1,NRT
      GMAT(J,I)=FMAT(J,I)/A(I,1)
  192 CONTINUE
  191 CONTINUE
      DO 87 I=1,NDIM
      DO 88 J=1,NRT
      DMAT(I,J)=0.0
      DO 89 K=1,NRT
      DMAT(I,J)=DMAT(I,J)+D(I,K)*GMAT(K,J)
   89 CONTINUE
   88 CONTINUE
   87 CONTINUE
      DO 91 I=1,NR
      DO 92 J=1,NRT
      A(I,J)=0.0
      DO 93 K=1,NDIM
      A(I,J)=A(I,J)+U(I,K)*DMAT(K,J)
   93 CONTINUE
   92 CONTINUE
   91 CONTINUE
      DO 95 I=1,NQ
      DO 96 J=1,NRT
      U(I,J)=0.0
      DO 97 K=1,NR
      U(I,J)=U(I,J)+B(I,K)*A(K,J)
   97 CONTINUE
   96 CONTINUE
   95 CONTINUE
      DO 98 I=1,NQ
      DO 99 J=1,NR
      A(I,J)=0.0
   99 CONTINUE
   98 CONTINUE
      DO 100 I=1,NOAT
```

```
      DO 101 M=1,3
      L=3*I+M-3
      DO 102 J=1,NRT
      A(L,J)=U(L,J)/AMASS(I)
102   CONTINUE
101   CONTINUE
100   CONTINUE
      DO 103 I=1,NRT
      WRITE(1,104)I
104   FORMAT(1H ,20X,33HCARTESIAN DISPLACEMENT FOR OMEGA(,I1,1H),/
     Z25X,1HX,20X,1HY,20X,1HZ)
      WRITE(1,105)(AJ,I),J=1,NQ)
105   FORMAT(3(15X,F9.5))
103   CONTINUE
      DO 221 I=1,NDIM
      DO 221 J=1,NDIM
      DMAT(I,J)=0.0
      D(I,J)=0.0
221   CONTINUE
      DO 222 I=1,NR
      DO 222 J=1,NR
      A(I,J)=0.0
222   CONTINUE
      DO 223 I=1,NDIM
      R(I)=0.0
223   CONTINUE
135   CONTINUE
  4   CONTINUE
      CALL EXIT
      END
```

Appendix 2

Symmetry coordinates for biphenyl and its 4-4' disubstituted derivatives for the D_2 point group

A Species

$$S_1 = R_{1-7}$$
$$S_2 = 2^{-1}(r_{8-18} + r_{12-22} + r_{6-17} + r_{2-13})$$
$$S_3 = 2^{-1}(r_{9-19} + r_{11-21} + r_{5-16} + r_{3-14})$$
$$S_4 = 2^{-\frac{1}{2}}(r_{10-20} + r_{4-15})$$
$$S_5 = 2^{-1}(R_{7-8} + R_{12-7} + R_{6-1} + R_{1-2})$$
$$S_6 = 2^{-1}(R_{5-6} + R_{2-3} + R_{8-9} + R_{11-12})$$
$$S_7 = 2^{-1}(R_{9-10} + R_{10-11} + R_{4-5} + R_{3-4})$$
$$S_8 = 2^{-\frac{1}{2}}(\alpha_1 + \alpha_7)$$
$$S_9 = 2^{-\frac{1}{2}}(\alpha_{10} + \alpha_4)$$
$$S_{10} = 2^{-1}(\alpha_{12} + \alpha_8 + \alpha_6 + \alpha_2)$$
$$S_{11} = 2^{-1}(\alpha_3 + \alpha_5 + \alpha_9 + \alpha_{11})$$
$$S_{12} = 2^{-1}(\gamma_{8-18} - \gamma_{12-22} - \gamma_{17-6} + \gamma_{13-2})$$
$$S_{13} = 2^{-1}(\gamma_{9-19} - \gamma_{21-11} - \gamma_{16-5} + \gamma_{14-3})$$
$$S_{14} = 2^{-1}(\beta_{8-18} - \beta_{22-12} - \beta_{17-6} + \beta_{13-2})$$
$$S_{15} = 2^{-1}(\beta_{19-9} - \beta_{21-11} - \beta_{16-5} + \beta_{14-3})$$
$$S_{16} = 2^{-1}(\phi_{8-9} + \phi_{11-12} + \phi_{5-6} + \phi_{2-3})$$
$$S_{17} = 2^{-1}(\phi_{7-8} + \phi_{12-7} + \phi_{6-1} + \phi_{1-2})$$
$$S_{18} = 2^{-1}(\phi_{9-10} + \phi_{10-11} + \phi_{4-5} + \phi_{3-4})$$

B1 Species

$$S_1 = 2^{-1}(r_{8-18} - r_{12-22} - r_{6-17} + r_{2-13})$$
$$S_2 = 2^{-1}(r_{9-19} - r_{11-21} - r_{5-16} + r_{3-14})$$
$$S_3 = 2^{-1}(R_{7-8} - R_{7-12} + R_{1-2} - R_{1-6})$$
$$S_4 = 2^{-1}(R_{8-9} - R_{11-12} + R_{2-3} - R_{5-6})$$
$$S_5 = 2^{-1}(R_{9-10} - R_{10-11} + R_{3-4} - R_{4-5})$$
$$S_6 = 2^{-1}(\alpha_8 - \alpha_{12} + \alpha_2 - \alpha_6)$$
$$S_7 = 2^{-1}(\alpha_9 - \alpha_{11} + \alpha_3 - \alpha_5)$$
$$S_8 = 2^{-1}(\gamma_{8-18} + \gamma_{12-22} + \gamma_{2-13} + \gamma_{6-17})$$
$$S_9 = 2^{-1}(\gamma_{9-19} + \gamma_{11-21} + \gamma_{3-14} + \gamma_{5-16})$$
$$S_{10} = 2^{-1}(\beta_{8-18} + \beta_{12-22} + \beta_{2-13} + \beta_{6-17})$$
$$S_{11} = 2^{-1}(\beta_{9-19} + \beta_{11-21} + \beta_{3-14} + \beta_{5-16})$$
$$S_{12} = 2^{-1}(\phi_{8-9} - \phi_{11-12} + \phi_{2-3} - \phi_{5-6})$$
$$S_{13} = 2^{-1}(\phi_{7-8} - \phi_{12-7} + \phi_{1-2} - \phi_{6-1})$$
$$S_{14} = 2^{-1}(\phi_{9-10} - \phi_{10-11} + \phi_{3-4} - \phi_{4-5})$$
$$S_{15} = 2^{-\frac{1}{2}}(\beta_{10-20} + \beta_{4-15})$$
$$S_{16} = 2^{-\frac{1}{2}}(\beta_{1-7} + \beta_{7-1})$$
$$S_{17} = 2^{-\frac{1}{2}}(\gamma_{1-7} + \gamma_{7-1})$$
$$S_{18} = 2^{-\frac{1}{2}}(\gamma_{10-20} + \gamma_{4-15})$$

B2 Species

$$S_1 = 2^{-1}(r_{8-18} - r_{12-22} - r_{2-13} + r_{6-17}$$

$$S_2 = 2^{-1}(r_{9-19} - r_{11-21} - r_{3-14} + r_{5-16})$$

$$S_3 = 2^{-1}(R_{7-8} - R_{7-12} - R_{1-2} + R_{6-1})$$

$$S_4 = 2^{-1}(R_{8-9} - R_{11-12} - R_{2-3} + R_{5-6})$$

$$S_5 = 2^{-1}(R_{9-10} - R_{10-11} - R_{1-4} + R_{4-5})$$

$$S_6 = 2^{-1}(\alpha_8 - \alpha_{12} - \alpha_2 + \alpha_6)$$

$$S_7 = 2^{-1}(\alpha_9 - \alpha_{11} - \alpha_3 + \alpha_5)$$

$$S_8 = 2^{-1}(\gamma_{8-18} + \gamma_{12-22} - \gamma_{2-13} - \gamma_{6-17})$$

$$S_9 = 2^{-1}(\gamma_{9-19} + \gamma_{11-21} - \gamma_{3-14} - \gamma_{5-16})$$

$$S_{10} = 2^{-1}(\beta_{8-18} + \beta_{12-22} - \beta_{2-13} - \beta_{6-17})$$

$$S_{11} = 2^{-1}(\beta_{9-19} + \beta_{11-21} - \beta_{3-14} - \beta_{5-16})$$

$$S_{12} = 2^{-1}(\phi_{8-9} - \phi_{11-12} - \phi_{2-3} + \phi_{5-6})$$

$$S_{13} = 2^{-1}(\phi_{7-8} - \phi_{12-7} - \phi_{1-2} + \phi_{6-1})$$

$$S_{14} = 2^{-1}(\phi_{9-10} - \phi_{10-11} - \phi_{3-4} + \phi_{4-5})$$

$$S_{15} = 2^{-\frac{1}{2}}(\beta_{10-20} - \beta_{4-15})$$

$$S_{16} = 2^{-\frac{1}{2}}(\beta_{7-1} - \beta_{1-7})$$

$$S_{17} = 2^{-\frac{1}{2}}(\gamma_{10-20} - \gamma_{4-15})$$

$$S_{18} = 2^{-\frac{1}{2}}(\gamma_{1-7} - \gamma_{7-1})$$

B3 Species

$$S_1 = 2^{-1}(r_{8-18} + r_{12-22} - r_{2-} - r_{6-17})$$
$$S_2 = 2^{-1}(r_{9-19} + r_{11-21} - r_{3-14} - r_{5-16})$$
$$S_3 = 2^{-\frac{1}{2}}(r_{10-20} - r_{4-15})$$
$$S_4 = 2^{-1}(R_{7-8} + R_{7-12} - R_{6-1} - R_{1-2})$$
$$S_5 = 2^{-1}(R_{8-9} + R_{11-12} - R_{5-6} - R_{2-3})$$
$$S_6 = 2^{-1}(R_{9-10} + R_{10-11} - R_{4-5} - R_{3-4})$$
$$S_7 = 2^{-\frac{1}{2}}(\alpha_7 - \alpha_1)$$
$$S_8 = 2^{-\frac{1}{2}}(\alpha_{10} - \alpha_4)$$
$$S_9 = 2^{-1}(\alpha_8 + \alpha_{12} - \alpha_2 - \alpha_6)$$
$$S_{10} = 2^{-1}(\alpha_9 + \alpha_{11} - \alpha_3 - \alpha_5)$$
$$S_{11} = 2^{-1}(\gamma_{8-18} - \gamma_{12-22} - \gamma_{2-13} + \gamma_{6-17})$$
$$S_{12} = 2^{-1}(\gamma_{9-19} - \gamma_{11-21} - \gamma_{3-14} + \gamma_{5-16})$$
$$S_{13} = 2^{-1}(\beta_{8-18} - \beta_{12-22} - \beta_{2-13} + \beta_{6-17})$$
$$S_{14} = 2^{-1}(\beta_{9-19} - \beta_{11-21} - \beta_{3-14} + \beta_{5-16})$$
$$S_{15} = 2^{-1}(\phi_{8-9} + \phi_{11-21} - \phi_{2-3} - \phi_{5-6})$$
$$S_{16} = 2^{-1}(\phi_{7-8} + \phi_{12-7} - \phi_{1-2} - \phi_{6-1})$$
$$S_{17} = 2^{-1}(\phi_{9-10} + \phi_{10-11} - \phi_{3-4} - \phi_{4-5})$$

Potential energy distribution of a simplified valence force field for biphenyl (diagonal constants only)

	S_1	S_2	S_3	S_4	S_5	S_6	S_7	S_8	S_9	S_{10}	S_{11}	S_{12}	S_{13}	S_{14}	S_{15}	S_{16}	S_{17}	S_{18}
Ag																		
3073		61	6	32														
3072		5	93															
3069		33		66														
1690	19				30	26		7						11				
1527	6					21	25							9	31			
1338	29					22				5				23	14			
1192														51	45			
1024					19		36			15	14			6	7			
998					9	22	37	6	7	8	9							
745	13				28				31		18							
272	32				11			29	6	16								
Au																		
963												37	37			19		
833												40	40				10	10
409												16	16			48	10	10
B1g																		
3070	50	49																
3069	49	50																

	S_1	S_2	S_3	S_4	S_5	S_6	S_7	S_8	S_9	S_{10}	S_{11}	S_{12}	S_{13}	S_{14}	S_{15}	S_{16}	S_{17}	S_{18}
1609			40		38													
1449			9	14	17					8	21				36			
1337			13		11					44	17				6			
1292			17	38	25					12	8							
1155			9	13						8	32				33			
1069			11	26	19					20	7				6	6		
607						45	47											
342																89		
B1u																		
987								8	35			8		22				26
898								48				11	6	9				23
726								30	23			9						32
703									39			11	24	17			9	
431													16	37			34	10
91													41				52	
B2u																		
3070	34	66																
3069	66	34																
1608			39		40		5								6			

	S_1	S_2	S_3	S_4	S_5	S_6	S_7	S_8	S_9	S_{10}	S_{11}	S_{12}	S_{13}	S_{14}	S_{15}	S_{16}	S_{17}	S_{18}
1430			9	14							31				39			
1326				29	17	26				23								
1295				30	16					39	11							
1161			8	10						9	35				36			
1055			14	32	19					14	7				6			
622						44	47											
96																90		
B2g																		
987								10	34			8		22			25	
909								50				8	8	10			20	5
755								15	16			15					32	22
694									47			9	16	14				14
515								5						28			12	55
239								11					65	11				9

	S_1	S_2	S_3	S_4	S_5	S_6	S_7	S_8	S_9	S_{10}	S_{11}	S_{12}	S_{13}	S_{14}	S_{15}	S_{16}	S_{17}	S_{18}
B3u																		
3073	61	6	32															
3072	5	93																
3069	33		66															
1610				15	52	12							7	6				
1483				14		15							33	35				
1193													48	48				
1040				43		20	8	7					9	8				
1020						15	9	8	30	29								
992				23	32	39												
611							29	31	15	16								
B3g																		
963											37	37			19			
833											40	40				10	10	
409											16	16			48	10	10	

Potential energy distribution of a simplified valence force field for 4-4'difluorobiphenyl (%)

	S_1	S_2	S_3	S_4	S_5	S_6	S_7	S_8	S_9	S_{10}	S_{11}	S_{12}	S_{13}	S_{14}	S_{15}	S_{16}	S_{17}	S_{18}
Ag																		
3073		10	89															
3072		89	10															
1664	20				31	25	3	7		3				10				
1535	5			7	3	18	28		5					8	27			
1347	29					23		3		4	3			24	13			
1241				56		16	11		7		4			3				
1143														49	50			
1022					23		28		3	18	19			4	4			
835	4			15	23	9	25	9	7	6								
653	14			22	13		8		27		12							
229	29				10	5		27	10	15	3							
Au																		
958												38	37			19	3	3
829												40	42				9	9
409												16	16			49	10	9

	S_1	S_2	S_3	S_4	S_5	S_6	S_7	S_8	S_9	S_{10}	S_{11}	S_{12}	S_{13}	S_{14}	S_{15}	S_{16}	S_{17}	S_{18}
B1g																		
3070	19	80																
3069	80	19																
1583			41		40											5		
1391			20	6	22					21	17				6	6		
1293										43	53							
1274			19	55	18					6								
1095			15	10	15					24	24				5	5		
610						48	46											
444															68	25		
301				8											18	70		
B1u																		
946								31	41			18						
821								38	33				10	5				10
711								23				20	9	13			16	18
494													20				14	60
280									11					56			29	
55													43	6			43	

	S_1	S_2	S_3	S_4	S_5	S_6	S_7	S_8	S_9	S_{10}	S_{11}	S_{12}	S_{13}	S_{14}	S_{15}	S_{16}	S_{17}	S_{18}
B2u																		
3070	11	88																
3069	88	11																
1586			41		42													
1361			27		21					10	30				6			
1291			15	46	17						21							
1279				19	5					62	11							
1088			17	16	15					17	25				6			
619						47	45											
417															85			
75																90		
B2g																		
949								34	39			17						
838								38	32				10	7			7	7
727								5				24		6			20	38
520								5						9			46	37
382									6				30	22			17	22
150								7	9				45	34				5

	S_1	S_2	S_3	S_4	S_5	S_6	S_7	S_8	S_9	S_{10}	S_{11}	S_{12}	S_{13}	S_{14}	S_{15}	S_{16}	S_{17}	S_{18}
B_{3u}																		
3073	10	89																
3072	89	10																
1586				13	50	16								5				
1494			4	15		14							33	30				
1245			55		10	11		8		5			5					
1144													47	52				
1032				69	12	4							6	4				
1016					9	27	8	9	24	22								
800			27		5	30	21		14									
525			12		6		17	39	8	15								
B_{3g}																		
958											38	37			19	4		
829											40	42				9	9	
409											16	16			49	10	9	

Appendix 5

NMRFIT is a programme written to plot the output of either DUNKEN or PERT incorporating CALCOMP subroutines.

```
      PROGRAM NMRFIT(INPUT,OUTPUT,TAPE25,TAPE27,TAPE6=OUTPUT)
      DIMENSION X(5003),Y(5003),MARY(4),FR(100),SIZE(100)
      COMMON FRINC,NL,W,FR1,FR,SIZE
      CALL START
      READ 2,W,NLINES
    2 FORMAT(F6.0,I3)
      PRINT 7, W,NLINES
    7 FORMAT(1H1,20X,16HHALF-BAND WIDTH=,F6.3/21X,14HORIG NO
     ZLINES=,I3////)
      READ 3,(FR(I),SIZE(I),I=1,NLINES)
    3 FORMAT(6(F7.3,F6.3))
      PRINT 8
    8 FORMAT(1H ,20X,9HFREQUENCY,20X,9HINTENSITY/)
      DO 10 I=1,NLINES
      PRINT 11, FR(I),SIZE(I)
   11 FORMAT(1H ,22X,F7.3,24X,F6.3)
   10 CONTINUE
      READ 4,NPROB
    4 FORMAT(I1)
      DO 5 NYC=1,NPROB
      READ 6,MARY,FR1,FR2
    6 FORMAT(4A10,2F7.3)
      PRINT 12, MARY,FR1,FR2
   12 FORMAT(1H ,20X,4A10/,22X,13HINITIAL FREQ=,F7.3/22X,11HFINAL
     ZFREQ=,F7.3)
      NL=0
   31 DO 30 J=1,NLINES
      IF(FR(J).GE.FR1) GO TO 28
      GO TO 31
   28 IF(FR(J).LE.FR2) GO TO 27
      GO TO 31
   27 NL=NL+1
      FR(NL)=FR(J)
      SIZE(NL)=SIZE(J)
   30 CONTINUE
      FRINC=(FR2-FR1)/5000.0
      CALL PLOT(9.0,14.0,3)
      CALL SYMBOL(9.0,14.0,0.28,15HNMR SPECTRUM OF,0.0,15)
      CALL SYMBOL(9.0,13.5,0.28,MARY,0.0,22)
      CALL CURVE(X,Y)
```

```
      PRINT 14,(I,X(I),I,Y(I),I=1500,2000)
   14 FORMAT(4(2HX(I4,2H)=F8.3,2X,2HY(I4,2H)=F7.4))
      CALL PLOT(3.0,2.0,-3)
      CALL SCALE(X,20.0,5001,-1)
      CALL SCALE(Y,10.0,5001,1)
      CALL AXIS(0.0,0.0,12HFREQUENCY HZ,-12,20.0,00.0,X(5002),X(5003))
      CALL AXIS(0.0,0.0,9HINTENSITY,+9,10.0,090.0,Y(5003))
      CALL LINE(X,Y,5001,1,0,0)
      CALL PLOT(24.0,-2.0,-3)
    5 CONTINUE
      CALL ENPLOT(4.0)
      END
```

```
      SUBROUTINE CURVE(X,Y)
      DIMENSION X(5003),Y(5003),FR(100),SIZE(100)
      COMMON FRINC,NL,W,FR1,SIZE
      DO 2 J=1,5001
      Y(J)=0.1
      X(J)=FR1+J*FRINC
    2 CONTINUE
      DO 3 I=1,NL
      M=IFIX(FR(I)/FRINC)
      N=IFIX(5.0*W/FRINC)
      NN=2*N+1
      DO 4 L=1,NN
      LN=L-N-1
      LA=M+LN
      Y(LA)=Y(LA)+SIZE(I)/(1.0+(2.0/W*LN*FRINC)**2)
    4 CONTINUE
    3 CONTINUE
      RETURN
      END
```

References

1. Y. Morino, IXth European Congress on Molecular Spectroscopy, I.U.P.A.C. (1969).

2. K. Machida and J. Overend, J. Chem. Phys., 50, 4429, (1969).

3. E. B. Wilson, J. C. Decius and P. C. Cross, Molecular Vibrations, McGraw-Hill, New York (1955).

4. D. Steele, Theory of Vibrational Spectroscopy, Saunders, (1971).

5. G. Varsanyi, Vibrational Spectra of Benzene Derivatives, Academic Press (1971).

6. F. A. Cotton, Chemical Applications of Group Theory, New York, Interscience, (1967).

7. R. P. Bell, Trans. Faraday Soc., 41, 293 (1945).

8. I. Harada and T. Shimanouchi, J. Chem. Phys., 44, 2016 (1966).

9. J. R. Scherer and J. Overend, J. Chem. Phys., 33, 1681 (1960).

10. J. R. Scherer and J. Overend, Spectrochim. Acta, 17, 719 (1961).

11. D. F. Heath and J. W. Linnett, Trans. Faraday Soc., 44, 556 (1948).

12. J. C. Duinker, Doctorate Thesis, University of Amsterdam, (1964).

13. J. C. Decius, J. Chem. Phys., 38, 241 (1963).

14. S. J. Cyvin and N. B. Slater, Nature, 188, 485 (1960).

15. M. Gussoni and G. Zerbi, J. Mol. Spect., 26, 485 (1968).

16. R. G. Snyder and J. H. Schachtschneider, Spectrochim. Acta, 21, 169 (1965).

17. Y. Morino and K. Kuchitsu, J. Chem. Phys., 20, 1809 (1952).

18. J. Dale, Acta Chem. Scand., 11, 640 (1957).

19. J. E. Katon and E. R. Lippincott, Spectrochim. Acta, 15, 627 (1959).

20. D. Steele and E. R. Lippincott, J. Mol. Spect., 6, 238 (1961).

21. G. V. Peregudov, Opt. Spect., 9, 155 (1960).

22. B. Pasquier and J. M. Lebas, J. Chem. Phys., 64, 765 (1966).

23. G. Zerbi and S. Sandroni, Spectrochim. Acta, 24A, 483 (1968).

24. G. Zerbi and S. Sandroni, Spectrochim. Acta, 24A, 511 (1968).

25. J. Dahr, Indian J. Phys., 7, 43 (1932).

26. J. Trotter, Acta Cryst., 14, 1135 (1961).

27. R. A. Hoffmann, P. O. Kinell and G. Bergström, Arkiv. Kemi., 15, 534 (1960).

28. K. Mocbius, Z. Naturforsch, 20a, 1093 (1965).

29. O. Bastiansen, Acta Chem. Scand., 3, 408 (1949).

30. H. Suzuki, Bull. Chem. Soc. Japan, 32, 1340 (1959).

31. S. Ashdown, T. F. Crowdy and D. Steele, Lab. Pract., 15, 868 (1966).

32. K. Radcliffe and D. Steele, Spectrochim. Acta, 25A, 597 (1969).

33. V. Eaton and D. Steele, Unpublished Data.

34. K. Krebs, S. Sandroni and G. Zerbi, J. Chem. Phys., 40, 3502 (1964).

35. E. C. Lim and Y. H. Li, J. Chem. Phys., 52, 12 (1970).

36. I. J. Wagner, J. Am. Chem. Soc., 89, 2820 (1967).

37. A. Imamura and R. Hoffmann, J. Am. Chem. Soc., 90, 5379 (1968).

38. A. F. Miller, W. G. Fateley and R. E. Witkowski, Spectrochim. Acta, 23A, 891 (1967).

39. G. Casalone, C. Mariani, A. Mugnoli and M. Simonetta, Mol. Phys., 15, 4, 339 (1968).

40. A. Finch, P. N. Gates, K. Radcliff, F. Dickson and F. Bentley, Chemical Applications of Far-Infrared Spectroscopy, Academic Press (1970).

41. P. Nanni, F. Viani and V. Lorenzelli, J. Mol. Struct., 6, 133 (1970).

42. R. E. Buckles and N. G. Wheeler, Org. Syn., 31, 29 (1951).

43. R. M. Barrett and D. Steele, Unpublished Data.

44. D. Steele, T. R. Nanney and E. R. Lippincott, Spectrochim. Acta, 22, 849 (1966).

45. D. Steele, Spectrochim. Acta, 25A, 959 (1969).

46. I. Mills, Centenary Lecture of the Chemical Society (April 1971).

47. R. G. Jones and H. Gilman, Org. Reactions, 6, 352 (1951).

48. R. I. Akawie, J. M. Scarborough and J. G. Burr, J. Org. Chem., 24, 946 (1959).

49. G. Zerbi and S. Sandroni, Spectrochim. Acta, 26A, 1951 (1970).

50. M. Hanack, Conformational Theory, Academic Press, New York, (1965).

51. E. L. Eliel et al, Conformational Analysis, Interscience, New York (1966).

52. H. Booth, Chapter 7, Progress in N.M.R. Spectroscopy, J. W. Emsley, J. Feeney and L. H. Sutcliffe, Vol. 5, Pergamon Press.

53. M. Larnaudie, J. Phys. Radium, 15, 650 (1954).

54. H. E. Hallam and T. C. Ray, J. Chem. Soc., 2337 (1964).

55. D. H. R. Barton, J. E. Page and C. W. Shoppee, J. Chem. Soc., 331 (1956).

56. I. O. C. Ekejuiba and H. E. Hallam, J. Mol. Structure, 6, 341 (1970).

57. R. G. Snyder and G. Zerbi, Spectrochim. Acta, 23A, 391 (1967).

58. R. G. Snyder and J. H. Schachtschneider, J. Mol. Spect., 30, 290 (1969).

59. R. G. Snyder, J. Mol. Spect., 28, 273 (1968).

60. G. W. C. Kaye and T. H. Laby, Tables of Physical and Chemical Constants, Longmans (1966).

61. R. F. Nystrom and W. G. Brown, J. Am. Chem. Soc., 69, 2549 (1947).

62. Chem. Abs., 50, 13892c, (1956).

63. F. R. Jensen and L. H. Gale, J. Org. Chem., 25, 2075 (1961).

64. R. A. Pickering and C. C. Price, J. Am. Chem. Soc., 80, 4931 (1958).

65. P. Klaeboe, J. J. Lothe and K. Lunde, Acta Chem. Scand., 10, 1465 (1956).

66. K. Kozima and K. Sakashita, Bull. Chem. Soc. Japan, 31, 796 (1958).

67. A. J. Berlin and F. R. Jensen, Chem. Ind., 998 (1960).

68. G. Chuirdoglu, L. Kleiner, W. Masschelein and J. Reisse, Bull. Soc. Chim. Belges, 69, 143 (1960).

69. N. Muller and W. C. Tosch, J. Chem. Phys., 37, 1167 (1962).

70. A. L. Anet and A. J. R. Bourn, J. Am. Chem. Soc., 89, 760 (1967).

71. H. S. Gutowsky and C. H. Holm, J. Chem. Phys., 25, 1228 (1956).

72. F. R. Jensen, D. S. Noyce, C. H. Sederholm and A. J. Berlin, J. Am. Chem. Soc., 82, 1256 (1960).

73. E. L. Eliel, Chem. Ind., 568 (1959).

74. A. J. Berlin and F. R. Jensen, Chem. Ind., 998 (1960).

75. J. Reisse, J. C. Celotti and G. Chiurdoglu, Tetrahedron Letters, 7, 397 (1965).

76. E. L. Eliel and M. H. Gianni, Tetrahedron Letters, 97 (1962).

77. L. W. Reeves and K. O. Strømme, Can. J. Chem., 38, 1241 (1960).

78. F. A. Bovey, E. W. Anderson, F. P. Hood and R. L. Kornegay, J. Chem. Phys., 40, 3099 (1964).

79. F. R. Jensen, C. H. Bushweller and B. H. Beck, J. Am. Chem. Soc., 91, 344 (1969).

80. G. Gatti, A. L. Segre and C. Morandi, J. Chem. Soc. (B), 1203 (1967).

81. R. J. Kurland, M. B. Rubin and W. B. Wise, J. Chem. Phys., 40, 2426 (1964).

82. A. Allerhand, H. S. Gutowsky, J. Jonas and R. A. Meinzer, J. Am. Chem. Soc., 88, 3185 (1966).

83. J. A. Pople, W. G. Schneider and H. J. Bernstein, High-Resolution Nuclear Magnetic Resonance, McGraw-Hill (1959).

84. R. M. Lynden-Bell and R. K. Harris, Nuclear Magnetic Resonance Spectroscopy, Nelson (1969).

85. C. R. Patrick and G. S. Prosser, Nature, 187, 1021 (1960).

86. D. V. Fenby and R. L. Scott, J. Phys. Chem., 71, 4103 (1967).

87. E. M. Dantzler and C. M. Knobler, J. Phys. Chem., 73, 1602 (1969).

88. W. J. Gaw and F. L. Swinton, Trans. Faraday Soc., 64, 2023 (1968).

89. W. A. Duncan, J. P. Sheridan and F. L. Swinton, Trans. Faraday Soc., 62, 1090 (1966).

90. M. E. Baur, D. A. Horsma, C. M. Knobler and P. Perez, J. Phys. Chem., 73, 641 (1969).

91. J. C. A. Boeyens and F. H. Herbstein, J. Phys. Chem., 69, 2153 (1965).

92. W. Wheatley, Ph.D. Thesis, University of London, (1968).

93. D. Steele and D. H. Whiffen, Trans. Faraday Soc., 55, 369 (1959).

94. L. Delbouille, Bull. Classe Sci. Acad. Roy. Belg., 44, 971 (1958).

95. T. Fujiyama and B. Crawford, J. Phys. Chem., 72, 2174 (1968).

96. W. J. Hurley, J. Chem. Education, 43, 5, 237 (1966).

97. L. Pauling and E. B. Wilson, Introduction to Quantum Mechanics, McGraw-Hill, New York (1935).

98. R. G. Gordon, Advances in Magnetic Resonance, Vol. 3, Academic Press (1968).

99. R. G. Gordon, J. Chem. Phys., 43, 1307 (1965).

100. R. G. Gordon, J. Chem. Phys., 39, 2788 (1963).

101. S. Bratoz, J. Rios and Y. Guissani, J. Chem. Phys., 52, 439 (1969).

102. L. D. Favro, Phys. Rev., 119, 53 (1960).

103. W. G. Rothschild, Chem. Phys. Letters, 9, 2, 149 (1971).

104. T. Fujiyama and B. Crawford, J. Phys. Chem., 73, 4040 (1969).

105. W. G. Rothschild, J. Chem. Phys., 53, 990 (1970).

106. P. Konynenburg and W. A. Steele, J. Chem. Phys., 56, 4776 (1972).

Journal of Molecular Structure
Elsevier Publishing Company, Amsterdam. Printed in the Netherlands

THE VIBRATIONAL SPECTRA AND DIHEDRAL ANGLES OF BIPHENYL AND THE 4,4′-DIHALOGENOBIPHENYLS

R. M. BARRETT AND D. STEELE

Department of Chemistry, Royal Holloway College, University of London, Englefield Green, Surrey (England)

(Received July 13th, 1971)

ABSTRACT

The vibrational frequencies of biphenyl and its 4,4′-dihalogen derivatives have been computed for various values of the dihedral angle between the two rings. It is shown that certain modes with frequencies below 700 cm^{-1} are sensitive to this angle. Agreement between experimental and calculated frequencies is good. The spectra of biphenyl and 4,4′-difluorobiphenyl are in complete accord with a planar D_{2h} structure in the crystal phase. In solution, melt and gas the dihedral angle of these systems is $45 \pm 15°$. The observed frequency shifts of certain A modes are shown to be due to considerable force constant changes for the central C–C bond and its neighbouring internal angle deformations. No significant frequency shifts with phase changes were observed for 4,4′-dichloro- or 4,4′-dibromobiphenyl. In these cases the structures are D_2.

INTRODUCTION

Biphenyl poses some interesting structural problems. It is known to be planar (D_{2h} configuration) in the crystal[1,2] and to have a staggered configuration in the vapour phase with a dihedral angle[3] of $45 \pm 10°$. NMR data show a non-planar configuration in solution but is inconclusive as to the dihedral angle[4]. In principle the vibrational spectra of the various possible configurations should show marked differences. It has been an embarrassing fact that despite many studies in the past[5–12] convincing evidence of spectral changes accompanying a change of state has been sadly lacking. Only one paper[12] reports data showing such evidence, and the spectral interpretation here is based on qualitative arguments. This raises the question as to whether or not vibrational spectroscopy really can give unequivocal evidence for structure. In view of this important issue it was decided to re-examine the spectra from theoretical and practical viewpoints. It will be shown

that drastic changes do occur in the spectra of biphenyl and one of its 4,4′-di-substituted derivatives on change of phase. The contradiction between earlier and the present work is due in part, but not entirely, to the fact that the low-frequency spectra, both Raman and infrared had been inadequately examined.

Spectral changes can arise from two sources: changes in restoring forces and changes in coupling conditions resulting from different geometries. As the dihedral angle changes, the π orbital overlap will vary and possibly lead to changes in bond orders and restoring forces on the nuclei. The experimental evidence is that π orbital overlap between the rings is very weak. The only positive data is that the inter-ring bond length in the crystal is 1.50 Å, a value only slightly less than the accepted value of 1.54 Å for a C–C single bond. Electron diffraction data yield a value of 1.48 Å for this bond in the vapour phase. This small bond length decrease, if real, may imply a slightly higher bond order, but still near unity, and a steric interaction between the 2,2′ substituents. Zerbi and Sandroni[10] sought evidence for coupling between the rings by carrying out a perturbation analysis of planar biphenyl using two simple quadratic force fields. Their results indicated that the extent of delocalization of π bonds across the inter-ring C–C bond must be very small. They also believed that evidence for steric interactions between substituents (hydrogen) on the two rings was weak. These conclusions lead to the predictions that the restoring forces will be changed by very little when biphenyl loses its planarity. We shall show that there are some force constant changes whose affect on the spectra can be distinguished from those due to changes in the kinetic energy expressions. The latter however are responsible almost entirely for the observed spectral variations. Thus the dihedral angles in solution may be estimated subject to the limitation of the accuracy of calculations for the planar case. Discrepancies between the calculated and observed frequencies for the planar configuration have large effects on the perturbations produced by changes in the dihedral angles.

Substitution on the aromatic rings leads to changes in the stabilities of the planar configurations through inductive and mesomeric effects, shown by the fact that the 4,4′-dichloro- and -dibromobiphenyls are twisted in the crystal and solution phases, whereas biphenyl itself and its 4,4′-difluoro derivative are planar in the crystal and twisted in solution.

SPECTRAL PREDICTIONS BASED ON SYMMETRY CONSIDERATIONS

As the dihedral angle is rotated from 0° to 90° so the nuclear geometry changes from D_{2h} through D_2 to D_{2d}. In the D_{2h} configuration the in-plane and out-of-plane vibrations do not interact if high order effects such as Coriolis coupling are ignored. For a significant rotation about the central bond – one large enough to change the shape of the vibrational potential wells – the centre of symmetry is

effectively lost and the symmetry classes of the D_{2h} group coalesce in pairs. Each pair is constituted from a gerade and an ungerade species and from an out-of-plane and an in-plane species of the D_{2h} configuration (Fig. 1). Thus, provided the in-plane and out-of-plane vibrational wavefunctions mix, the vibrations constituting the pairs of classes will push one another apart and the mixing of the wavefunctions will lead to a relaxation of the spectral activities. On this basis changes can be predicted.

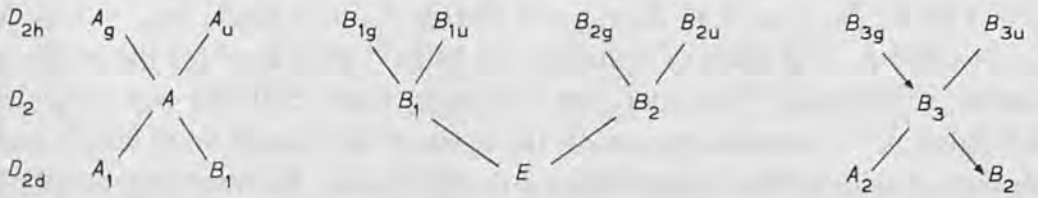

Fig. 1. Relationships between vibrations of different symmetry species for biphenyl in the D_{2h}, D_2 and D_{2d} configurations.

In first-order perturbation theory the interaction between levels depends

(i) on the interaction integral $\langle\psi_a|H_{ab}|\psi_b\rangle$; rotation of the rings with respect to one another will not affect this integral if the vibrational wavefunctions are localized in the rings;

(ii) inversely on the difference between the energy levels. This implies that interaction will be weak unless there are similar vibrational frequencies in the species which coalesce.

The in-plane and out-of-plane fundamental frequencies range from 3000 to 70 cm^{-1}, and 1000 cm^{-1} down respectively. It follows from (ii) that the perturbations will lie below 1000 cm^{-1}. This range can be narrowed. Coupling can only occur through those modes which span the ring. As will be explained below interaction cannot occur in the A species. This precludes any interaction through the CC stretch. Other internal deformations which span the ring and may lead to coupling are γ_C (out-of-plane deformation of the C_1 external to the ring), β_C (in-plane deformation of C_1) and δ, or ϕ (ring torsion). The natural frequency of the γ_{CH} deformation lies well above that of the only in-plane deformation coordinate to span the ring, β_C, being about 900 cm^{-1} compared to 300 cm^{-1}. Again interaction is predicted to be weak. The primary perturbations arise from ϕ, β_C interactions.

Calculations reported below show that no interaction occurs between the a_g and a_u, nor between the b_{3g} and b_{3u}, vibrations on reduction of the symmetry, though this is formally allowed. The explanation is that in the a_u and b_{3g} vibrations the nuclei lying on the C_2 axis passing through C_1 and C_1' cannot move without violating the appropriate transformation properties of the species. Coupling can only occur through the C_2 and C_6 carbons. As is easily shown the symmetry cartesian

co-ordinates of these nuclei for A_u, A_g, B_{3u} and B_{3g} representations rotate with the rings and hence remain orthogonal for all dihedral angles.

CALCULATIONS

All calculations were performed on a CDC 6600 computer using Fortran programmes. The logic of the programmes is as reported previously[13]. The aromatic rings were assumed to be regular hexagons and the bond lengths were taken as $R_{CC} = 1.40$ Å; $R_{C_1C_{1'}} = 1.48$ Å; $r_{CH} = 1.084$ Å; $r_{CF} = 1.30$ Å; $r_{CCl} = 1.70$ Å and $r_{CBr} = 1.865$ Å. The fields of Duinker and Mills[14] were used for the in-plane deformation coordinates. The inter-ring stretching force constant was assumed to be 4.9 mdyn $Å^{-1}$ – a value chosen on the basis of the known bond length and a simple force constant/bond length relation for CC bonds. No inter-ring coupling constants were introduced in view of the uncertainty concerning any resonance interaction. All out-of-plane force constants are transferred directly from derived fields for benzene and mono- and *p*-di-halogenobenzenes[15]. As there are no data on values for angle bending constants for a carbon substituent on a ring we assumed that the energy required for a unit angular deformation was independent of the substituent. This has been shown to be a reasonable first approximation[15]. The values chosen were based on the benzene values. All constants are given in Table 1.

In this work we have not used the force field of Zerbi and Sandroni[10] since it was derived from a perturbation analysis using their biphenyl assignments and we wished our conclusions to be independent of this earlier work. It is extremely encouraging that our computed frequencies (Tables 2 to 5) are in almost as good an agreement with the assignments as their perturbed field.

EXPERIMENTAL

Calculations were carried out on the London University CDC 6600. Biphenyl was purchased from B.D.H. Ltd., 4,4′-difluorobiphenyl from Koch-Lights Ltd., 4,4′-dichlorobiphenyl from Pfaltz & Bauer Inc. and 4,4′-dibromobiphenyl was synthesized according to Buckles and Wheeler[16]. The near infrared spectra (1700–200 cm^{-1}) were recorded with a Perkin–Elmer 325 and the far infrared spectra (400–40 cm^{-1}) with a R.I.I.C. FS 720. All solid interferometric spectra were recorded at liquid nitrogen temperature to prevent evaporation of the sample under vacuum. Raman spectra were recorded with either a Cary 81 (180° scattering and He/Ne 6328 Å exciting line) or a Spex Ramalog (90° scattering and Ar^+ 5147 Å exciting line). Molten Raman spectra were taken in a specially designed glass heating finger at University College and the gas-phase spectra using facilities at Southampton University.

TABLE 1

THE QUADRATIC FORCE CONSTANTS USED IN CALCULATING THE FREQUENCIES OF THE SYSTEMS $XC_6H_4 \cdot C_6H_4X$

Interaction constants are shown in parentheses. The units are mdyn $Å^{-1}$ for stretching constants, mdyn rad^{-1} for stretch/bend interactions and mdyn Å rad^{-2} for bending constants.

Force constant for coordinate	*X = H*	*X = F*	*X = Cl*	*X = Br*
r_i^2 (H)	5.125	5.125	5.125	5.125
r_i^2 (X)	—	5.80	3.70	3.12
β_i^2 (H)	1.035	1.012	1.028	1.036
β_i^2 (X)	—	1.741	1.656	1.117
R_i^2	7.015	6.97	6.87	6.95
β^2 (C)	1.035	1.012	1.028	1.036
R_i^2 (C)	4.9	4.9	4.9	4.9
α_i^2 (H)	1.103	1.070	1.213	1.149
α_i^2 (X)	—	1.394	1.405	1.207
(R_i, R_{i+1})	0.531	0.526	0.480	0.558
(R_i, β_i)	0.364	0.347	0.379	0.414
$(R_i, \beta_i(X))$	—	0.448	0.425	0.476
$(r_i, \alpha_i(X))$	—	−0.637	−0.772	−0.557
(β_i, β_{i+1})	0.028	0.047	0.022	0.015
(β_i, β_{i+2})	−0.022	−0.022	−0.019	−0.008
(β_i, β_{i+3})	−0.032	−0.073	−0.065	−0.080
(α_i, α_{i+1})	−0.098	−0.096	0.000	−0.043
(R_i, α_i)	0.442	0.463	0.441	0.462
$(r_i\ (X), R_i)$	—	0.429	0.334	0.336
(β_i, α_{i+1})	0.064	0.064	0.064	0.064
γ_H^2	0.307	0.306	0.311	0.310
γ_X^2	—	0.359	0.354	0.321
ϕ_{HH}^2	0.0706	0.0700	0.0700	0.0700
ϕ_{HX}^2	—	0.0676	0.0561	0.0684
$(\gamma_H \gamma_H^o)$	0.0153	0.0155	0.0145	0.0155
$(\gamma_H \gamma_H^m)$	−0.0129	−0.0132	−0.0153	−0.0148
$(\gamma_H \gamma_H^p)$	−0.0141	−0.0142	−0.0135	−0.0159
$(\gamma_H \gamma_X^o)$	—	0.0234	0.0284	0.0281
$(\gamma_H \gamma_X^m)$	—	−0.0058	−0.0116	−0.0040
$(\gamma_H \gamma_X^p)$	—	−0.0056	0.0013	0.0160
$(\phi\phi_o)$	−0.0137	−0.0141	−0.0131	−0.0129
$(\gamma_H\ \phi_o)$	0.0182	0.0187	0.0190	0.0191
$(\gamma_X\ \phi_o)$		−0.0195	−0.0081	−0.0123
$(\gamma_X\ \phi_m)$		−0.0122	−0.0055	−0.0115

Note: $(R_i, R_{i+1}) = -(R_i, R_{i+2}) = (R_i, R_{i+3})$

TABLE 2

CALCULATED AND OBSERVED FREQUENCIES (cm^{-1}) FOR BIPHENYL FOR VARIOUS DIHEDRAL ANGLES

Calculated frequencies for all θ	*Observed frequencies*				
	Raman			*Infrared*	
	Solid	*Liquid*	*Gas*	*Solid*	*Liquid*
A Species ($D_{2h}-A_g$, A_u)					
A_g					
3073, 3072, 3069	No measurements				
1690	1610 vs	1612 vs	1613 vs	—	—
1527	1513 m	1509 m (0.27)	1505 w	—	—
1338	1276 vs	1285 vs (0.18)	1282 vs	—	—
1192	1205 w	1192 m (br) (0.18)	—	—	—
1024	1036 s	1031 s (0.06)	1029 m	—	—
998	1002 vs	1004 vs (0.09)	1003 vs	—	—
745	743 sh/739 m	741 vs (0.08)	740 s	—	—
272	330 m	316 m (0.18)	307 s	—	315 w
A_u					
963	—	967* m (0.29)	964* w	—	964* vw
833	846* w	841* m (0.33)	838* w	—	838* m
409	409* vw	410* m (0.56)	405* m	—	403* s
B_3 Species ($D_{2h}-B_{3u}$, B_{3g})					
B_{3u}					
3073, 3072, 3069	No measurements				
1610	—	—		1597 s	1595* s
1483	—	—	—	1480 vs	1481 s
1193	—	—	—	1181 m	1174 w
1040	—	—	—	1041 s	1042 s
1020	—	—	—	1006 s	1007 s
992	—	—	—	985 w	990 w
611	—	—	—	610 m	609 s
B_{3g}					
963	—	969* m (0.29)	964* w	—	964* vw
833	846* w	841* m (0.33)	838* w	—	838* m
409	409* vw	410* m (0.56)	405* m	—	403*s

θ=0°	*30°*	*60°*	*90°*					
B_1 Species ($D_{2h}-B_{1g}$, B_{1u})								
B_{1g}								
3070, 3069	3070, 3069	3070, 3069	3070, 3069	No measurements				
1609	1608	1606	1605	1592 vs	1595 s	1596 vs	—	1595* vs
1449	1448	1443	1439	1462 w	1462 w	—	—	1455* m
1337	1336	1332	1328	1333 w	—	—	—	1317 w
1292	1293	1294	1296	1263 sh-w	1249 m	1233 m	—	—
1155	1155	1156	1158	1165/1149 m	1158 m (0.81)	—	—	—
1069	1068	1065	1062	1097 w	1094 w	—	—	—
607	608	610	613	610 m	614 m (0.75)	615 w	—	—
342	326	300	275	—	—	—	—	367 m

TABLE 2 (continued)

Calculated frequencies for θ =				*Observed frequencies*				
				Raman			*Infrared*	
0°	*30°*	*60°*	*90°*	*Solid*	*Liquid*	*Gas*	*Solid*	*Liquid*
B_{1u}								
987	987	987	987	—	—	—	968 w	964* vw
898	899	900	902	—	—	—	903 s	902 s
726	728	735	746	—	—	—	729 vs	735 vs
703	703	703	703	—	—	—	695 vs	697 vs
431	449	479	502	—	—	—	458 s	486 s
91	91	91	91	—	—	—	73 w	77 w
B_2 Species (D_{2h}—B_{2u}, B_{2g})								
B_{2u}								
3070	3070	3070	3070	—	—	—	—	—
3069	3069	3069	3069	—	—	—	—	—
1608	1607	1605	1605	—	—	—	1568 s	1567 s
1430	1431	1433	1439	—	—	—	1428 vs	1430 s
1326	1326	1326	1328	—	—	—	1344 m	1337 w
1295	1296	1296	1296	—	—	—	1268 w	1266 m
1161	1160	1159	1158	—	—	—	1154 w/1169 s	1155 m
1055	1055	1058	1062	—	—	—	1075 m/1090 s	1072 s
622	621	617	613	—	626 w	—	626 w	—
96	95	93	91	—	—	—	118 vs	112 vs
B_{2g}								
987	987	987	987	978 w	987	—	—	979 vw
909	908	906	902	—	—	—	—	917 m
755	755	752	746	779/786 m	782 m	—	—	778 s
694	696	699	703	—	—	—	—	670 m
515	514	512	502	546 w	546 w	—	—	543 s
239	244	257	275	251 m	269 m (0.88)	265 w	—	269 m
Unassigned observed frequencies								
							1690 w	1683 w
							1650 w	1655 w
				1620 sh				
							1617 w	1612 w
							1380 w	1381 m
							1307 w	1300 w
							1280 w	1280 w
							1110 m	1107 w
								670 w
							174 w	
89 m, 52 m, 41 m, 22 m	Lattice nodes							

* Double assignment.
vs, s, m, w, vw, sh, very strong, strong, medium, weak, very weak, shoulder respectively.
The species symbols refer to $\theta = 0$ (D_{2h} configuration). The mode correlation for $\theta \neq 0$ is made on the basis of eigenvector similarities.

TABLE 3

CALCULATED AND OBSERVED FREQUENCIES (cm^{-1}) FOR 4,4′-DIFLUOROBIPHENYL FOR VARIOUS DIHEDRAL ANGLES

Calculated frequencies for all θ	*Observed frequencies*				
	Raman			*Infrared*	
	Solid	*Liquid*	*Gas*	*Solid*	*Liquid*
A Species ($D_{2h}-A_g$, A_u)					
A_g					
3073, 3072	No measurements				
1664	1603 vs	1607 vs (0.44)	1604 s	—	—
1535	1529 m	1524 m (0.39)	1519 m	—	—
1346	1323 w	1320 w	—	—	—
1241	1277 vs	1283 vs (0.27)	1284 vs	—	—
1143	1169 vs	1167 m (0.12)	1163 m	—	—
1022	1017 w	1017 w	—	—	—
835	846 vs	843 vs (0.09)	840 vs	—	—
653	660 s	661 m (0.74)	658 w	—	—
229	277 vs	264 s (0.22)	255 vs	—	—
A_u					
958	—	—	—	—	—
829	823* w	824* s	812* s	—	—
409	—	423* m (0.68)	415* w	—	420* m
B_3 Species ($D_{2h}-B_{3u}$, B_{3g})					
B_{3u}					
3073, 3072	No measurements				
1586	—	—	—	1600 vs	1600 vs
1494	—	—	—	1495 vs	1496 vs
1245	—	—	—	1235 vs	1230 vs
1144	—	—	—	1158 s	1153 s
1032	—	—	—	1016 s	1018 s
1016	—	—	—	1007 s	1008 s
800	—	808 sh	—	804 vs	806 s
525	—	—	—	518 s	515 s
B_{3g}					
958	966 vw	—	—	—	—
829	823* w	824* s or 812* m	812* s	—	—
409	—	423* m (0.68)	415* w	—	420* m
θ=0° 30° 60° 90°					
B_1 Species ($D_{2h}-B_{1g}$, B_{1u})					
B_{1g}					
3070 3070 3070 3070, 3069 3069 3069 3069	No measurements				
1583 1582 1581 1581	1554 w	1553 w	—	—	1555 w
1391 1388 1381 1373	—	—	—	—	—
1293 1292 1291 1288	1257 m	1259 sh	1267 sh	—	—
1274 1275 1278 1281	1245 vw	1239 w	1242 w	—	—
1095 1094 1092 1091	1098 m	1100 w	—	—	—
610 610 611 613	627 s	632 m (0.91)	633 w	—	630 w
444 441 435 428	464 vw	—	—	—	454 m
301 325 349 365	340 vw	—	—	—	358 m

TABLE 3 (continued)

Calculated frequencies for θ =				*Observed frequencies*				
				Raman			*Infrared*	
0°	*30°*	*60°*	*90°*	*Solid*	*Liquid*	*Gas*	*Solid*	*Liquid*
B_{1u}								
945	945	945	946	—	—	—	935 m	932 vw
							or 956 m	or 952 vw
820	821	822	826	—	—	—	822 vs	821 vs
709	712	720	729	—	—	—	702 m	704 w
494	500	511	520	—	—	—	499/505 vs	515* s
280	254	233	196	—	—	—	283 m	255 m
55	56	58	61	—	—	—	71 vw	72 w
B_2 Species ($D_{2h}-B_{2u}$, B_{2g})								
B_{2u}								
3070	3070	3070	3070	No measurements				
3069	3069	3069	3069					
1586	1585	1583	1581	—	—	—	1585 s	1586 m
1361	1362	1366	1373	—	—	—	1393 m	1394 m
1291	1290	1288	1288	—	—	—	1317 s	1302 s
1279	1280	1282	1281	—	—	—	1286 w	1283 vw
1088	1088	1089	1091	—	—	—	1124 s/1108	1095 s
619	618	616	613	—	641 sh	—	642 w	638 w
417	418	423	428	—	—	—	414 m	415 w
75	72	66	61	—	—	—	84 w	96 vw
B_{2g}								
949	949	947	946	938 vw	—	—	—	—
838	834	830	826	846* vs	843* vs (0.09)	—	—	847 s
727	727	729	729	722 s	728 m (0.90)	728 w	—	726 m
520	522	522	520	540 vw	—	—	—	542 m
382	381	376	365	395 s	392 m (0.81)	389 w	—	390 s
150	157	173	196	180 vw	183 m	178 w	—	182 vw
Unassigned observed frequencies								
							1687 w	
							1660 m	1660 w
							1645 m	
				1626 m	1638 w	1636 w		
								1516 w
								1476 m
							1450 m	1458 w
							1343 w	1350 w
				1176 m				
				1113 w				
							761 m	755 w
							145 w	
								101 w

Same abbreviations as in Table 2.

TABLE 4

CALCULATED AND OBSERVED FREQUENCIES (cm^{-1}) FOR 4,4′-DICHLOROBIPHENYL FOR VARIOUS DIHEDRAL ANGLES

Calculated frequencies for all θ				*Observed frequencies*				
				Raman			*Infrared*	
				Solid	*Liquid*	*Gas*	*Solid*	*Liquid*
A Species ($D_{2h}-A_g$, A_u)								
A_g								
3072				No measurements				
3072								
1653				1597 vs	1597 vs	1595 vs	—	—
1503				1495	—	1505 vw	—	—
1334				1287 vs	1284 vs	1275 vs	—	—
1174				1184 vs	1191 m	1186 m	—	—
1088				1098 vs	1098 s	1096 m	—	—
1012				1016 s	1018 m	1013 w	—	—
788				773 s	773 m	768 s	—	—
521				545* s	543* m	536 w	540 sh	—
198				227 s	226 s	219 s	227 vw	—
A_u								
964				973 w	—	953 vw	971 vw	—
832				822* m	824* m	817 w	822 sh-w	
408				421 w	413* m	406 m	410* s	414* s
B_3 Species ($D_{2h}-B_{3u}$, B_{3g})								
B_{3u}								
3072				No measurements				
3072								
1563				—	—	—	1588 m	1593* m
1468				—	—	—	1474 vs	1474 s
1174				—	—	—	1172 w/ 1186 m	1180 w
1097				1078 m	1077 m	1070 sh	1087 vs	1092 vs
1025				1019 sh-w	—	—	1019 vs	1019 m
997				1000 vw	—	—	1003 vs	1004 s
712				706 w	—	—	702 s	704 s
420				424 sh-m	423 sh	—	420 m	423 w
B_{3g}								
964				966 w			962 w	957 w
832				828 m	824* m	—	832* w	829* w
408				414 w	413* m	406 m	410* s	414* s
θ=0°	*30°*	*60°*	*90°*					
B_1 Species ($D_{2h}-B_{1g}$, B_{1u})								
B_{1g}								
3070	3070	3070	3072	No measurements				
3070	3070	3070	3072					
1566	1565	1564	1564	1549 m	—	—	1556 w	—
1387	1385	1380	1375	1380 vw	—	—	—	—
1287	1287	1287	1290	1275 m	—	—	—	—
1284	1285	1285	1283	1242 w	—	—	—	—
1106	1105	1103	1100	1123 m	1124 m	1123 m	1117 w	1114 w
621	621	622	624	628 m	629 m	627 w	624 w	626 w
387	383	373	363	373 m	370 w	—	372 w	369 m
242	261	277	289	274 m	—	—	271 w	270 m

TABLE 4 (continued)

Calculated frequencies for θ =				*Observed frequencies*				
				Raman			*Infrared*	
0°	*30°*	*60°*	*90°*	*Solid*	*Liquid*	*Gas*	*Solid*	*Liquid*
B_{1u}								
940	940	941	941	—	—	—	943 w	941 w
809	810	813	820	—	—	—	814 vs	812 vs
695	698	705	712	—	—	—	698 sh-m	696 w
472	481	498	512	—	—	—	504/510 s	501 s
233	211	185	161	219 w-sh	—	—	215 w	—
42	43	45	48	—	—	—	63 w?	—
B_2 *Species* ($D_{2h}-B_{2u}$, B_{2g})								
B_{2u}								
3070	3070	3070	3070	—	—	—	—	—
3070	3070	3070	3070	—	—	—	—	—
1569	1568	1566	1564	—	—	—	1595 m	1593 m
1368	1368	1370	1375	1394 vw	—	—	1387 s	1389 s
1296	1295	1293	1290	1307 sh	—	—	1300 w	1300 w
1279	1279	1281	1283	—	—	—	1271 w	—
1095	1095	1097	1100	—	—	—	1100 s	100 sh-w
630	629	627	624	639 w	639 w	—	637 w	637 w
306	303	297	289	—	—	—	—	—
63	59	54	48	—	—	—	87–95 m	—
B_{2g}								
944	943	942	941	—	—	—	949 vw	—
832	831	826	820	853 w	847 w	—	850 s	843 m
707	708	711	712	727 m	—	—	723 m	722 w
518	518	517	512	542* m	543* m	—	545 s	538 m
345	348	355	363	309 m	309 m	—	306 w	306 m
119	126	141	161	150 vw	154 vw		157 w	—
Unassigned observed frequencies								
							1675 w	1667 w
							1640 w	1635 w
				1633 w				
				1516 m	1513 vw			
							1488 m	1484 s
				1453 vw			1455 m	1450 vw
				1417 vw			1410 m	1411 vw
				1224 vw				
							762 m	757 m
				116 vs				
				104 vs				
				56 m				
				42 m				

Same abbreviations as in Table 2.

TABLE 5

CALCULATED AND OBSERVED FREQUENCIES (cm^{-1}) FOR 4,4′-DIBROMOBIPHENYL FOR VARIOUS DIHEDRAL ANGLES

Calculated frequencies for all θ	*Observed frequencies*		
	Raman	*Infrared*	
	Solid	*Solid*	*Liquid*
A Species ($D_{2h}-A_g$, A_u)			
A_g			
3072, 3072	No measurements		
1651	1587 vs	—	—
1496	1498 m	—	—
1339	1282 vs	—	—
1168	1184 s	—	—
1066	1069 s	—	—
1016	1010 s	—	—
771	757 s	—	—
443	460 s	—	—
147	167 s	—	—
A_u			
972	969 w	970 vw	—
827	818 m	814 m-sh	—
411	408 m	—	—
B_3 *Species* ($D_{2h}-B_{3u}$, B_{3g})			
B_{3u}			
3072, 3072	No measurements		
1560	—	1584 m	—
1462	—	1471 vs	1470 s
1169	—	1166 vw	—
1077	—	1067 vs	1071 s
1028	1015 sh-w	1016 vs	1016 m
1001	—	1001 vs	1000 s
679	671 w	672 s	672 s
321	—	315 vs	316 vs
B_{3g}			
972	962 w	962 w	—
827	824 m	822 w	—
411	415 s	410 m	412 s

TABLE 5 (continued)

Calculated frequencies for θ =				*Observed frequencies*		
				Raman	*Infrared*	
0°	*30°*	*60°*	*90°*	*Solid*	*Solid*	*Liquid*
B_1 *Species* ($D_{2h}-B_{1g}$, B_{1u})						
B_{1g}						
3070	3070	3070	3070	—	—	—
3069	3069	3069	3059	—	—	—
1546	1546	1548	1552	1538 vw	—	—
1375	1374	1370	1367	—	—	—
1285	1284	1283	1281	1263 w-sh	—	—
1234	1235	1238	1242	1224 w	—	—
1095	1094	1092	1090	1083 m	1076 s	1079 m
616	616	617	618	623 m	623 w	624 vw
361	357	349	340	354 m	356 w	355 w
182	176	161	144	237 w	237 w	—
B_{1u}						
925	925	925	926	—	944 vw	—
816	817	820	827	—	810 vs	808 vs
696	698	704	710	—	668 m	668 w
460	471	492	509	—	500/506 m	497 s
220	220	221	222	192 w	190 vw	—
33	34	35	39	—	73 w	—
B_2 *Species* ($D_{2h}-B_{2u}$, B_{2g})						
B_{2u}						
3070	3070	3070	3069	—	—	—
3069	3069	3069	3069	—	—	—
1564	1562	1556	1552	—	1590 w	1588 w
1364	1364	1365	1367	—	1382 s	1383 m
1279	1279	1280	1281	—	1300 w	1300 vw
1248	1247	1245	1242	—	—	—
1087	1087	1088	1090	1103 vw	1100 m	1100 w
625	624	622	618	632 w	635 w	635 w
223	223	223	222	—	—	—
50	48	43	39	98 vs	89 w	—
B_{2g}						
928	928	927	926	—	949 vw	—
839	837	833	827	844 w	848 m	841 m
703	705	708	710	720 w	720 m	718 w
519	518	516	509	540 w	542 m	537 m
328	330	335	340	270 m	271 m	—
108	113	127	144	—	145 vw	—
Unassigned observed frequencies						
					1670 w	
					1635 w	
				1628 w		
				1490 m	1485 s	1485/1480 m
					1452 w	
				1271 w		
				1235 vw		
				1201 vw-sh		
					1117 w	1114 vw
					538 sh-w	537 m
				112 vs	108 vw	

Same abbreviations as in Table 2.

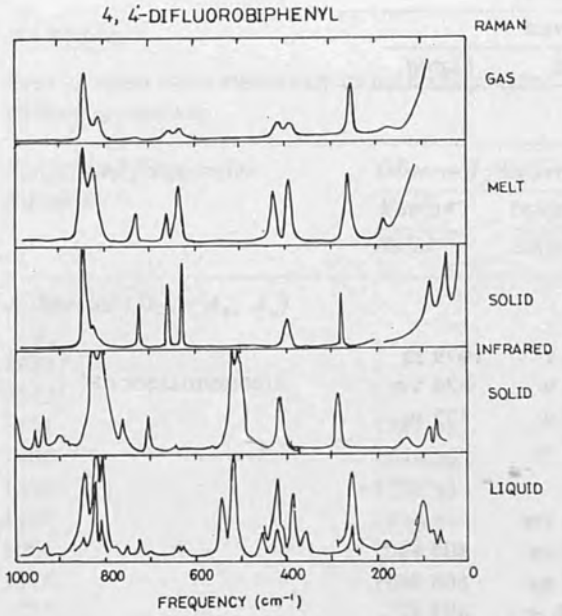

Fig. 2. Solid, melt and gaseous Raman and solid and liquid infrared spectra of 4,4′-difluorobiphenyl.

Composite spectra of 4,4′-difluoro- and -dichloro-biphenyls are shown in Figs. 2 and 3. The spectra of biphenyl have been adequately presented previously and those of 4,4′-dibromobiphenyl are sufficiently similar to those of the dichloro compound not to warrant reproduction. In Fig. 4 the absorption spectrum of a crystallized melt of 4,4′-difluorobiphenyl is compared with that of the same compound as measured in an alkali halide disc.

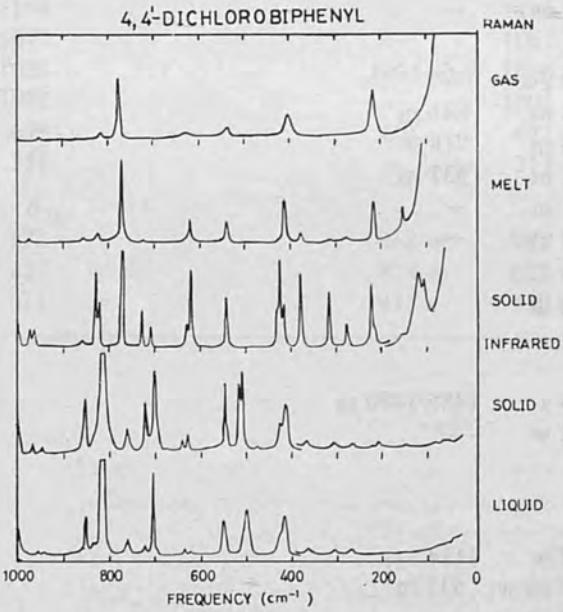

Fig. 3. Solid, melt and gaseous Raman and solid and liquid infrared spectra of 4,4′-dichlorobiphenyl.

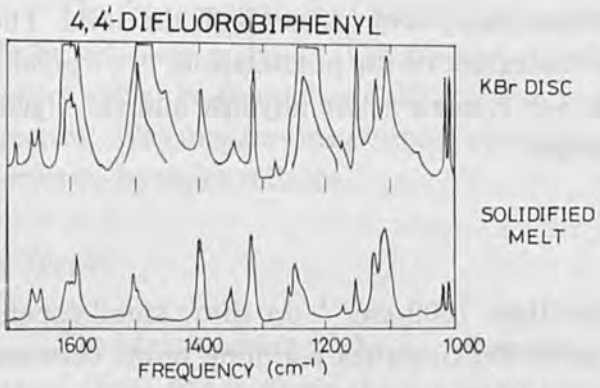

Fig. 4. Infrared absorbtions of 4,4'-difluorobiphenyl between 1000–1700 cm^{-1}.

INTERPRETATION OF THE SPECTRA OF BIPHENYL

Previous investigations have established the majority of the assignments for planar biphenyl beyond any reasonable doubt. We shall therefore refer only to the main points of interest.

A Species

The agreement between calculated and observed A_g frequencies is quite pleasing – especially in view of the fact that no attempt has been made to improve the fit by varying the transferred benzene force field. The greatest discrepancy is for the highest ring mode, which is 5 % high. In our experience this is a characteristic failing of the field used.

The assignments present no problem – all the bands being strongly polarized in the melt and remaining sharp in the gaseous phase. The calculated A_g and A_u frequencies do not vary with dihedral angle. The observed changes are indeed small (Table 2) for all, except the lowest mode, and are probably associated with small variations in the C–C force constants. We found it rather surprising that the lowest mode varied so strongly with phase until we examined the eigenvectors. About 30 % of the energy of this mode is associated with stretching of the central C–C bond and a further 27½ % arises from the adjacent ring angle deformation. This dependence then shows that there is indeed a reduction in these force constants as the molecule goes from planar solid to solution to gaseous phase. This change must be quite large, perhaps as high as 30 %, to account for the 7 % variation in frequency. Study of the deuterated biphenyls may elucidate the problem of the relative contributions of the two internal deformations. For the present we content ourselves with the observation that the variation from melt to gaseous phase is at least half of that from solid to melt.

The Raman polarization data positively identifies the A modes of the melt derived from the A_u modes of the planar configuration. Three moderate to strong

polarized bands appear in the melt where there were no bands in the solid. The extent of the increase in intensity, and the extent of the polarization, is surprising in view of the facts that the A_u modes are Raman active anyhow and the eigenvectors do not change with dihedral angle.

B_1 Species

The calculated frequencies greater than 1000 cm^{-1} do show small depenences on dihedral angle due to changes in the G matrix coupling terms between what were in-plane symmetry co-ordinates. The major angle dependence however is predicted to arise from interaction between the lowest b_{1g} and the second lowest b_{1u} vibrations. Both exhibit about 20 % shift in change of dihedral angle from 0° to 90°. Experimentally the b_{1u} band shifts 28 cm^{-1} at 458 cm^{-1}. No Raman band was observed in the liquid phase at the new frequency of this mode. In accord with this failure we could not find a Raman band in the crystal which could be assigned to the b_{1g} vibration, but an infrared band of moderate strength appears in the infrared at 367 cm^{-1}. The observed frequency shift of the b_{1u} band is in accord with a dihedral angle in solution of near 40°. However it should be noted that the b_{1g} and b_{1u} frequencies are calculated to be about 50 and 30 cm^{-1} high respectively. The interaction between the levels is sensitive to their frequency separation for reasons discussed earlier, and therefore the above deduction has an uncertainty of at least 10°. It is our hope that the studies of force fields and deuterated species which are in progress will allow these error limits to be decreased.

The major assignment problems in this species arise from the weakness of the associated Raman and infrared bands. It is reassuring that our calculations have vindicated the agreement of earlier studies in locating and assigning these fundamental transitions.

With the exception of the perturbation discussed earlier no effects of interaction between the b_{1g} and b_{1u} modes are found.

B_2 Species

As with the B_1 species, the higher frequency modes show up to 10 cm^{-1} calculated shift with a dihedral angle change from 0° to 90°. Interaction between the two lowest b_{2u} and b_{2g} vibrations is significant, though not as great as with the b_1 pair discussed earlier. Experimentally the frequency shifts are indeed small – the greatest being 18 cm^{-1} (lowest b_{2g} mode) – but there are strong intensity effects due to the strength of the b_{2u} and b_{2g} bands for the planar configuration. Thus the b_{2g} vibration at 546 cm^{-1} gives rise to a strong infrared band in the melt, or in solution, due to interaction with the 626 cm^{-1} band. Surprisingly the 626 cm^{-1} band disappears in solution, but this is not because of a frequency shift since a moderate strength Raman band now occurs at 626 cm^{-1}.

The frequency shift of the lowest b_{2g} mode, if attributed entirely to G matrix effects indicates a dihedral angle change of just over 60°. This result is rather suspect since the frequency shift from melt to vapour is 4 cm^{-1} in the opposite direction. We consider this estimate too high and believe the deduction from the B_1 species to be more reliable.

B_3 Species

The identification of the b_{3u} vibrations is facilitated by the marked polarization of these bands along the c axis of the crystal[7,9]. No marked frequency or intensity effects are expected or observed with the single exception that the b_{3g} band at 838 cm^{-1} gives rise to a moderate strength infrared band.

DISCUSSION

The agreement between the spectral frequencies reported here and those reported by Zerbi and Sandroni[9] and by Pasquier and Lebas[12] is very good. Our assignments differ from those of Pasquier and Lebas only in minor details. This is an encouraging fact since their paper has come to our attention only since the completion of our work, and their assignments were arrived at essentially by qualitative arguments. The assignments of Zerbi and Sandroni for the in-plane species are again in good agreement as might be expected since they too were based on calculations, though for the planar case only.

The one outstanding gap in our present knowledge is the frequency of the torsion mode. Zerbi and Sandroni suggest that this might be 70 cm^{-1} corresponding to an absorption in the neutron scattering spectrum. As a band appears at this frequency in the electromagnetic absorption spectrum and has alternative explanations as a fundamental this assignment may be discounted. In a recent analysis of the fluorescence spectrum[17] a long sequence of bands of frequency 635 cm^{-1} was reported. On the assumption that the excited state was planar whilst the ground state was non-planar the authors pointed out that a progression in the torsion might be expected, and they assigned the long sequence accordingly. This is not tenable as such a high frequency would require an enormous torsion barrier.

A semi-empirical computation of internal energy of biphenyl as a function of dihedral angle, $H_2C_2C_1$ angle and C_1C_1' bond length has been made[18]. The results were in excellent accord with known properties. The most stable configuration predicted for the free molecule had a dihedral angle of about 35° and a C_1C_1' bond length of about 1.50 Å. A planar configuration was predicted for the crystal with a slightly longer C_1–C_1' bond length of 1.52 Å. The barrier height predicted was 2.5 kcal $mole^{-1}$ at $\chi = 0°$ and 3.7 kcal $mole^{-1}$ at $\chi = 90°$. An assumed barrier

height of 12.5 J mole^{-1} (3 kcal mole^{-1}) and a two-fold barrier, then, with $F = 0.377$ cm^{-1} a torsion frequency of approximately 60 cm^{-1} is predicted.

The predicted π orbital overlap energy between the rings decreases sharply with the dihedral angle. The flatness of the internal energy–dihedral angle curve is due to the simultaneous sharp drop in steric repulsion. The small change in bond length observed on passing from crystal to vapour does not therefore preclude a considerable change in the inter-ring force constant. Such a change is suggested by the behaviour of the lowest a_g mode.

INTERPRETATION OF THE SPECTRA OF 4,4′-DIFLUOROBIPHENYL

In marked contrast to the biphenyl history there is no earlier detailed analysis of the spectrum. However the similarity in the spectra of biphenyl and of its difluoro derivative – especially in the dependence of bands on phase and crystal orientation – allows a ready interpretation of the latter which is based on the earlier analyses of biphenyl itself.

A Species

As with biphenyl no frequency shifts with dihedral angle change are predicted. The actual Raman bands due to the a_g and a_u modes are readily identified by the band polarizations and the sharpness of the bands in the vapour phase. Only the highest a_u mode is not located. Just as with biphenyl, the observed frequency shifts, on passing from solid to liquid to vapour, are small, with the single exception of that for the lowest a_g mode. The potential distribution is similar to that for biphenyl, and in principle this again should allow reasonable estimates for the change in bond order of the central C–C bond to be determined. A significant answer however could only be given after a careful analysis of the force field to ascertain the relative contributions due to the ring angle and the C–C stretch force constants. This difficulty is made clear when it is realised that the vibrations at 1603 and 1323 cm^{-1} both have over 20 % of their energy in the central C–C stretching mode and both, in contrast to the 277 cm^{-1} vibration, are calculated too high.

B_1 Species

The intensity of many of the b_{1g} Raman bands is very weak – just as for biphenyl. Only three of the eight non C–H stretching modes can be located with any certainty. Strong interactions or the dihedral angle changes are predicted between the two lowest b_{1g} modes and the b_{1u} modes. Strong new infrared bands at 357 and 456 cm^{-1} are clearly due to these formerly b_{1g} modes. The other interacting vibrations of the b_{1u} species in the planar case, show considerable frequency

shifts (10 % for a band at 283 cm^{-1}), but in accord with the weakness of the Raman activity of the b_{1g} modes, no Raman bands can be located at the displaced frequencies.

The observed frequency shift of the 283 cm^{-1} band would indicate a dihedral angle of about 32° in the solution. However the main interaction between this mode and the b_{1u} species is with the b_{1g} vibration at 464 cm^{-1}. The observed difference in the energies of the two modes is 181 hc erg compared with a calculated value of 164 hc. The greater observed difference will lead to an underestimate of angle. An angle of 35° to 45° appears to be more realistic.

B_2 Species

The general comments about frequency shifts and intensity changes made for this species of biphenyl apply equally well to 4,4′-difluorobiphenyl. Shifts are small, but intensity changes are quite dramatic. In particular the strong infrared bands of the solution at 847, 726 and 542 cm^{-1} are due to formerly b_{2g} vibrations.

B_3 Species

The behaviour of the bands due to the B_3 species vibrations on allowing a melt to crystallize on a plate in itself gives good evidence for planarity, or near planarity, of the rings in 4,4′-difluorobiphenyl. It also suggests that the crystal structure is very similar to that of biphenyl in that the molecular axes along which the b_{3u} transition moments are orientated are all parallel and are perpendicular to the plate. This is shown as a very strong dichroic ratio for the b_{3u} bands as measured by relative intensities in the crystallized melt spectrum and in a KBr disc. Frequency shifts and activity changes are small.

INTERPRETATION OF THE SPECTRA OF 4,4′-DICHLOROBIPHENYL AND 4,4′-DIBROMOBIPHENYL

In contrast to biphenyl and its 4,4′-difluoro derivative, the dichloro and dibromo derivatives show no significant frequency or intensity variations with change of state. The spectra can be fairly readily interpreted by comparison with the solution or molten state spectra of difluorobiphenyl on making allowance for the heavier masses of the substituents.

In a recent publication[18] the spectra of 4,4′-dichlorobiphenyl were briefly reported and interpreted on the basis of a planar system. The arguments presented in support of this were the similarity to the spectral frequencies of biphenyl itself and the simplicity of the spectrum. Neither argument is acceptable on the present much more extensive evidence. The major argument against a D_{2h} structure must be the almost total coincidence between observed infrared and Raman frequencies below 1000 cm^{-1}.

It would be possible to assign the principal bands on the basis of the D_{2d} structure. The major evidence against this is the polarization of the Raman band at 413 cm^{-1}. No measurements of polarization were made on the other weaker fundamentals derived from the A_u vibrations of the D_{2h} species.

Just as for difluorobiphenyl and for biphenyl there are considerable intensity changes of bands between a KBr disc spectrum and a solidified melt spectrum. The greatest changes occur for those bands which are certainly b_3 fundamentals. In these instances the bands are weaker in the solidified melt. On the other hand not all bands which exhibit this intensity decrease can arise from b_3 transitions. The principal deduction must be that the long axes are once more oriented almost perpendicular to the plane of major crystal development. This serves to assist vibrational assignments. A good example is afforded by the complex region around 1100 cm^{-1}. In the crystallized melt spectrum a band at 1087 cm^{-1} is strongly reduced in intensity relative to neighbouring bands. From this we deduce that the associated transition is of a different species to that of its neighbours and that it is to be identified as the b_3. From similar arguments our desire to assign one of the pair of infrared bands at 1186 and 1172 cm^{-1} to a b_3 fundamental, which is the only fundamental apart from an a expected in this region, has to be tempered by the lack of any orientation effects on the strengths of the bands.

Doublets near 970, 830 and 415 cm^{-1} should clearly be assigned to the pairs of bands due to the a and b_3 out-of-plane type vibrations. That such doublets exist is further support for the D_2 structure.

The spectra of 4,4′-dibromobiphenyl are very similar to those of the dichloro analogue. Difficulty was experienced in obtaining a uniform crystallised melt spectrum. The material tended to form globules on the surface and crystallise in random orientations thereby probably explaining the fact that no marked intensity changes were observed.

On the existing evidence it is not possible to estimate quantitatively the dihedral angles in these molecules. However the similarity of the spectra with those of solutions of biphenyl and its 4,4′-difluoro derivative suggests similar angles.

CONCLUSION

It has been clearly demonstrated that change in conformation for biphenyl and 4,4′-difluorobiphenyl from D_{2h} to D_2 symmetry is accompanied by changes in spectral activities and shifts of certain normal modes. The only high frequency shift observed was $\nu_5(B_{2u})$ for difluorobiphenyl and this tallies with an observed shift for $\nu_5(B_{2u})$ of 4,4′-dideuterobiphenyl from 1322 cm^{-1} in the solid state to 1308 cm^{-1} in solution. This can be explained in terms of lack of steric hindrance in the *ortho* hydrogens on twisting which would be expected to affect the β-CH bending modes.

Both the lowest a_{1g} modes for biphenyl and 4,4′-difluorobiphenyl are affected by a decrease of 15 cm^{-1} and 13 cm^{-1} respectively from solid to liquid and 9 cm^{-1} from liquid to gas. These shifts have to be explained in terms of force constant changes about the central joining bond.

Several frequencies of these systems are predicted to shift. Comparison of calculated dihedral angle dependence and observed shifts leads to estimates for the dihedral angles of near 45°. A more accurate estimate of the dihedral angles in solution for these two molecules is being undertaken by using supplementary data from the deuterated species. With the additional observables the force field is being refined for D_{2h} symmetry, and then the dihedral angle will be varied until the practical shifts on the modes which move correspond to the theoretically predicted shift.

The conformations of 4,4′-dichloro- and 4,4′-dibromobiphenyl have been shown to be D_2 irrespective of phase. The estimation of the angle here is more difficult because the frequency fit is not as good. The very poor solubilities of dichloro- and dibromobiphenyl in common organic solvents compared with biphenyl and difluorobiphenyl indicates a difference in physical properties which may be related to structure.

ACKNOWLEDGEMENTS

One of us (R.M.B.) wishes to thank the Science Research Council for a studentship. We also acknowledge a grant by the Science Research Council towards the purchase of a Perkin–Elmer 325 spectrometer.

REFERENCES

1 A. Hargreaves and S. H. Rizvi, *Acta Crystallogr.*, 15 (1962) 365.
2 J. Trotter, *Acta Crystallogr.*, 14 (1961) 1135.
3 O. Bastiansen, *Acta Chem. Scand.*, 3 (1949) 408.
4 R. A. Hoffman, P. O. Kinell and G. Bergström, *Ark. Kemi*, 15 (1960) 534.
5 J. Dale, *Acta Chem. Scand.*, 11 (1957) 640.
6 J. E. Katon and E. R. Lippincott, *Spectrochim. Acta*, 15 (1959) 627.
7 D. Steele and E. R. Lippincott, *J. Mol. Spectrosc.*, 6 (1961) 238.
8 G. V. Peregudov, *Opt. Spectrosc. (USSR)*, 9 (1960) 155.
9 G. Zerbi and S. Sandroni, *Spectrochim. Acta*, 24 A(1968) 483.
10 G. Zerbi and S. Sandroni, *Spectrochim. Acta*, 24A (1968) 511.
11 G. Zerbi and S. Sandroni, *Spectrochim. Acta*, 26A (1970) 1951.
12 B. Pasquier and J. M. Lebas, *J. Chim. Phys.*, 64 (1966) 765.
13 D. Steele, *J. Mol. Spectrosc.*, 15 (1965) 333.
14 J. C. Duinker, *Thesis for Doctorate of Natural Sciences*, University of Amsterdam, 1964.
15 K. Radcliffe and D. Steele, *Spectrochim. Acta*, 25A (1969) 597.
16 R. E. Buckles and N. G. Wheeler, *Org. Syn.*, 31 (1951) 29.
17 E. C. Lim and Y. H. Li, *J. Chem. Phys.*, 52 (1970) 6416.
18 G. Casalone, C. Mariani, A. Mugnoli and M. Simonetta, *Mol. Phys.*, 15 (1968) 339.